Atténuation des interférences dans les réseaux mobiles 5G : Contamination pilote des liaisons montantes dans le schéma massif MIMO TDD

Ahmad Abboud

Thèse de doctorat

Université de Limoges

Université de Limoges

École Doctorale Sciences et Ingénierie pour l'Information, Mathématiques (ED 521)

Laboratoire XLIM, Département C_2S_2: Composants Circuits Signaux et Systèmes Hautes Fréquences, ENSIL - Ecole Nationale Supérieure d'Ingénieurs de Limoges

Thèse pour obtenir le grade de

Docteur de l'Université de Limoges

Spécialité : Gestion des interférences dans le réseau mobile 5G

Présentée et soutenue par

Ahmad Abboud

Le 22 septembre 2017

Interference Mitigation in 5G Mobile Networks

Uplink Pilot Contamination in TDD Massive MIMO Scheme

Thèse dirigée par **Jean-Pierre Cances**, **Ali Jaber** et **Vahid Meghdadi**

JURY :

Président du jury

M. **Gilles Burel**, Professeur des Universités, UBO (Université de Bretagne Occidentale), Université de Bretagne Occidentale, laboratoire Labsticc

Rapporteurs

M. **Guillaume Ferré**: MCF HDR, Laboratoire IMS Bordeaux, ENSEIRB Mat-Méca

M. **Samir Saoudi**, Professeur des Universités, Institut Mines-Télécom Atlantique

Examinateurs

M. **Yannis Pousset**, Faculté de Sciences Fondamentales et Appliquées, Université de Poitiers, labo Xlim, axe SRI

M. **Vahid Meghdadi**, directeur, Co-encadrant de thèse, ENSIL Limoges, 16 rue Atlantis, 87068 Limoges cédex, Labo: Xlim, axe SRI

M. **Jean-Pierre Cances**, directeur, Co-encadrant de thèse ENSIL Limoges, 16 rue Atlantis, 87068 Limoges cédex, Labo: Xlim, axe SRI

Abstract

By the revolution of Cloud Computing and Smartphones, an enormous amount of data should traverse the network every second where most of this data are delivered by mobiles using internet services. The fast growth in bandwidth and QoS demands makes the 4th G mobile networks insufficient. The next generation system must afford a sum rate from 100Mbps up to 1Gbps per User Terminal (UT), with a connection density that exceeds 1M connection/Km2, the mobility of high-speed vehicles up to 500 km/hr and an End to End (E2E) delay less than 10ms. A promising candidate that can offer those demands is the Multi-User Multi-Cell Massive Multiple-Input Multiple-Output (MIMO) wireless system. However, Massive MIMO capacity is upper bounded by the Inter-cell Interference (ICI) due to pilot reuse and thus, pilot contamination.

In this thesis, we investigate the uplink pilot contamination in Time Division Duplexing (TDD) training scheme of massive MIMO wireless networks. Assuming block-fading channel, the coherence interval will lag for a limited duration, where channel estimation, symbol reception, and symbol precoding must be done within the same interval. Having said that, the training pilot length is limited. Likewise, the number of User Terminal's (UT's) per interference region is also limited. Inspired by the variation of coherence interval size among UT's, this research introduces two independent novel contributions to deal with uplink pilot contamination in massive MIMO. The first contribution maps the Base Station (BS) cell coverage region into a Channel State Information (CSI) Map. This map is created and updated using a special machine-learning algorithm, and it is exploited to predict UT CSI instead of estimating their channels. In view of this, training overhead and uplink pilots are reduced significantly. The second contribution classifies UT's based on the size of their channel coherence interval. Furthermore, we apply a pilot shifting technique to shift similar pilots to different time position (that considered empty due to empty pilot TDD frames).

Simulation results show a scaled increase in the performance of massive MIMO especially in the performance of energy and spectral efficiency, UT per cell and sum-rate. In particular, the third contribution evolves multi-cell massive MIMO to a single cell performance and even overcome single conventional huge in the energy efficiency and UT per cell.

Acknowledgment

First, I would like to express my elite gratefulness and appreciations to my first supervisor Prof. Jean-Pierre Cances for his supervision and provision. I would like to thank him for inspiring my research, for tolerating me to grow as a researcher, and for providing me this valuable prospect to follow a Ph.D. I am also thankful for my second, supervisors, Prof. Ali Jaber, from the Lebanese University, and I would like to thank Prof. Vahid Megdadi, from the University of Limoges, for his insightful debates.
It is my great honor to work with, Dr. Oussam Habachi and I am thankful for his significant contribution to this work.
Also, I would like to take this opportunity to thank my teachers from the high school, namely Mr. Bassam Saad, Mr. Ali Elaik for their encouragements.
In the end, my superior gratitude goes to my family for their unconditional love and tremendous support.
Thank you all for helping me in all my quests.

Ahmad Abboud
Limoges-France, July 2017.

Table of Content

List of Figures

List of Tables

Nomenclature

General Symbols

$(.)^T$	*denote transpose*
$(.)^H$	*Hermitian transpose*
$(.)^*$	*denote the conjugate*
det(A)	*denote the determinant of A*
$\odot$	*denote element-wise multiplication*
$\|\|A\|\|$	*denote the Frobenius norm and used for L^2-norm.*
max {.}	*maximum value of a set*
min {.}	*minimum value of a set*
E [.]	*statistical expectation*
$\mathcal{CN}(mean, \sigma)$	*complex circular symmetric normal distribution*
$\boldsymbol{H}$	*channel coefficient matrix*
K	*Number of users per cell*
M	*Number of antennas per base station*
L	*Number of cells*
τ_p	*Pilot sequence length*
S	*Symbol vector*
$\boldsymbol{y}$	*signal vector*
σ	*Standard deviation*
P	*Power vector*
$[.]^{UL}$	*Corresponds to Uplink session*

Note:
Bold small letter, used to denote vectors
Bold capital letter, used to denote matrix

General Abbreviations

BS	*Base Station*
UT	*User Terminal*
LoS	*Line of Sight*
DoF	*Degree of Freedom*
SNR	*Signal to Noise Ratio*
SINR	*Signal to Interference Noise Ratio*
MIMO	*Multiple Input Multiple Output*
MRC	*Maximal Ratio Combination*
ZF	*Zero Forcing*
MMSE	*Minimum Mean Square Error*
DPC	*Dirty Paper Coding*
TDD	*Time Division Duplexing*
FDD	*Frequency Division Duplexing*

5G	*Fifth Generation*
IoT	*Internet of the Things*
CSI	*Channel State Information*
QCSI	*Quantized Channel State Information*
SDN	*Software Defined Network*
NFV	*Network Function Virtualization*
RRH	*Remote Radio Head*
BBU	*Baseband Unit*

Chapter 1: Introduction

It's much easier to get a reception from someone if there is an introduction versus randomly trying to get in front of people~ Brad Feld

This chapter will introduce a background on the 5th generation wireless technology demands and features. Further, it will clarify the position and the scope of this research within the literature. After reading this chapter, the intention behind researching on 5th generation wireless networks and the scope of this thesis will be clear.

1 The 5th Generation Wireless Communication Systems

1.1 The fifth Generation Demand Features

An enormous amount of data has to cross the network, and internet services deliver most of this data. The QoS demands, and the rapid growth in bandwidth make 4G mobile networks insufficient to afford user requirements. The next generation mobile network should provide a bandwidth from 100Mbps up to 1Gbps per User Terminal (UT), and a density of connection that exceeds 1M connection/Km^2 and high-speed vehicles mobility of up to 500 km/hr and an End-to-End (E2E) delay less than 10ms [1].
The 5G network needs to be elastic to afford Network-as-a-Service (NaaS) and simple SDN control. Also, Power effective, Security and Cost-effective Services must be provided. Furthermore, Quality of Experience (QoE) and Network Intelligence (NI), should be included.

1.2 Ongoing Global Research and Framework on 5th Generation

Many projects on 5G are ongoing in both industry and academic. In this section, we will introduce the most important proposals. In Europe, the main leading projects are 5G Private Public Partnership (5G PPP) [2] and Horizon 2020[3]. China introduces the main project by IMT-2020 (5G) Promotion Group [4]. Intel Strategic Research Alliance (ISRA) [5] in the USA leads new research on 5G networks. In [6], a software defined decentralized mobile network architecture (SoftNet) suggests distributed data forwarding, a dynamically defined architecture, multi-RATs coordination, and decentralized mobility management. SoftNet afforded features, includes a flexible and high capacity network in contrast to 4G mobile networks.
C-RAN or Cloud Radio Access Networks provides low operating expenses, as well as high energy and spectral efficiency. It separates the baseband processing from the radio units, permitting the processing power to be shared at a central location. Thus, dropping the required element redundancy by splitting BBU and RRH, where BBU pool offered as a centralized cloud service and Remote Radio Heads (RRH's) are distributed among the network ends. This architecture solves many challenges struggle network flexibility but introduce a new challenge by flooding front-haul links with signaling data to the Baseband Unit (BBU) resources [7]. Recent research on C-RAN virtualization reduces signaling overhead by logically grouping macro cells with collocated small cells that can provide the core network with a simplified overview [8]. C-RAN projects have been initiated in many organizations such as the European Commission's Seventh Framework program and the Next Generation Mobile Networks (NGMN) project.
SoftRAN is a software-defined control plane applied to radio access networks. It integrates all base stations in a local area as a virtual big BS containing radio access elements and a central controller [9].

SoftRAN suggests a logically centralized entity, which makes control plane decisions for all the radio elements in the geographical area. Nevertheless, this architecture still lacks some elasticity, where user terminals deal with the virtual BS as a separate BSs. SoftRAN arranges this issue by running multiple handovers between the same pair of base stations.

2 MOTIVATIONS AND PRIOR WORK

In 2010, Thomas L. Marzetta from Bell Labs posted a paper [10] on what can be considered as a strive to make full use of MIMO. Let the number of base station antennas develop barring restriction in MU-MIMO scenarios. The first important phenomenon is that the effects of additive receive noise and small-scale fading disappear, as does intra-cellular interference among users. The only remaining impairment is inter-cellular interference from transmissions that are associated with the equal pilot sequence used in channel estimation and that paper concludes that the throughput per cell and the number of users per cell are unbiased, the spectral efficiency is independent of the system bandwidth and required transmit strength per bit vanishes. Although some marvelous consequences are a situation to the system model and propagation assumptions used in the paper, Dr. Marzetta pointed out an essential route in which mobile systems may evolve. Scaling up MIMO provides many extra degrees of freedom in the spatial domain than any of trendy systems. This issue rescues us from the state of affairs that wireless spectrum has to turn out to be congested and expensive, mainly in frequency bands beneath 6 GHz. In contrast to traditional MU-MIMO with up to eight antennas, we name MIMO with a large variety of antennas "massive MIMO", "very-large MIMO" or "large-scale MIMO".
In massive MIMO operation, we take on consideration an MU-MIMO scenario, where a base station geared up with a large number of antennas serves many terminals in the same time-frequency resource. Processing efforts can be done at the base station side, and terminals have the simple and inexpensive hardware. Until now, many theoretical and experimental research has been executed in the massive MIMO context, e.g., [11]–[15]. These studies have proven that massive MIMO can considerably improve spectral efficiency while reducing radiated output power with the aid of at least an order of magnitude. In addition, real-time large MIMO testbeds are being carried out, and demonstrations are reported in [16], [17].

In light of this, massive MIMO can be considered a promising system for the next 5^{th} generation wireless mobile technology. This is due to the high capacity, spectral and energy efficiency that can be afforded. For instance, in a scenario of 80 antennae at the BS and a sixteen UT Closely located with NLOS, a sum-rate capacity at the downlink reaches 40 b/s/Hz using Dirty Paper Coding (DPC) [18]. However, certain essential characteristics of massive can limit the performance and challenge the implementation of this technology. That is to say, uplink pilot contamination, limited pool of orthogonal pilot sequence within the coherence interval and training overhead are considered as the main aspects that face the implementation of massive MIMO.
The use of TDD scheme in massive MIMO is considered as a higher alternative when channel reciprocity is regarded for channel estimation [19]. However, the principal constraint is the coherence interval length. The use of non-orthogonal pilot indicators in multi-cell introduces the trouble of pilot contamination. The effect of pilot contamination is shown to be profound in the multi-cell state of affairs with a high-frequency reuse factor of one. Some researchers suggest the use of fractional frequency reuse to mitigate the impact of pilot contamination [20]. However, several other researchers have proposed extraordinary techniques in reducing the outcomes of pilot contamination for a reuse factor heigher than one. The majority of the reviewed papers think about the worst-case situation and uniform distribution when analyzing the consequences of pilot contamination. Low bound on achievable rate have been derived based on best and imperfect channel estimation and for uniformly dispensed UTs in L cells with a finite number of BS antennas [21]. Other viable causes of pilot contamination, such as hardware impairment and non-reciprocal are also studied in [12], [22].

This work studies uplink pilot contamination in massive MIMO systems and proposes two novel techniques to mitigate pilot contamination by exploiting the coherence interval characteristics of UTs.

Also, the reduction in training overhead and transmitted energy makes this work a breakthrough in the literature.

3 CONTRIBUTIONS

The problem of pilot contamination has received significant interest from the ongoing research on massive MIMO. Theoretical evaluation has recognized pilot contamination as an imperative restriction on the throughput of massive MIMO systems [23]. Throughout this thesis, our goal is to propose techniques to mitigate uplink pilot contamination. Our contribution had proved its ability to mitigate contamination, increase sum-rate, increase energy and spectral efficiency as well as the number of user terminal per cell.

The contribution of this research can be presented as follows:

First, for the indoor scenario, we introduce the CSI Map, where BS stores the CSI of each UT at each position of the covered region. We use graph theory to represent this map. Each node stores a quantized version of the CSI, which is previously estimated from a UT in a particular location. The nodes are connected with directed weighted edges that represent the transition of a UT between two channel states. We develop an algorithm that creates and update the map during the learning phase, and we suggest the use of Expectimax search to predict the next possible CSI of a monitored UT within the map. Furthermore, we use Garbage Collector (GC) algorithm to remove rarely visited nodes to reduce the complexity of the CSI Map.

Second, another novel technique to reduce training overhead was introduced. In this contribution, we classify UTs based on their coherence interval into several classes. Users of the first class, i.e. high mobility users, were considered to upload their pilots in each frame similar to traditional reciprocity TDD protocol. In contrast, low mobility UTs related to class n must upload their pilots once every n frame due to their larger coherence interval. Exploiting the pilot sparsity of frames related to class $n > 1$, we shift frames with pilots to an empty time space. The proposed method, reduce the number of uploaded pilots eventually as well as the training overhead. The added value of applying user classification with pilot shifting, reduce the uplink pilot contamination and increase the system performance in the dimension of energy and spectral efficiency. It also increases the system sum-rate and the cell density. Worth to mention that the proposed technique can be used jointly with any other pilot decontamination techniques if the number of UTs is still higher than the number of orthogonal pilots.

4 ORGANIZATION

The organization of the thesis is as follows:

- Chapter 2 reviews the massive MIMO concept, including the advantages and challenges facing this technology.
- Chapter 3 was dedicated to massive MIMO channel measurements and processing. In this chapter, uplink and downlink processing will be considered including linear and non-linear processing.
- Chapter 4 introduce the interference challenge in 5G networks and focus on uplink pilot contamination in massive MIMO mobile technology. It also summarizes some literature techniques to mitigate uplink pilot contamination.
- Chapter 5 proposes our first novel technique to mitigate uplink pilot contamination in massive MIMO. It introduces the CSI map that will be used to predict channel rather than estimating it. The numerical results of applying this technique were also presented in this chapter.
- Chapter 6 proposes our second novel technique to mitigate uplink pilot contamination. In this chapter, we introduce the pilot shifting in sparse pilot frames. This method describes how to classify users based on their mobility profile and skip sending pilots for low mobility users. At the end of this chapter, numerical results were introduced to prove the ability of the proposed technique to overcome conventional massive MIMO.
- Chapter 7 concludes this thesis and introduce some future research direction to extend this work.

5 CONFERENCES AND PUBLICATIONS

5.1 Refereed Papers

1- Title: Forecasting and Skipping To Reduce Transmission Energy In WSN
Authors: Ahmad Abboud, Abdel-Karim Yazbek, Jean-Pierre Cances, Vahid Meghdadi
Journal: International Journal of Research in Engineering and Science
Domain: Electronics Engineering
Published: June 2016
ISSN: 2320-9364
Description:
The fundamental concept behind this research is the is the ability to use previously stored pattern at the base station to estimate the measured data from the sensor before requesting which limit the content of the transmitted to include only the error variance.

2- **Title:** Indoor Massive MIMO: Uplink Pilot Mitigation Using Channel State Information Map
Authors: Ahmad Abboud, Jean-Pierre Cances, Ali H. Jaber, Vahid Meghdadi
Journal: Journal of Algorithms and Computational Technology
Domain: Networking and Internet Architecture
Year: 2016
Pre-Print: arXiv:1605.00082
Description:
This research proposes a novel method to mitigate uplink pilot contamination effect in an indoor Massive MIMO system by exploitation of stored channel state information CSI to precode new vectors based on the prediction.
[This work was introduced in "19th IEEE International Conference on Computational Science and Engineering (CSE 2016)- Paris, France"]

5.2 Submitted Papers

1- Title: Channel Coherence Classification with Pilot Shifting
Authors: Ahmad Abboud, Oussama Habachi, Jean-Pierre Cances, Vahid Meghdadi, Ali Jaber

Description:
In this work, we classify users based on their coherence interval length where channel training is done once each coherence interval for each group. Then we make use of the pilot sparsity in long coherence intervals to shift similar pilot sequences into an empty training slot.
[This work was accepted in 3nd International Symposium on Ubiquitous Networking (UNet'17) as Invited Paper].

2- Title: CSI Map for Indoor Massive MIMO
Description: An improved version of the Indoor massive MIMO paper that consider a garbage collection algorithm to decrease the size of the CSI map and upgrade the algorithm used to learn new CSI.
[This paper was accepted in "SAI Computing Conference 2017" and will be available in IEEE Explorer soon]

5.3 Papers in Preparation or Revision

1- Title: Spatio-temporal User Specific Mobility Profile in Smart Cities Wireless Networks
Authors: Ahmad Abboud, Oussama Habachi, Jean-Pierre Cances, Vahid Meghdadi, Ali Jaber
Description: This paper exploits the user mobility profile in wireless networks to improve decision making on various services in smart cities. As a methodology, Naïve Net is used to represent the conditional transition probability of specific user connected between sites in the network where the tessellation weight of the sites and the particular period of transition was taken as features. Then a decision network will represent the optimal utility to take action based on the transition probability of the Naïve net. The studied Model of User Mobility takes into consideration three dimensions (User specific, period specific and site specific) which make it flexible and powerful to query out critical what-if scenarios to make an optimal decision considering city resources management.

2- Title: Smart Massive MIMO: An Infrastructure Toward 5th Generation Smart Cities Network
Authors: Ahmad Abboud, Jean-Pierre Cances, Vahid Meghdadi, Ali Jaber
Journal: arXiv preprint arXiv:1606.02107
Description: On the Optimizing of Wireless Networks and toward improving the future 5G Mobile Network Infrastructure, we propose a novel infrastructure that can serve for the next Smart City Network. Our proposed Infrastructure takes into consideration most future demands and challenges, includes Capacity, Reliability, Scalability, and Flexibility. To deal with these issues, we suggest a wireless network infrastructure that is based on latest technologies of Massive MIMO systems.

3- Title: Concatenated Channel Estimation for Massive MIMO systems
Description: This work introduces a novel idea that theoretically enables the implementation of an unlimited number of user terminal within each cell without encountering pilot contamination, even with a limited number of orthogonal pilot sequences.
This technique is done by estimating the CSI in an initial frame and correct this CSI at each training iteration using a short-reused pilot. The method considered useful only after exploiting the coherence block overlapping. In other words, the correction phase is done within the same coherence interval, which elongates the age of the CSI at each iteration.

6 REFERENCES

[1] "METIS 2020," 2013. [Online]. Available: https://www.metis2020.com/.
[2] "5G-PPP," 2016. [Online]. Available: https://5g-ppp.eu/.
[3] "HORIZON 2020," 2016. [Online]. Available: https://ec.europa.eu/programmes/horizon2020/.
[4] "IMT-2020," 2016. [Online]. Available: http://www.imt-2020.cn/en/.
[5] "Intel Labs," 2013. [Online]. Available: http://blogs.intel.com/intellabs/2013/07/15/next-generation-wireless-communication-5g-transforming-the-wireless-user-experience/.
[6] H. Wang, S. Chen, H. Xu, M. Ai, and Y. Shi, "SoftNet: A software defined decentralized mobile network architecture toward 5G," *IEEE Netw.*, vol. 29, no. 2, pp. 16–22, 2015.
[7] M. Peng, C. Wang, V. Lau, and H. V. Poor, "Fronthaul-constrained cloud radio access networks: Insights and challenges," *IEEE Wirel. Commun.*, vol. 22, no. 2, pp. 152–160, 2015.
[8] A. W. Dawson, M. K. Marina, and F. J. Garcia, "On the benefits of RAN virtualisation in C-RAN based mobile networks," *Proc. - 2014 3rd Eur. Work. Software-Defined Networks, EWSDN 2014*, pp. 103–108, 2014.
[9] A. Gudipati, D. Perry, L. E. Li, and S. Katti, "SoftRAN: Software defined radio access network," in *Proceedings of the second ACM SIGCOMM workshop on Hot topics in software defined networking*, 2013, pp. 25–30.
[10] T. L. Marzetta, "Noncooperative cellular wireless with unlimited numbers of base station antennas," *IEEE Trans. Wirel. Commun.*, vol. 9, no. 11, pp. 3590–3600, 2010.
[11] F. Rusek *et al.*, "Scaling up MIMO : Opportunities and challenges with very large arrays," *IEEE*

Signal Process. Mag., vol. 30, no. 1, pp. 40–60, 2013.
[12] E. Björnson, J. Hoydis, and M. Kountouris, "Massive MIMO Systems With Non-Ideal Hardware : Energy Efficiency , Estimation , and Capacity Limits," vol. 60, no. 11, pp. 7112–7139, 2014.
[13] L. You, X. Gao, X.-G. Xia, N. Ma, and Y. Peng, "Massive MIMO Transmission with Pilot Reuse in Single Cell," *2014 IEEE Int. Conf. Commun.*, no. JUNE 2014, pp. 4783–4788, 2014.
[14] E. Björnson, E. G. Larsson, and M. Debbah, "Massive MIMO for Maximal Spectral Efficiency: How Many Users and Pilots Should Be Allocated?," in *IEEE Transactions on Wireless Communications*, 2016, vol. 15, no. 2, pp. 1293–1308.
[15] H. Q. Ngo, E. G. Larsson, and T. L. Marzetta, "Energy and spectral efficiency of very large multiuser MIMO systems," *IEEE Trans. Commun.*, vol. 61, no. 4, pp. 1436–1449, 2013.
[16] A. Osseiran *et al.*, "Scenarios for 5G mobile and wireless communications: The vision of the METIS project," *IEEE Commun. Mag.*, vol. 52, no. 5, pp. 26–35, 2014.
[17] J. Vieira *et al.*, "A flexible 100-antenna testbed for Massive MIMO," in *2014 IEEE Globecom Workshops, GC Wkshps 2014*, 2014, pp. 287–293.
[18] X. Gao, O. Edfors, F. Rusek, and F. Tufvesson, "Massive MIMO performance evaluation based on measured propagation data," pp. 1–12, 2015.
[19] T. L. Marzetta, "Massive MIMO: An Introduction," *Bell Labs Tech. J.*, vol. 20, pp. 11–22, 2015.
[20] L. Su and C. Yang, "Fractional frequency reuse aided pilot decontamination for massive MIMO systems," in *IEEE Vehicular Technology Conference*, 2015, vol. 2015.
[21] M. M. System, O. Elijah, S. Member, C. Y. Leow, and T. A. Rahman, "A Comprehensive Survey of Pilot Contamination in Massive MIMO—5G System," *IEEE Commun. Surv. Tutorials*, vol. 18, no. c, pp. 905–923, 2015.
[22] E. Björnson, J. Hoydis, M. Kountouris, and M. Debbah, "Hardware impairments in large-scale MISO systems: Energy efficiency, estimation, and capacity limits," in *2013 18th International Conference on Digital Signal Processing, DSP 2013*, 2013.
[23] J. Jose, A. Ashikhmin, T. L. Marzetta, and S. Vishwanath, "Pilot contamination and precoding in multi-cell TDD systems," *IEEE Trans. Wirel. Commun.*, vol. 10, no. 8, pp. 2640–2651, 2011.

Chapter 2: Massive MIMO Overview

> Life is like riding a bicycle. *To* keep *your balance, you must* keep *moving.* ~ *Albert Einstein*

This chapter introduces the intention behind increasing the number of antennas at the base station as well as the evolution from MIMO to Massive MIMO. In details, it investigates the Massive MIMO system, its benefits, and its challenges. Furthermore, we investigate the uplink pilot contamination problem and the used method in the literature to mitigate uplink pilot contamination will be discussed.

1 From MIMO to Massive MIMO

Generally, MIMO systems are divided into two categories: single-user MIMO (SU-MIMO) and multi-user MIMO (MU-MIMO). In SU-MIMO, the transmitter and receiver are outfitted with more than one antennas. The performance is enhanced in terms of coverage, link reliability, and sum rate can be executed via strategies such as beamforming, diversity-oriented space-time coding, and spatial multiplexing of numerous data streams. These methods cannot be thoroughly used at the same time, therefore we commonly add a tradeoff between them. For example, adaptive switching between spatial diversity and multiplexing schemes is adopted in LTE [1].

The situation with MU-MIMO is radically different. The wireless channel is now spatially shared by way of different UTs, and the users transmit and obtain barring joint encoding and detection amongst them. By exploiting differences in spatial signatures at the BS antenna array caused by way of spatially dispersed users, the BS communicates concurrently to the users. Thus, overall performance beneficial properties regarding sum rates of all users can be impressive. An important venture is, however, the interference among the co-channel users [2]. Signal processing in MU-MIMO regularly targets at suppressing inter-user interference, thus spatial channel knowledge turns into another indispensable in contrast to SU-MIMO.

Massive MIMO is a new notion that makes use of hundreds of antennas at the BS to serve tens of UTs simultaneously in the same time-frequency resource. Massive MIMO mostly approves us to reap all the benefits of conventional MIMO on a large scale. In Massive MIMO systems, a huge number of BS antennas enhance spectral efficiency and radiated energy efficiency as compared to the present wireless technologies. The BS antennas make use of the idea of beamforming using transmitting solely in the preferred directions so that the radiated energy is centered in a small area and interference is minimized [3].

Massive MIMO systems enable an extend in theoretical sum-rate and a reduction in uplink (UL) and downlink (DL) energy consumption. The uplink power should be scaled down by way of relatively increasing the number of BS antennas [4]. All these motivations make Massive MIMO a conceivable solution for future broadband technologies. As the range of antennas at the BS increases, linear receivers such as (MRC) and (MMSE) turn out to be optimal. As a result, the acquisition of CSI turns into fundamental for the operation of Massive MIMO systems [5], [6]. Note that the acquisition of CSI is achieved via pilot sequences. Since the pilots require orthogonality between the antennas and all users operate in the same time-frequency resource, such structures have an inherent quandary due to pilot contamination. It is shown that the principal limiting element in growing the number of BS antennas is the pilot contamination [6].

2 MASSIVE MIMO SYSTEM

2.1 System Characteristics

Massive MIMO is a form of MU-MIMO structures where the variety of BS antennas and the numbers of UTs are huge. In Massive MIMO, thousands of BS antennas concurrently serve tens or hundreds of users in the same frequency resources. Some essential points of Massive MIMO are:

2.1.1 Scalability

The BS learns the channels via uplink training, with TDD operation. The time required for channel estimation is impartial of the number of BS antennas. Therefore, the broad range of BS antennas can be made as large as favored with no extension in the channel estimation overhead. Furthermore, the signal processing at every UT is essential and does not depend on other UTs existence, de-multiplexing signal processing is carried out at the UTs. Adding or losing some UTs from service does no longer have an effect on other UT activities.

2.1.1.1 Massive MIMO prefers TDD Scheme

Using FDD, the channel estimation overhead relies upon on the number of BS antennas M. By contrast, using TDD, the channel estimation overhead is unbiased of M. In Massive MIMO, M is large, and hence, TDD operation is preferable. For instance, suppose that the coherence interval is $T = 200$ symbols (corresponding to a coherence time of 1 *ms* and a coherence bandwidth of 200 *kHz*). Then, in FDD systems, the quantity of BS antennas and the amount of UTs are limited through $M + K < 200$, while in TDD systems, the constraint on M and K is $2K < 200$. From *fig 2.2.1,* we can see that the FDD place is tons smaller than the TDD region. With TDD, adding more antennas does now not affect the sources needed for the channel acquisition.

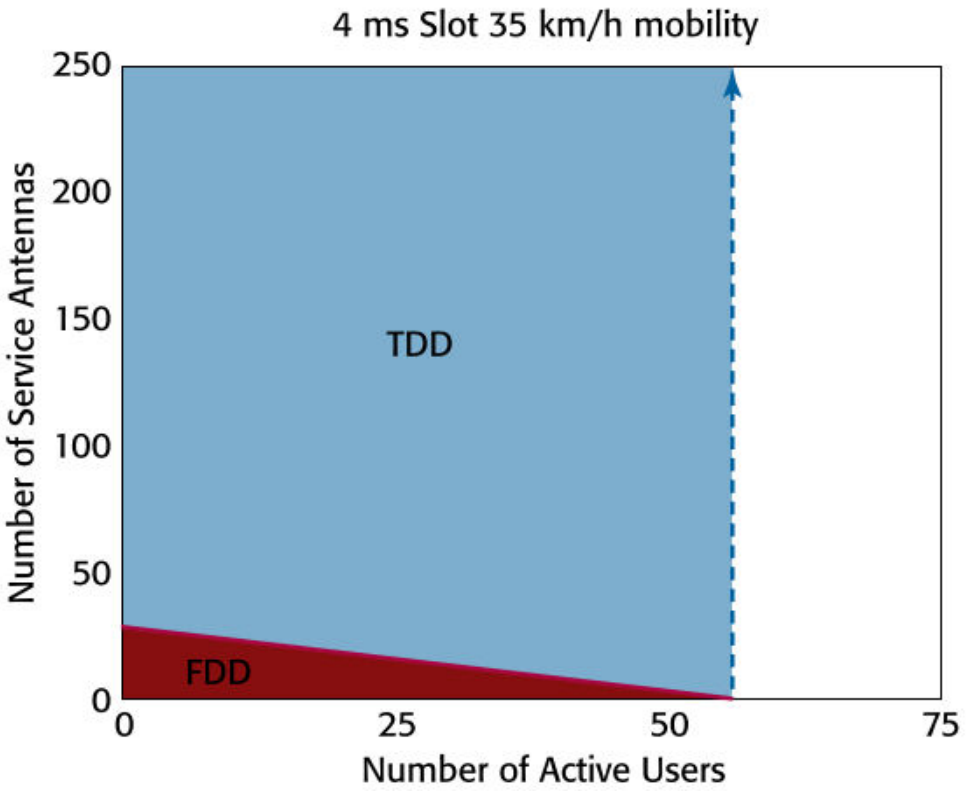

Figure 2.2.1 TDD enables Massive MIMO scalability for mobile users, while FDD is strictly limited to small systems [7].

Figure 2.2.1 indicates the overwhelming gain of TDD over FDD for UTs. The vertical axis is the number of BS antennas, and the horizontal axis is the quantity of UTs. The light-to-medium blue location indicates the gadget dimensions accessible with TDD versus the much smaller red area for FDD. The slot duration is four *ms*, which allows 35 km/h mobility at 1.9 GHz. To reduce pilot contamination, the orthogonal pilot sequences selected seven times longer than necessary.

2.1.2 Antenna Array Should Not be Physically Large

For instance, think about a cylindrical array of 128 antennas, comprising four circles of 16 dual-polarized antenna elements. According to [8], at 2.6 GHz, the distance between adjecent antennas is about 6 cm, which is 1/2 a wavelength, and hence, this array occupies a physical dimension of 28cm × 29cm solely.

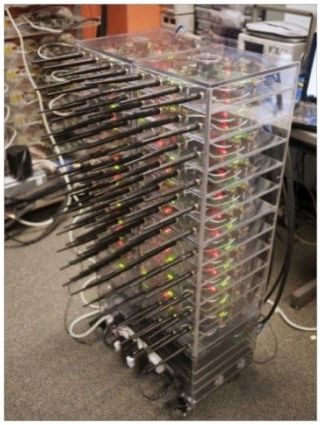

Figure 2.2.2 The Rice University Argos

2.1.3 Massive MIMO Offers Favorable Propagation

Favorable propagation, described as mutual orthogonality amongst the vector-valued channels to the terminals, is one of the key factors of the radio channel that is utilized in Massive MIMO [9]. However, there has been little work on this matter in detail. As the used number of BS antennas goes huge, Massive MIMO tends to have favorable propagation. This reality holds due to the regulation of large numbers.

2.2 Massive MIMO Processing

Processing in Massive MIMO takes place in TDD scheme within three phases, Channel Estimation (includes upload pilots), uplink data receiving and downlink data (see *Fig* 2.2.3).

The three stages are done within 2-time divisions that lag for not more than the coherence interval length.

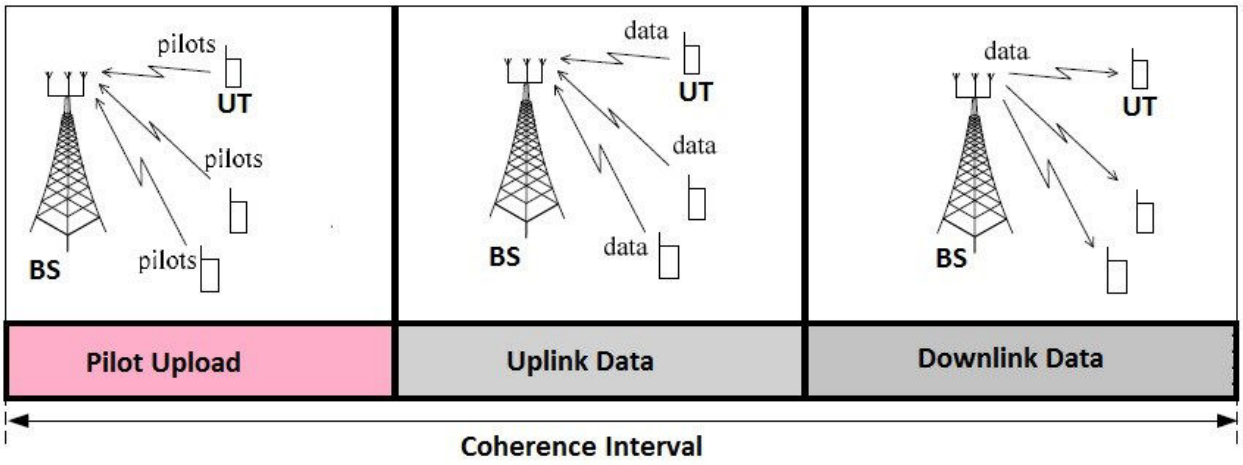

Figure 2.2.3 Three stages within a TDD fram, first from the right uplink pilot then uplink data and at last downlink data

2.2.1 Channel Estimation

At the reverse link, the BS needs the channel state information to become aware of the signals transmitted from the UTs in the uplink, and to precode the signals in the downlink. This channel information is acquired via the uplink training. Each user is assigned an orthogonal pilot sequence and sends his pilot sequence to the BS. Due to the pilot sequences orthogonality, the BS is aware of the pilots transmitted from all user terminals, and then estimates the channels based on the received pilot signals. Also, each user may need partial information of CSI to discover the signals transmitted from the BS coherently. Downlink training can typically obtain these statistics. Since the BS makes use of linear precoding strategies to beamform the indicators to the users, the user desires solely on the active channel reap to notice its favored signals. Hence, the BS can spend a brief time to beamform pilots in the downlink for channel acquisition at the UT.

2.2.2 Uplink Data

After channel estimation, the BS can receive the uploaded data for each UT using the estimated version of the CSI. This estimation is done at the same reverse link of the coherence interval. The uploaded data from each UT is assumed to share the same frequency-time domain, where the BS uses the spatial multiplexing signature acquired from the CSI to separate the received data streams. Linear receivers include (MRC, MMSE, ZF) can efficiently receive the uploaded data stream without the need for complex non-linear receivers.

2.2.3 Downlink Data

The third phase of the TDD frame is the downlink data phase. The forward link is typically considered shorter than the reverse link, where the downlink data only occupy it. Within the same coherence interval, the BS uses the estimated CSI to precode the downlink data stream. Many techniques can do precoding in Massive MIMO but due to the law of large number Massive MIMO systems can use linear precoders (as MRT, MMSE, and ZF) to perform the task.

3 MASSIVE MIMO TYPES

3.1 Single-User MIMO

Owing to the physical hassle of terminals, the number of antennas at the terminal is typically a lot much less than *M*. Therefore, SU-MIMO structures fall into case 1 when a massive amount of antennas are geared up at the base station, and hence reap the advantages of channel orthogonalization if favorable channel propagation circumstance holds. However, the SU-MIMO channels can be extraordinarily correlated due to the fact of the short distance of antennas at the terminal side and viable line-of-sight

environment. From the energy efficiency point of view, the use of a massive antenna array to serve a single or a small quantity of UTs may additionally not be wise. Hence, in this case, the achieve of massive MIMO for SU-MIMO can also be limited.

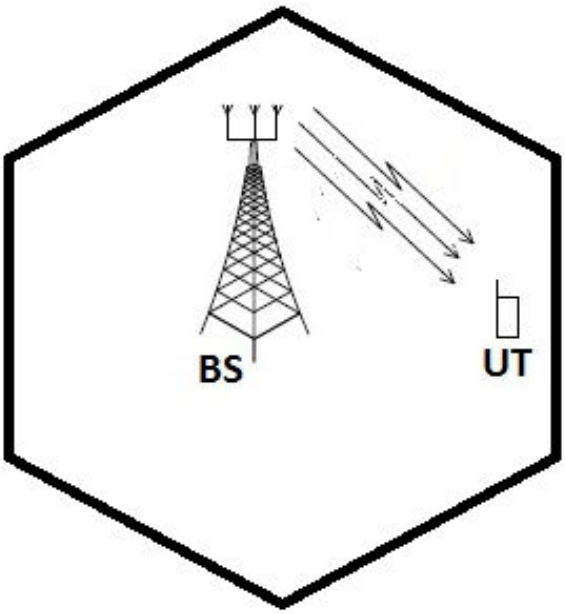

Figure 2.3.1 Single-User Massive MIMO

$$\boldsymbol{y} = \sqrt{Pu}\boldsymbol{h}s + \boldsymbol{w} \qquad (2.3.1)$$

Denote by Pu, the uplink SNR, by $\boldsymbol{h}$, the channel response vector, by s, the symbole vector and by $\boldsymbol{w}$ the AWGN noise vector.

3.2 Multi-User Massive MIMO

When more than one terminals are allowed to access identical time–frequency resource, MU-MIMO offers greater system efficiency in contrast to SU-MIMO. In this section, we take into consideration a single-cell MU-MIMO systems, where the BS is serving *K* UTs with every terminal being equipped with one antenna. The received signal at the BS of an uplink MU-MIMO system is:

$$\boldsymbol{y} = \sum_{\boldsymbol{k=1}}^{\boldsymbol{K}} \sqrt{Pu}\boldsymbol{h_k}s_k + \boldsymbol{w} \qquad (2.3.2)$$

$$\boldsymbol{y} = \sqrt{Pu}\boldsymbol{H}\boldsymbol{s} + \boldsymbol{w} \qquad (2.3.3)$$

$\boldsymbol{y}$ is $M \times 1$ received signal matrix, $\boldsymbol{h_k} \in \boldsymbol{H}$. *e.g.* $\boldsymbol{H} = [\boldsymbol{h_1} \dots \boldsymbol{h_k} \dots \boldsymbol{h_K}]$ represents the channel vector between the BS antennas and the k^{th} UT, $s_k \in \boldsymbol{s}$. *e.g.* $\boldsymbol{s}^T = [s_1 \dots s_k \dots s_K]$ represents the symbol transmitted by k^{th} UT and $\boldsymbol{w}$ represents the Additive White Gaussian Noise (AWGN).

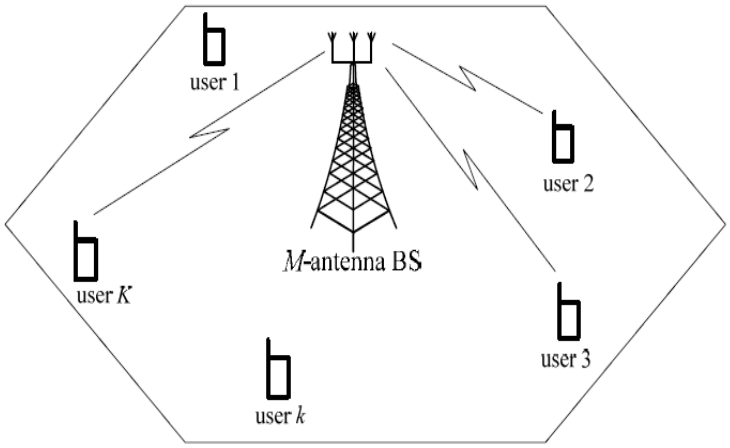

Figure 2.3.2 Multi-user Massive MIMO System. M-antennas BS serves the K single antenna UT.

When $K \geq 2$, the obtained signal of every UT interferes with those of the other terminals, and hence we should anticipate that the mutual information of every terminal for MU-MIMO is smaller than that for SU-MIMO given the same transmitted power at each terminal. However, when $M \gg K$, the channel orthogonalizing kicks in, such that the obtained signal of every terminal is nearly orthogonal, that is, interference-free in the favored sign house below favourable channel propagation condition. Also, given that the terminals are autonomous, the favorable channel propagation condition is usually comfortable due to the fact the antennas at the terminals are almost uncorrelated and uncoupled [8]. It suggests that the Massive MIMO is the desire of the MU-MIMO setup.

3.3 Multi-User Massive MIMO with Multi-Cell scenario

In this section, we contemplate the restriction of non-cooperative cellular multiuser MIMO systems as M grows without limit. For a single cell, as properly as for multi-cell MIMO, the outcome impact of letting M increase without limits is that thermal noise and small-scale Rayleigh fading vanishes. However, as we will discuss, with more than one cell the interference from distinct cells due to pilot contamination will persist. The idea of pilot pollution is novel in a cellular MU-MIMO context and is illustrated in Fig 2.3.3. However, used to be a problem in the context of CDMA, generally with the title "pilot contamination". The channel estimate computed with the aid of the base station in cell l being contaminated from the pilot transmission of cell j. The BS in cell l will beamform its signal partially alongside the channel to the terminals in the adjacent cell. Due to the beamforming, the interference to cell j does not vanish asymptotically as $M \to \infty$. We reflect on consideration on a cellular multi user MIMO-OFDM system with hexagonal cells and NFFT subcarriers. All cells serve K independent terminals and have M antennas at the BS. The BSs are assumed non-cooperative. The $M \times K$ composite channel matrix between the K UTs in cell l and the BS in cell j is denoted by $\boldsymbol{H_{jl}}$. Relying on reciprocity, the down link channel matrix between the BS in cell j and the terminals in cell l is presented by $\boldsymbol{H_{jl}^{T}}$. The received signal at the *j-th* BS will be as follows:

$$\boldsymbol{y_j} = \sum_{l=1}^{L} \sum_{\boldsymbol{k=1}}^{\boldsymbol{K}} \sqrt{Pu}\boldsymbol{h_{jlk}} s_{lk} + \boldsymbol{w} \qquad (2.3.4)$$

$$\boldsymbol{y_j} = \sum_{l=1}^{L} \sqrt{Pu}\boldsymbol{H_{jl}} \boldsymbol{s_l} + \boldsymbol{w} \qquad (2.3.5)$$

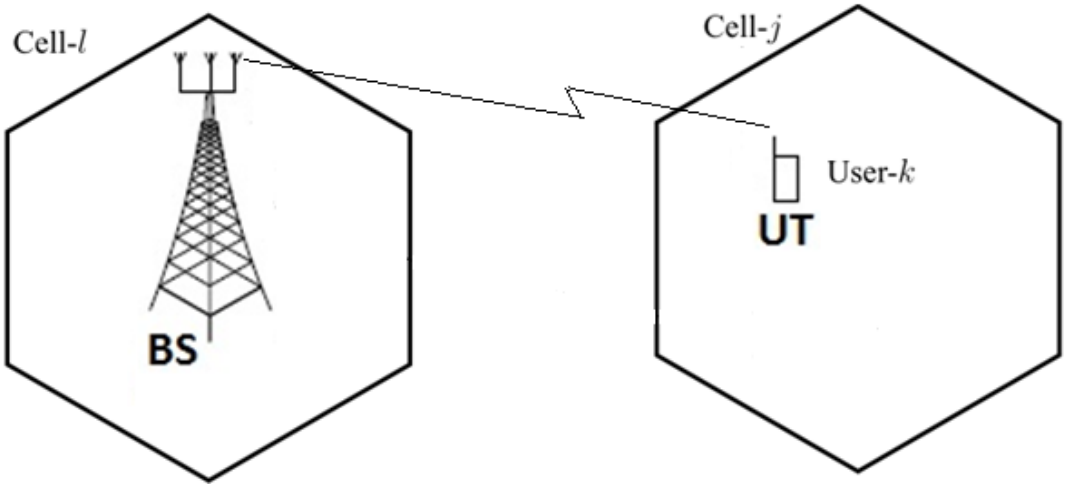

Figure 2.3.3 The base station in l-th cell and the k-th user in j-th cell

3.4 Distributed Massive MIMO

Distributed Massive MIMO can be handled as a distinct case of MU-MIMO to additionally supply greater system capacity using dispersed deployed antennas to transmit and receive signals. One scheme of disbursed Massive MIMO is to allow cooperation between the BS's in distinctive cells which reduces the inter-cell interference. However, synchronization turns into a quintessential problem even for dispensed antennas at the same BS. In some cases, the massive quantity of antennas at the base station can additionally be positioned in unique places [11] (e.g., on tops of buildings). In this case, synchronization is one issue, and the inexpensive RF front end might also introduce greater problems.

4 ON THE MASSIVE MIMO EFFECT

This section will discuss the effect of increasing the dimension of antennas on the overall system performance. To focus on the effect of increasing the number of antennas at the BS and within the UTs we will consider a single cell Massive MIMO scenario where K UTs with one antenna each, served with one BS holding M antennas. Two scenarios can be discussed, first considering increasing M without bounds where $M >> K$, the second scenario consider both M and K increased without bounds where $M \approx K$.

One of the most interesting performance metric to be considered in any communication system is the transmitted mutual information which is the measure of bit per channel use. Using the model in (2.3.3) and considering a Gaussian distribution of the symbols, the instantaneous mutual information, which is also referred as system capacity [12], is expressed as follows:

$$C = \log_2 \det(\boldsymbol{I}_K + \frac{Pu}{K}\boldsymbol{H}^H\boldsymbol{H}) = \log_2 \det(\boldsymbol{I}_M + \frac{Pu}{K}\boldsymbol{H}\boldsymbol{H}^H) \quad (2.4.1)$$

Since $\boldsymbol{H}$ is a random matrix [13], we can calculate the ergodic capacity $\mathbb{E}\{C\}$ as follows:

$$\mathbb{E}\{C\} = \mathrm{M}\,\mathbb{E}\{\log_2(1 + Pu\,\boldsymbol{\lambda})\} \quad (2.4.2)$$

where $\boldsymbol{\lambda}$ denotes the eigenvalues of the normalized Wishart matrix $\frac{\boldsymbol{H}\boldsymbol{H}^H}{\boldsymbol{K}}$ [14].

Considering the first scenario $M >> K$, where $\boldsymbol{H}$ is Gaussian i.i.d. random matrix, by the law of large numbers, $\frac{\boldsymbol{H}\boldsymbol{H}^H}{K} = \frac{\boldsymbol{H}\boldsymbol{H}^H}{M}(\frac{M}{K})$ tends to $(\frac{M}{K})\boldsymbol{I}$. This result means that, when M tends to ∞, the eigenvalues in (2.4.2) tends to $\left(\frac{M}{K}\right)$. For $M >> K$, the expectation of mutual information can be written as:

$$\mathbb{E}\{C\} \sim M \log_2(1 + Pu\frac{M}{K}) \quad (2.4.2)$$

Considering the second scenario, where *M* and *K* both increase without bounds, with a ratio, $F = \frac{M}{K}$, the eigenvalues will converge statistically according to Marchenko-Pastur law which is given in the following theorem:

Theorem 2.3.1*: Consider a matrix* $\boldsymbol{H} \in \mathbb{C}^{M\times K}$ *with i.i.d. entries* $\left(\frac{1}{\sqrt{K}}\boldsymbol{H}_{M,ij}\right)$*, such that* $H_{M,11}$ *has zero mean and unit variance. As* $K, M \to \infty$ *with* $\frac{M}{K} \to c \in (0,\infty)$*, the eigenvalues distribution* $\boldsymbol{R}_K = \boldsymbol{H}\boldsymbol{H}^{\boldsymbol{H}}$ *converges weakly and almost surely to a nonrandom distribution function* P_c *with a density function* p_c *that can be presented as follow:*

$$p_c(x) = (1 - c^{-1})^+\delta(x) + \frac{1}{2\pi cx}\sqrt{(x-a)^+(b-x)^+}$$

where $a = (1-\sqrt{c})^2$*,* $b = (1+\sqrt{c})^2$ *and* $\delta(x) = 1_{\{0\}}(x)$ *represents the Dirac function.*

The proof of *Theorem 2.3.1* can be found in [15].

Referring to the graphical illustration of the eigenvalues distribution in the figure below, one can infer the deterministic state of the eigenvalues as the number of BS antennas relative to the number of users, increases without limits (here referred as c).

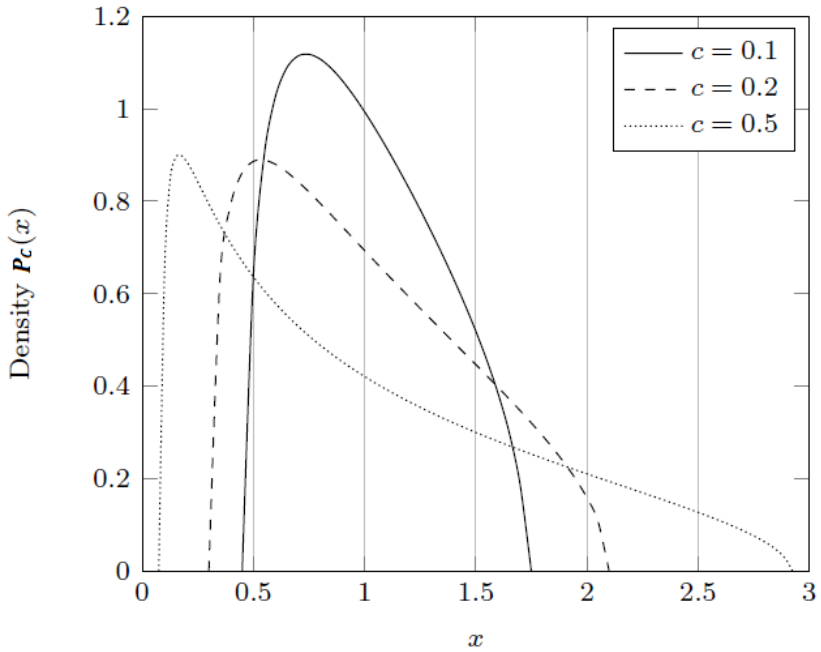

Figure 2.4.1 Probability density function (pdf) of the eigenvalues of x for different ratios of c

5 Massive MIMO Benefits

Massive MIMO technology exploits phase-coherent, where computationally it is a simple processing of signals from all the antennas at the base station. Some unique advantages of a large MU-MIMO system are mentioned below.

5.1 Increasing Capacity

The increase in capacity results from the aggressive spatial multiplexing used in massive MIMO. The quintessential precept that makes the dramatic increase in energy efficiency viable is that with a large number of antennas, power can be centered with intense sharpness into small areas in space.

The underlying physics is the coherent superposition of wavefronts. By accurately shaping the signals sent out through the antennas, the BS can make sure that all wavefronts jointly emitted using all antennas add up constructively at the places of the dedicated terminals, and destructively almost everywhere else. Interference between terminals can be suppressed even similarly with the aid of linear precoder, e.g., MMSE, ZF. However, this may come at the cost of more transmitted power.

By numerical analysis, the essential exchange between the energy efficiency regarding the total number of transmitted bits per Joule per terminal receiving provider of energy spent, and spectral efficiency relating to a total number of transmitted bits per Hz. The figure below (Figure 2.5.2) illustrates the relationship for the uplink, from the terminals to the base station.
Figure 2.5.2, indicates the exchange off for two cases: in purple, a reference system with one single antenna serving a single UT. In green, a system with one hundred antennas serving a single UT using traditional beamforming and at last, a massive MIMO system with a hundred antennas simultaneously serving forty UT's (blue, using ZF and red, using MRC).

Using of MRC receivers in contrast with ZF is not only its simpler complexity by using multiplication of the obtained signals by the conjugate channel responses, but also that it can be carried out in a distributed fashion, independently of every antenna unit. While ZF additionally works well for a traditional or moderate dimension MIMO system, MRC typically does not. The key factor behid the performance of MRC in massive MIMO is that the channel responses associated with distinct terminals tend to be nearly orthogonal when the number of base station antennas is large. The prediction in (Figure 2.5.2) relies primarily on an information theoretical analysis that considers intra-cell interference, as well as the energy cost and bandwidth of using pilots to estimate CSI in a high-mobility scenarios.

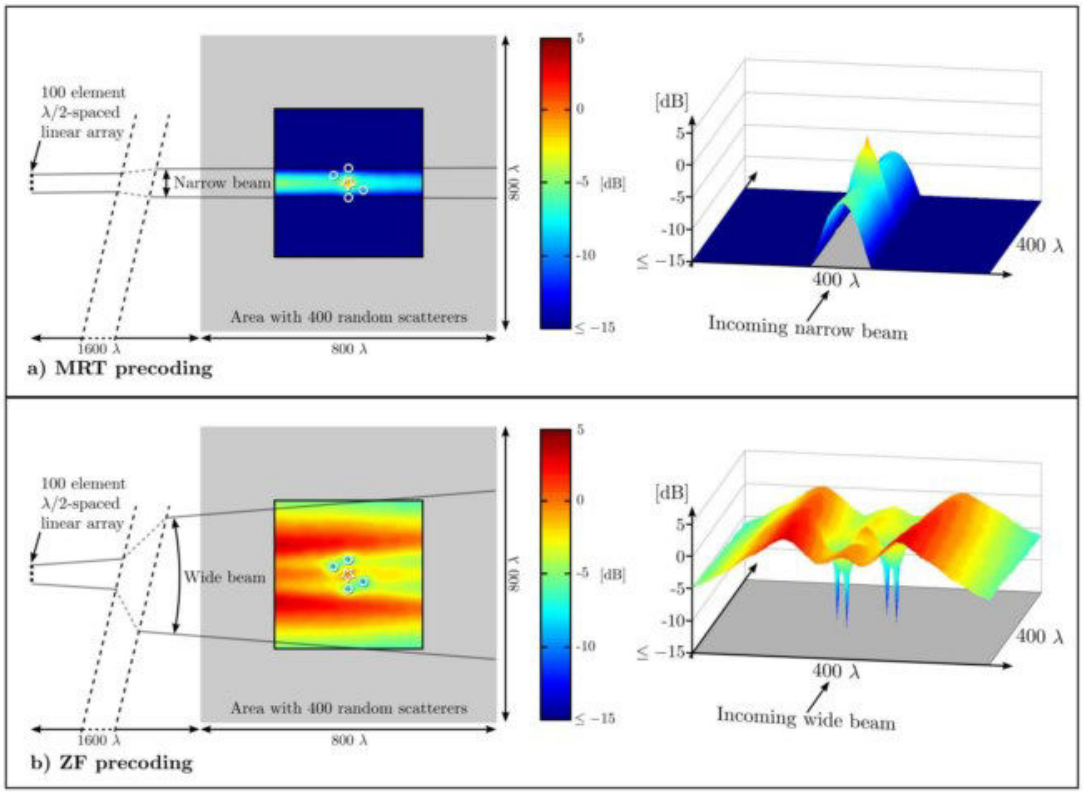

Figure 2.5.1 Linear precoding within a scattering environment of size 800λ×800λ [3].

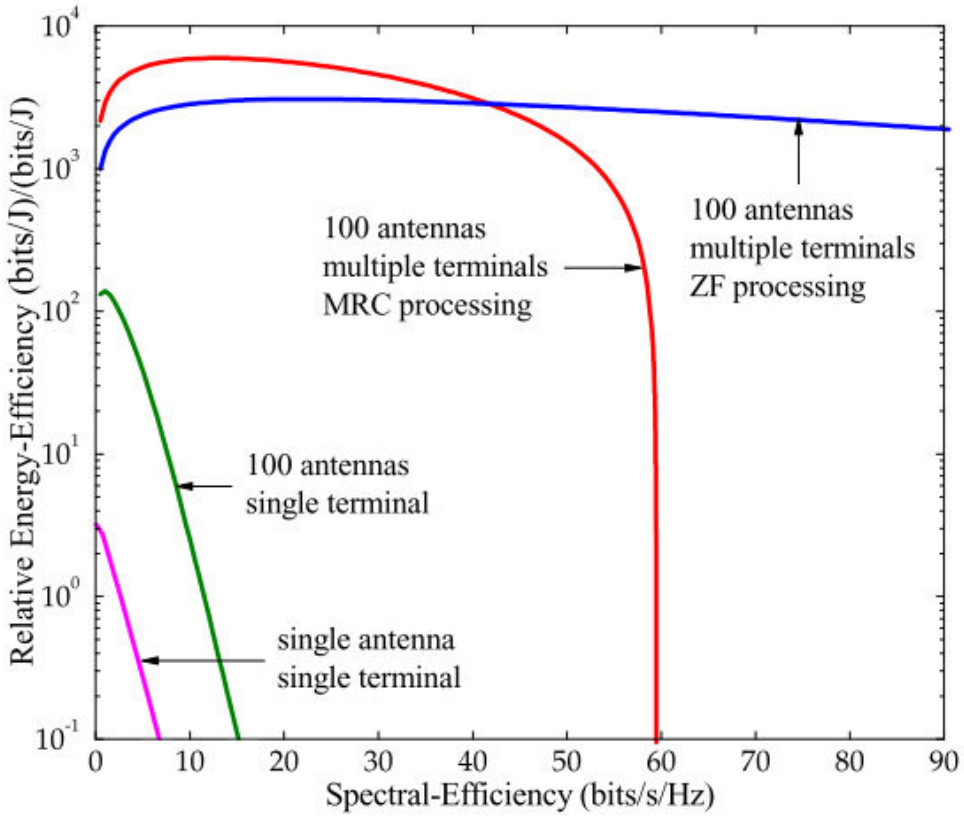

Figure 2.5.2 Spectral efficiency Vs Energy efficiency [4]

The purpose that the average spectral efficiency ten times higher than in traditional MIMO is that many terminals are served simultaneously, in the same time-frequency resource. When running in the 1 bit/dimension/UT regime, there is additionally some evidence that inter-symbol interference can be handled as extra thermal noise, therefore offering a way of disposing OFDM as an ability to combat inter-symbol interference [16].

To recognize the scale of the potential beneficial properties of Massive MIMO, think about an array consisting of 6400 omnidirectional antennas. A whole structure aspect of 6400 × (λ) ≈ 40 m^2, transmitting with a complete power of 120 Watts (every antenna radiating about 20 mW) over a 20 MHz bandwidth in the band (1900 MHz). The array serves 1000 fixed terminals randomly allocated in a disk of radius 6 km centered on the array, every terminal having an 8dB gain antenna. The peak of the antenna array is 30m, and the height of the terminals is 5m. Using the Hata-COST231 model we locate that the route loss is 127 dB at 1 km distance and the range-decay exponent is 3.52. With log-normal shadow fading with 8 dB standard deviation and 9 dB noise at the receiver, one-quarter of the TDD frame is spent on the transmission of uplink pilots. Furthermore, it is assumed that the channel is significantly steady over periods of 164 ms to estimate the channel gains with enough accuracy. The downlink data is transmitted through MRT beamforming mixed with strength control, where the 5% of the users that have the worst channels are omitted from service. Numerical averaging over random terminal places over the shadow fading indicates that 95% of the terminals will obtain a throughput of 21.2 Mb/s/UT. According to [3], the array in this example will provide the 1000 terminals a full downlink throughput of 20 Gb/s, ensuring in a sum spectral efficiency of 1000 bits/s/Hz. This given, would be sufficient to grant 20 Mbit/s broadband service to each of a 1000 UTs. The max-min power control provides similar service concurrently to 950 terminals. Other types of power control associated with time-division multiplexing ought to accommodate various traffic needs of a larger set of terminals. The MRC receiver and its counterpart MRT precoding are additionally regarded as matched filtering (MF) in the literature.

5.2 Increase Robustness Against Man-Made Interference and International Jamming

A serious cyber- security risk is the intentional jamming of private wireless systems (see Fig 2.5.3), that seems to be little regard to the public. Simple jammers can be sold off the Internet for a few $100, and tools that used to be military-grade can be put collectively using off-the-shelf software radio-based platforms for a few $1000. Numerous latest incidents, specifically in public security applications, illustrate the magnitude of the problem. During the EU summit in Gothenburg, Sweden, in 2001, demonstrators used a jammer positioned in a close by the apartment and while major phases of the riots, the chief commander could not attain any of the engaged seven-hundred police officers [17].Due to the shortage of bandwidth, spreading data over frequency is no longer possible, so the only way of enhancing the performance of wireless communications is to use a couple of antennas. Massive MIMO provides many extra DoF that can be used to cancel signals from intentional jammers. If Massive MIMO is implemented through the usage of uplink pilots for channel estimation, then smart jammers should make hazardous interference with modest transmission power. However, further smart implementations by joint channel estimation and decoding need to be capable to considerably lower that problem.

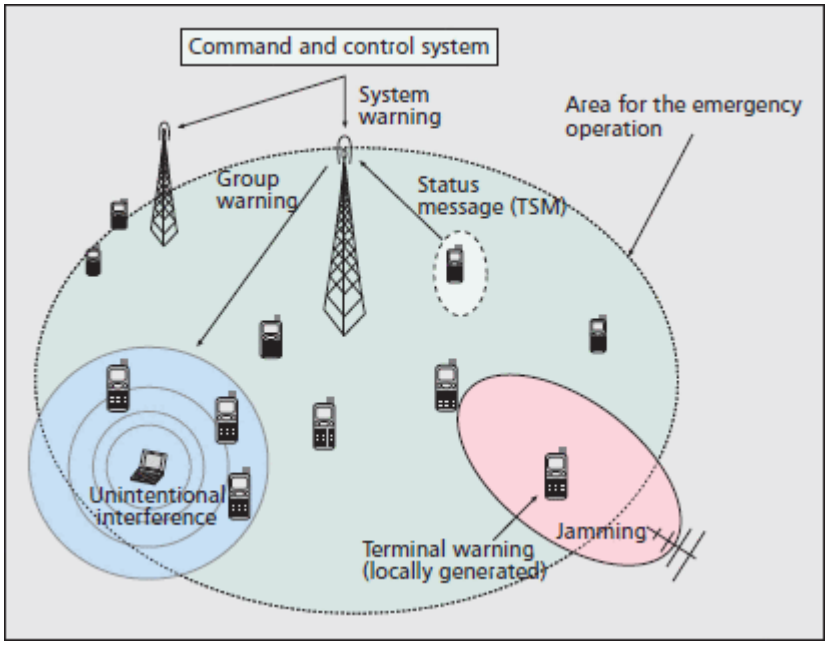

Figure 2.5.3 International Jamming [17]

5.3 Inexpensive and Low-Power Components

With Massive MIMO, expensive, ultra-linear 50W amplifiers used in traditional systems are changed by using 100's of cheap amplifiers with output power in the milli-Watt range. The distinction to traditional array designs, which use few antennas fed from high-power amplifiers, is significant. Several costly and cumbersome items, such as giant coaxial cables, can be eradicated. Massive MIMO reduces the constraints on accuracy and linearity of every item amplifier and RF chain. All that should be considered is their mixed action. In a way, Massive MIMO depends on the regulation of huge numbers to make sure that noise fading and hardware imperfections common out when signals from a huge number of antennas are mixed. The same characteristics that make Massive MIMO resilient in opposition to fading make the technology extraordinarily robust to failure. A Massive MIMO system has a huge spare of DoF. For example, with 200 antennas serving 20 terminals, 180 DoF are unused. This DoF can be used for hardware-friendly signal shaping. In particular, every antenna can transmit signals with minimum peak-to-average ratio [18] or even steady envelope [19] at a very modest penalty in phrase of the improved total radiated power. Such envelope signaling enables the use of extraordinarily low-cost and power-efficient RF amplifiers. The methods in [18], [19] should not be

burdened with traditional beamforming methods or equal-magnitude-weight beamforming techniques. This is with contrast with constant-envelope multi-user precoding where no beams are formed and the signals emitted through every antenna are no longer shaped using weighing of a symbol. Rather, a wave field is created such that when this wave field is sampled at the spots where the users are located, the terminals see precisely the signals that we favor them to see. The quintessential property of the Massive MIMO channel that makes this feasible is that the channel has a large null space: nearly anything can be put into this null space beside affecting what the terminals see. In particular, elements can be put into this null space that makes the transmitted waveforms fulfill the preferred envelope constraints. In spite of that, the advantageous channels between the base station and every terminal can take any signal group as input and does no longer require the use of PSK-type modulation. The extensively improved energy efficiency allows Massive MIMO systems to function with a total output RF power two orders of magnitude much less than with contemporary technology. This matter due to the fact the energy consumption of cellular base stations is a developing concern worldwide. Also, base stations that devour many orders of magnitude less power may want to be harvested by the wind or solar energy, and subsequently quickly deployed where no electricity.

5.4 Reduction in Latency

The furthermost restrictive factor in wireless communication systems is the presence of fading. The fading can render the obtained signal power very small at sometimes. This fact occurs when the signal dispatched from a base station travels through more than one path before it reaches the user terminal, and the waves ensuing from these multiple paths interfere destructively. Fading makes it difficult to construct low-latency wireless links. In case, the terminal is stuck in a fading dip, it must wait till the propagation channel has sufficiently modified until any symbol can be received. Massive MIMO depends on the regulation of large numbers and beamforming to keep away from fading problems so that fading no longer limits latency.

6 MASSIVE MIMO CHALLENGES

6.1 Uplink Pilot Contamination

In an ideal way, every terminal in a Massive MIMO system is assigned an orthogonal uplink pilot sequence. However, the maximum range of orthogonal pilot sequences that can exist is upper bounded by the length of the coherence interval divided by the channel delay spread. In accordance to [20], for a typical working scenario, the maximum quantity of orthogonal pilot sequences in a one-millisecond coherence interval is estimated to be about 200. It is convenient to exhaust the reachable resources of orthogonal pilot sequences in a multi-cellular system. The impact of re-using pilots from one cell to another, and the related adverse consequences, is called “pilot contamination”. Specifically, when the service array correlates its acquired pilot signal with the pilot sequence related to a particular terminal, it indeed obtains a channel estimate that is contaminated by a linear mixture of channels to the different terminals that share the identical pilot sequence. Downlink beamforming primarily based on the contaminated channel estimate brings in interference that is directed to the terminals that share the identical pilot sequence. Similar interference is concord with uplink transmissions. This attentive interference grows with the number of antennas at an equal rate as the preferred signal [20]. Even in part, correlated pilot sequences leads to directed interference. Pilot contamination as a fundamental phenomenon is not particular to Massive MIMO. However, its impact on Massive MIMO seems to be an awful much extra profound than in traditional MIMO [5], [20]. According to [20], it used to be argued that pilot contamination constitutes a remaining limit on performance, when the number of antennas is elevated beside binding, at least with receivers that depend on pilot channel estimation. While this argument has been contested lately [21], at least beneath some particular assumptions on the power control used, it seems possible that pilot contamination needs to be dealt with in some way.

Some approaches used to mitigate pilot contamination are listed below unless an extended survey on reducing uplink pilot contamination will be discussed in detail later in this thesis.

- **Pilot Allocation:** One way is to use a less-aggressive frequency reuse factor for the pilots. This technique pushes contaminating cells farther apart. It is additionally feasible to coordinate the use of pilots or adaptively allocate pilot sequences to the distinct terminals in the system [22]. (see fig 2.11 for more details see [22]).
- **Smart Estimation:** for instance, blind estimation algorithms [21] that avoid the use of pilots altogether [23] might also mitigate or remove the consequences of pilot contamination. The most promising path appears to be blind methods that jointly estimate the channels and the payload data (for performance see fig 2.6.1).
- **System Structure**: New precoding strategies that consider the system structure, such as pilot contamination precoding [6], can exploit cooperative transmission over a multiplicity of cells aside of the beamforming operation to nullify, at least partially, the directed interference that effects from pilot contamination. Unlike coordinated beamforming over a couple of cells which requires estimates of the right channels between the User terminals and the base station of the contaminating cells, pilot contamination precoding relies on the corresponding slow fading coefficients.

A lot of techniques developed to mitigate uplink pilot mitigation, mainly deployed under these approaches, however, none of the current methods had afforded an optimal solution.

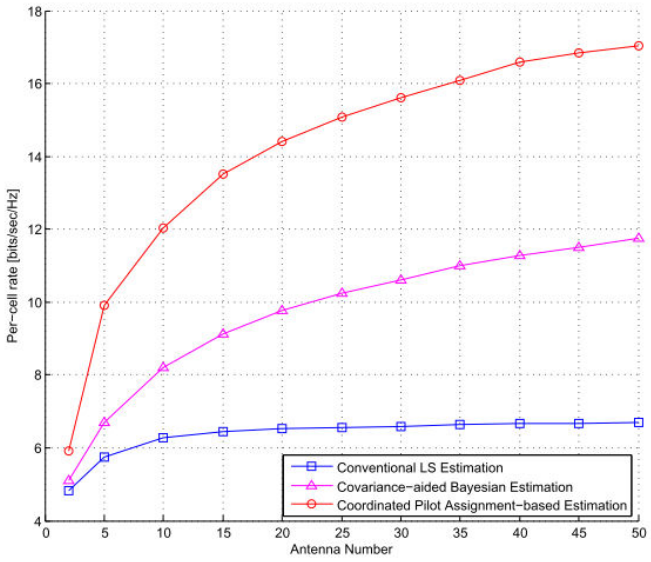

Figure 2.6.1 Per-cell rate vs. antenna number, 2-cell network, Gaussian distributed AOAs with σ = 10 degrees [22]

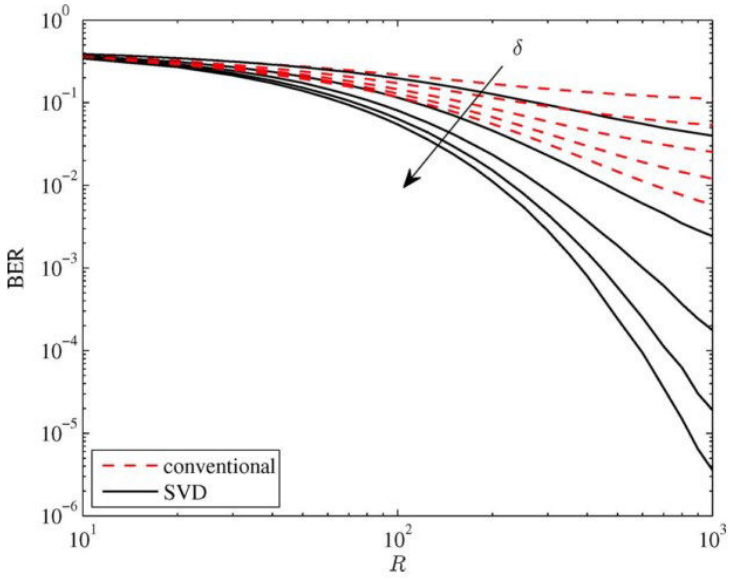

Figure 2.6.2 BER vs. number of receive antennas [21]

6.2 TDD Scheme

There seems to be a practical unanimity that the propagation channel itself is reciprocal, except the distribution is affected using materials with unusual magnetic properties. However, the hardware chains in the BS and UT transceivers might also no longer be reciprocal between the uplink and the downlink. Adjustment of the hardware chains does not appear to represent a serious trouble, and there are options in system calibration that have already been examined to some extent in practice [24], [25]. Specifically, [24] treats reciprocity calibration for a 64-antenna (see fig 2.6.3) system and claims practical empirical implementations.

Note that adjustment of the terminal uplink and downlink chains is now not required to obtain the full beamforming beneficial properties of Massive MIMO. If the base station tools are appropriately calibrated, then the array will indeed transmit a coherent beam to the terminal. There will still be some mismatch in the receiver chain of the terminal. However, this can be dealt with via transmitting pilots through the beam to the UT; the overhead for these additional pilots is minimal. Absolute calibration of the array is no longer required. Instead, as proposed in [24], one of the antennas can be handled as a locus, and signals can be switched between the reference antenna and each of the different antennas to derive a compensation aspect for that antenna. It may also be viable entirely to forbear from reciprocity calibration inside the array, for instance, if the maximum phase shift between the uplink chain and the downlink chain had been much less than sixty degrees then coherent beamforming would nevertheless take place even if with a viable 3 dB reduction in gain.

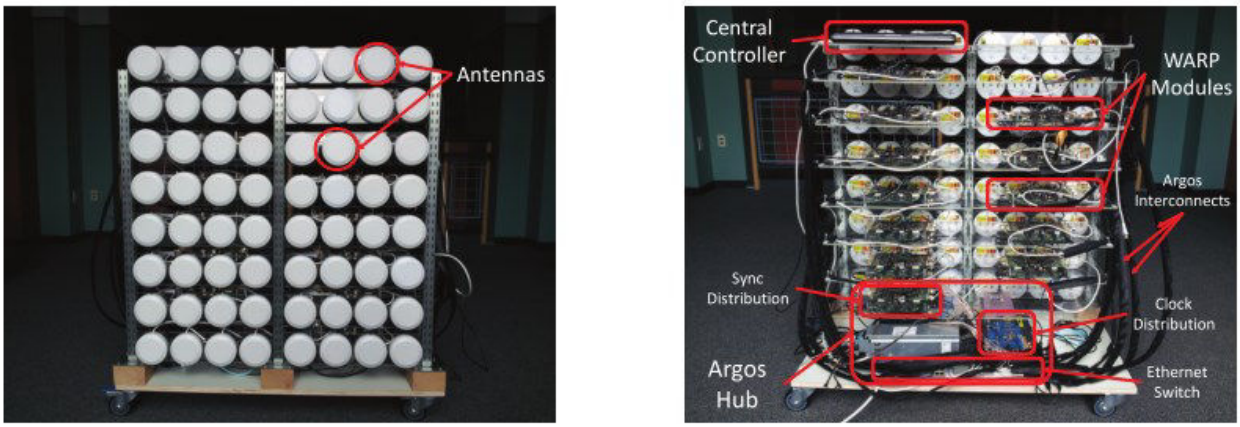

Figure 2.6.3 The prototype of Argos with 16 modules and 64 antennas. Left: front side. Right: backside [24]

6.3 Channel Response

Massive MIMO linear processing depends mainly on favorable propagation. Favorable propagation means that the propagation channel responses from the base station to distinct terminals are sufficiently different. To learn about the behavior of massive MIMO systems, channel measurements have to be carried out the usage of practical antenna arrays. This is due to the fact the channel performance using huge arrays differs from that experienced using traditional smaller arrays. Essential variations are that there may be large scale fading over the array and the small-scale signal information may also alternate over the array. It is additionally proper for physically smaller arrays with directional antenna elements pointing in a variety of directions (see fig 2.6.4).

Figure 2.6.4 Two large antenna arrays at the base station side: on left: a cylindrical array with 128 patch antenna on right: a virtual linear array with 128 omnidirectional antenna positions [26].

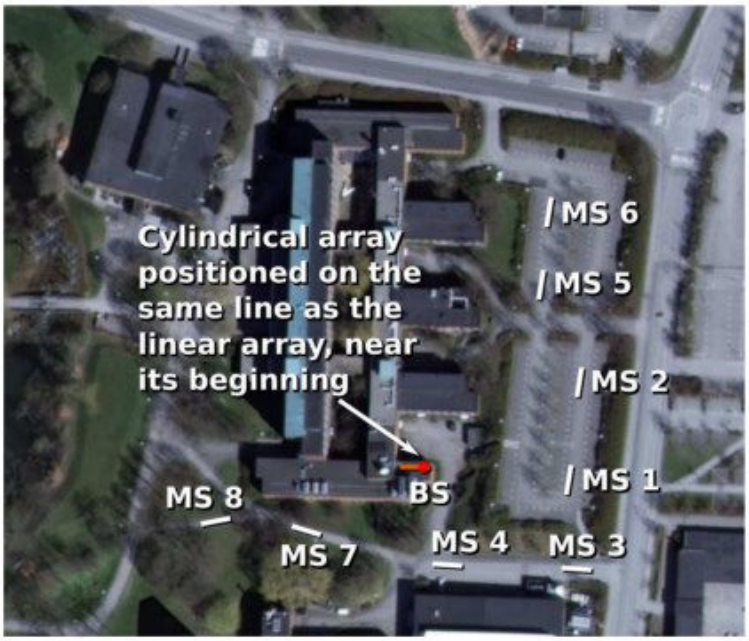

Figure 2.6.5 The measurement area at the campus of the Faculty of Engineering (LTH). The two BS antenna arrays were placed on the same roof of the E-building during two measurement campaigns [26].

The Dirty Paper Coding (DPC) sum-rate and the ZF sum-rate for an especially hard setup are proven in Fig. 2.6.6, where the UTs are tightly spaced and have LOS to the base station. For the i.i.d. channels both the DPC sum-rate and the ZF sum-rate converge to that of the interference-free case which is 13.8 bps/Hz.

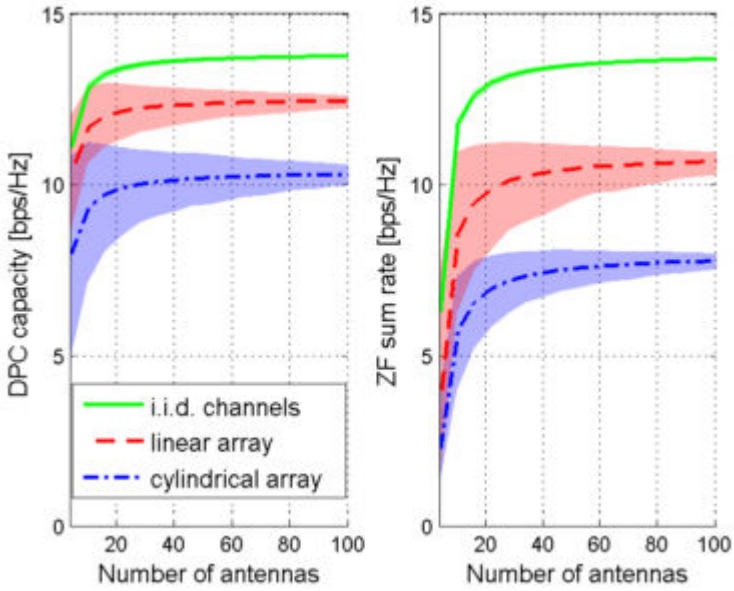

Figure 2.6.6 Four users close to each other at MS 2, with LOS to the base station antenna arrays [26], with dashed lines representing the average of the shadowed region arround .

Referring to Fig 2.6.6, the variance of the sum-rate decreases as the number of antennas increases, however slowly for the measured channels. The gradual decline can at least partially, be attributed to the shadow fading taking place throughout the arrays. In the case of a linear array in the form of shadowing via exterior objects along the array and for the cylindrical array as shadowing induced by directive antenna pointing in the wrong direction. The overall performance of the physically massive array tends to that of the theoretical i.i.d. case when the high diversity of antennas grows large. The short round array has inferior overall performance in contrast to the linear array owing to its smaller aperture it can't get to the bottom of the scatterers as well as the physically massive array and its directive antenna factors from time to time pointing in the wrong direction. Also, due to the truth that most of the scatterers are considered at the same horizontal angle, the opportunity to resolve scatters at specific elevations gives solely marginal contributions to the sum-rate in this scenario.

Worth to mention that when using extremely another complex, but nonetheless linear, precoding techniques such as ZF or MMSE, the convergence to the i.i.d. channel overall performance is increased and the variance of the sum-rate is decreased as the number of base station antennas is increased [26]. Another issue worth citing is that additionally for a very complicated propagation scenario, such as tightly spaced users in LOS conditions, it looks that the massive array is capable of separating the UTs to a practicable extent using the distinctive spatial signatures that the UTs have at the BS, due to the improved spatial resolution. This fact would not be feasible with conventional MIMO. Those conclusions are further presented after the observations in [27] where another outdoor measurement scenario is described and analyzed (see fig 2.6.7).

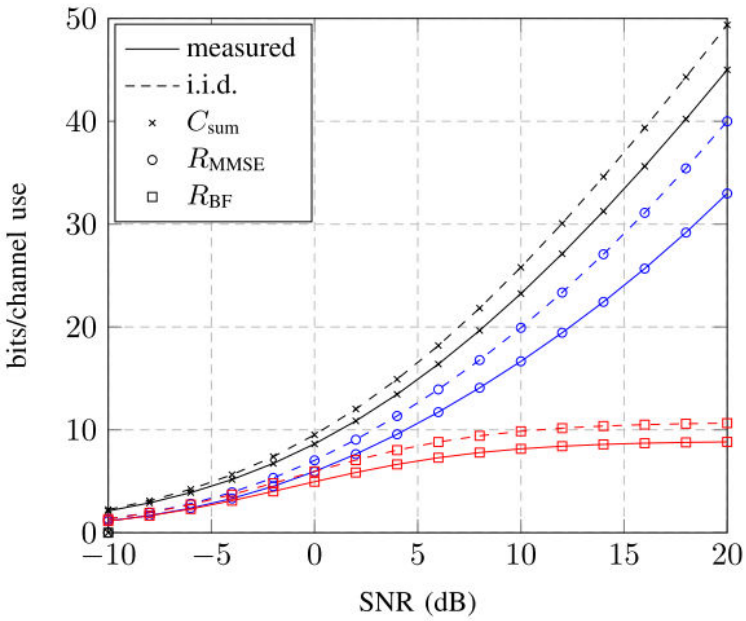

Figure 2.6.7 Average sum-capacity and sum-rates with linear precoding versus SNR with M = 10 antennas and K = 8 UTs [27].

7 CONCLUSION

This chapter had introduced an overview of massive MIMO technology. Starting from conventional MIMO to the next future 5G networks. Furthermore, it shed the lights on massive MIMO technology. It also introduces some main characteristics of massive MIMO includes scalability, favorable propagation and signal processing on the forward and downlink. Furthermore, the opportunities and challenges facing massive MIMO were briefly discussed. Hence, capacity increase, system robustness, and latency reduction were discussed as opportunities. However, uplink pilot contamination and channel response as discussed as challenges.

As a conclusion, there is a compelling clue that the assumptions on favorable propagation with massive MIMO, are appreciably legitimate in practice. Depending on the particular configuration of the huge array and the precoding algorithms used the convergence closer to the perfect overall performance can also be faster or slower, as the number of antennas is increased. However, with about 10 instances extra base station antennas than the number of users, it looks that it is viable to get a steady performance, not a long way from the theoretically perfect performance additionally underneath what is regarded very challenging propagation conditions.

8 REFERENCES

[1] J. Vicario and C. Antón-Haro, “Adaptive switching between spatial diversity and multiplexing: A cross-layer approach,” IST MWCS, 2005.

[2] D. Lee et al., “Coordinated multipoint transmission and reception in LTE-advanced: Deployment scenarios and operational challenges,” IEEE Commun. Mag., vol. 50, no. 2, pp. 148–155, 2012.

[3] E. Larsson, O. Edfors, F. Tufvesson, and T. Marzetta, “Massive MIMO for next generation wireless systems,” Commun. Mag. IEEE, vol. 52, no. 2, pp. 186–195, 2014.

[4] H. Q. Ngo, E. G. Larsson, and T. L. Marzetta, “Energy and spectral efficiency of very large multiuser MIMO systems,” IEEE Trans. Commun., vol. 61, no. 4, pp. 1436–1449, 2013.

[5] J. Hoydis, S. Ten Brink, and M. Debbah, “Massive MIMO in the UL/DL of cellular networks: How many antennas do we need?,” IEEE J. Sel. Areas Commun., vol. 31, no. 2, pp. 160–171, 2013.

[6] J. Jose, A. Ashikhmin, T. L. Marzetta, and S. Vishwanath, “Pilot Contamination and Precoding in Multi-Cell TDD Systems,” pp. 1–23, 2009.

[7] T. L. Marzetta, “Massive MIMO: An Introduction,” Bell Labs Tech. J., vol. 20, pp. 11–22, 2015.

[8] X. Gao, O. Edfors, F. Rusek, and F. Tufvesson, “Linear pre-coding performance in measured very-large MIMO channels,” IEEE Veh. Technol. Conf., 2011.
[9] H. Q. Ngo, E. G. Larsson, and T. L. Marzetta, “Aspects of favorable propagation in Massive MIMO,” Eur. Signal Process. Conf., no. 1, pp. 76–80, 2014.
[10] J. Jose, A. Ashikhmin, T. L. Marzetta, and S. Vishwanath, “Pilot contamination and precoding in multi-cell TDD systems,” IEEE Trans. Wirel. Commun., vol. 10, no. 8, pp. 2640–2651, 2011.
[11] F. Rusek et al., “Scaling up MIMO : Opportunities and challenges with very large arrays,” IEEE Signal Process. Mag., vol. 30, no. 1, pp. 40–60, 2013.
[12] E. Telatar, “Capacity of multi-antenna Gaussian channels,” Eur. Trans. Telecommun., vol. 10, no. 6, pp. 585–595, 1999.
[13] B. M. Hochwald, T. L. Marzetta, and V. Tarokh, “Multiple-antenna channel hardening and its implications for rate feedback and scheduling,” IEEE Trans. Inf. Theory, vol. 50, no. 9, pp. 1893–1909, 2004.
[14] A. Gupta and D. Nagar, Matrix variate distributions. 1999.
[15] R. Couillet and M. Debbah, Random matrix methods for wireless communications. 2011.
[16] A. Pitarokoilis, S. K. Mohammed, and E. G. Larsson, “On the optimality of single-carrier transmission in large-scale antenna systems,” IEEE Wirel. Commun. Lett., vol. 1, no. 4, pp. 276–279, 2012.
[17] P. Stenumgaard, D. Persson, E. Larsson, and K. Wiklundh, “An early-warning service for emerging communication problems in security and safety applications,” IEEE Commun. Mag., vol. 51, no. 5, pp. 186–192, 2013.
[18] C. Studer and E. G. Larsson, “PAR-aware large-scale multi-user MIMO-OFDM downlink,” IEEE J. Sel. Areas Commun., vol. 31, no. 2, pp. 303–313, 2013.
[19] S. K. Mohammed and E. G. Larsson, “Per-antenna constant envelope precoding for large multi-user MIMO systems,” IEEE Trans. Commun., vol. 61, no. 3, pp. 1059–1071, 2013.
[20] T. L. Marzetta, “Noncooperative cellular wireless with unlimited numbers of base station antennas,” IEEE Trans. Wirel. Commun., vol. 9, no. 11, pp. 3590–3600, 2010.
[21] R. R. Müller, L. Cottatellucci, and M. Vehkaperä, “Blind pilot decontamination,” IEEE J. Sel. Top. Signal Process., vol. 8, no. 5, pp. 773–786, 2014.
[22] and Y. L. Haifan Yin, David Gesbert Fellow, IEEE, Miltiades Filippou, “A Coordinated Approach to Channel Estimation in Large-scale Multiple-antenna Systems,” IEEE J. Sel. Top. Signal Process., vol. 4553, no. c, pp. 1–1, 2012.
[23] H. Q. Ngo and E. G. Larsson, “EVD-based channel estimation in multicell multiuser MIMO systems with very large antenna arrays,” in 2012 IEEE International Conference on Acoustics, Speech and Signal Processing (ICASSP), 2012, no. 1, pp. 3249–3252.
[24] C. Shepard et al., “Argos: practical many-antenna base stations,” Proc. 18th Annu. Int. Conf. Mob. Comput. Netw. - Mobicom ’12, p. 53, 2012.
[25] F. Kaltenberger, H. Jiang, M. Guillaud, and R. Knopp, “Relative channel reciprocity calibration in MIMO/TDD systems,” 2010 Futur. Netw. Mob. Summit, pp. 1–10, 2010.
[26] X. Gao, F. Tufvesson, O. Edfors, and F. Rusek, “Measured propagation characteristics for very-large,” pp. 295–299, 2012.
[27] J. Hoydis, C. Hoek, T. Wild, and S. ten Brink, “Channel measurements for large antenna arrays,” Wirel. Commun. Syst. (ISWCS), 2012 Int. Symp., pp. 811–815, 2012.

Chapter 3: Massive MIMO Detection and Precoding

The method of magnitude estimation provided a direct measure of sensation ~ Stanley Smith Stevens

This chapter will introduce a brief introduction to channel estimation and precoding techniques used in Massive MIMO, on advance low-performance analysis will take place to clarify the optimality of linear processing techniques in Massive MIMO systems.

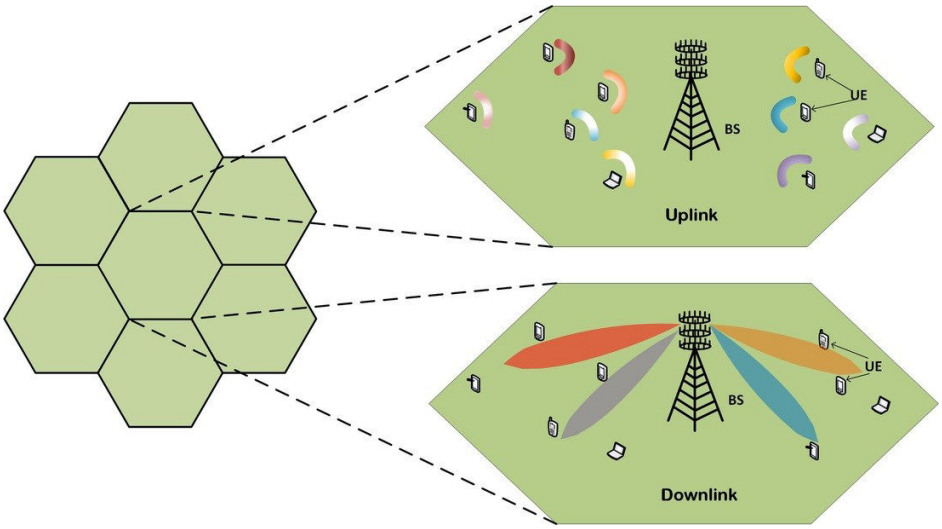

Figure 3.0 Multi-cell Massive MIMO

1 INTRODUCTION

Detection and precoding is an essential aspect in Massive MIMO systems. A dominant factor of any channel link is the effectiveness of its detection algorithm. Provided some information of the channel be accessible at the receiver side, one is to plan low complexity algorithms to retrieve statistics from the transmitted symbols. A decrease complexity leads to a reduction in arithmetic operations, which leads to decreased latency and improved energy efficiency. However, when decreasing complexity, one may be compromising on the overall performance of the receiver (e.g., lowering the diversity gain), which would possibly be undesirable. Since most advantageous detection is no longer possible for massive MIMO structures due to its exponential complexity, sub-optimal methods should be considered, studied and compared. An overview of the special feasible techniques will be presented in this chapter. Another motivation for the exhaustive research is the precoding process. Considering Massive MIMO system, one is attracted in the case where various UTs are served simultaneously because in that scenario the

possibilities of uncorrelated fading are higher. This leads to a channel matrix **H** with a higher rank, which is more preferred. In this chapter, the multiuser case will then be considered, and the effect of growing the range of BS antennas *M,* beyond bounds will be discussed. While assuming K << M, it will be certainly confirmed that linear processing methods perform near optimal and, capitalizing on that fact, algorithms for speedy computation and updates of inverse matrices will be evaluated.

2 DETECTION FUNDAMENTALS AND DEFINITIONS

The purpose of a MIMO detector is to decode the uplink K streams that were transmitted and combined with the channel. Under this scenario, the performance will depend mainly on the statistics of matrix **H** and average noise power. The basic definitions to assess the comportment of the various detectors will be presented. One of the important parameters to illustrate the anticipated performance of a detector is the orthogonality deficiency *od(**H**)*.
In what follows some fundamental definitions will be presented.

Orthogonality Deficiency:
By definition [1], for an $M \times K$ channel matrix $\mathbf{H} = [\mathbf{h_1}, \mathbf{h_2}, \dots, \mathbf{h_K}]$, the orthogonality deficiency $od(\mathbf{H})$ is represented as:

$$od(\boldsymbol{H}) = 1 - \frac{\det(\boldsymbol{H}\boldsymbol{H}^H)}{\prod_{i=1}^{K} \|\boldsymbol{h}_i\|^2}, \qquad (3.2.1)$$

with $\|\boldsymbol{h}_i\|$ being the L2 norm i-*th* column of **H**.
$od(\boldsymbol{H})$ is a measure of the orthogonality of the column vectors in matrix **H**, it is bounded by $0 \leq od(\boldsymbol{H}) \leq 1$ and it takes minimum value when **H** is orthogonal and maximum value when **H** is singular.

Signal-to-Noise Ratio:

The *SNR* measures how much the transmitted symbol power is above the additive noise at the receiver. Given a transmitted vector $\boldsymbol{x} \in \mathbb{C}^{K \times 1}$ with covariance matrix
$\mathbb{E}\{\boldsymbol{s}\boldsymbol{s}^{\boldsymbol{H}}\} = {\delta_s}^2 \boldsymbol{I}_K$ and AWGN $\boldsymbol{n} \in \mathbb{C}^{M \times 1}$ with distribution, $CN(0, {\delta_n}^2 \boldsymbol{I})$. Then the average input SNR will be given as follow:

$$SNR = K \frac{{\delta_s}^2}{{\delta_n}^2}. \qquad (3.2.2)$$

SNR is typically definite in logarithmic measure and broadly used to study bit error rate (BER) concert in communication systems. In this domain, the progression features of BER as a function of the SNR are often represented and are used in the literature to estimate the diversity order gain of the system.
Diversity Order Gain:
Signified as the average error probability, where it is a function of the SNR. Following [1], the diversity order gain G_d can be represented as:

$$G_d = \lim_{SNR \to \infty} \left(- \frac{\log Pe(SNR)}{\log SNR} \right), \qquad (3.2.3)$$

where $Pe()$ is the error probability function.

Spatial Multiplexing Gain:
A valuable metric is the multiplexing gain, which characterizes the growth of the spectral efficiency with the SNR, for a specified BER. Let *F(SNR)* be a set of codes of block length *b*, one at each SNR level, and *S(SNR)* represents the rate of the consistent code. Given this, the attainable spatial multiplexing gain G_m of the system is defined according to [2] as follows:

$$G_m = \lim_{SNR \to \infty} \left(- \frac{\log S(SNR)}{\log SNR} \right), \qquad (3.2.4)$$

This metric demonstrates the effect of capacity increases with SNR and relates to the maximum quantity of independent sub-channels, and it is upper bounded as $G_m \leq min(M, K)$. Given a specific BER value, the multiplexing gain G_m can illustrate the speed of change of spectral efficiency with the increase of the SNR at the same BER [3].

3 CHANNEL DIVERSITY AND MULTIPLEXING GAIN

Although, it can be revealed that MIMO system performance can be measured based on two interdependent gains [2]. Considering the slow Rayleigh fading wireless system with *K* transmit and *M* receive antennas. If the K antennas transmit the identical signal, multiple independent copies of the same symbol are received, follow-on a better consistent reception. This enhancement in reliability can be referred to it as "Diversity", for the considered situation this benefit is stated in the average BER, assuming high SNR regime, is made to decay with SNR^{-K} which performs significantly better than the SISO system with decay SNR^{-1}.

Alternative possible method to increase the system gain is to send dissimilar data streams through diverse antennas. In case of each link fade independently, the sum-rate can be increased by a specified value G_m.This approach is referred to it as "Spatial Multiplexing" and, for a high regime SNR, system capacity was proved to scale with *min (M, K)*.

Concisely, MIMO systems afford two independent forms of gain: "Diversity" and "Spatial Multiplexing". These gains are shown to be independent in such a way that increasing one may not certainly increase the other. Nevertheless, the trade-off between them can be stated in a simple way using essential system parameters.

Contemplate the mentioned scenario, where the block length contents $b \geq M + K - 1$, for a multiplexing gain G_m, the maximum attainable diversity gain is $G_d = (M - G_m)(K - G_m)$. This consequence can be construed as G_m antennas provide multiplexing gain, while the rest are exploited for diversity.

Consequently, there is a necessary trade-off between the two probable gains which is an optimization problem that many researchers were done to enhance both results.

4 MAXIMUM LIKELIHOOD DETECTION

Given signal $\boldsymbol{y}$ and channel $\boldsymbol{H}$, the role of the detector is to obtain an estimate $\hat{\boldsymbol{s}}$ of the transmitted symbol $\boldsymbol{s}$. Supposing that $\boldsymbol{s}$ is selected uniformly from a constellation $\mathcal{X}$, the optimal detector that reduces the error probability is called maximum likelihood (ML).

$$\hat{\boldsymbol{x}} = arg \min_{\hat{\boldsymbol{x}} \epsilon \mathcal{X}^K} \|\boldsymbol{y} - \boldsymbol{H}\boldsymbol{s}\|, \quad (3.4.1)$$

Maximum likelihood Geometrically selects the vector $\hat{\boldsymbol{x}}$ that produces the minimum Euclidian distance between received vector $\boldsymbol{y}$ and estimated message $\boldsymbol{H}\hat{\boldsymbol{s}}$. This is like a discrete optimization problem with $|\mathcal{X}|^K$ entries. This will lead to increase the complexity of the detector exponentially with an exponent of *K*, which is considered NP-hard problem [4], [5]. Although ML achieves optimal performance, its complexity is unrealistic for higher dimensions. Considering this complexity manner, suboptimal methods will be represented to make practical use of detectors in Massive MIMO systems.

5 FAVORABLE PROPAGATION

Adding more antennas at the BS, both linear and non-linear processing receivers approach sum rate capacity without interference. This issue can be seen in the figure below, where spectral efficiency converges to the same limit as *M* grows large.

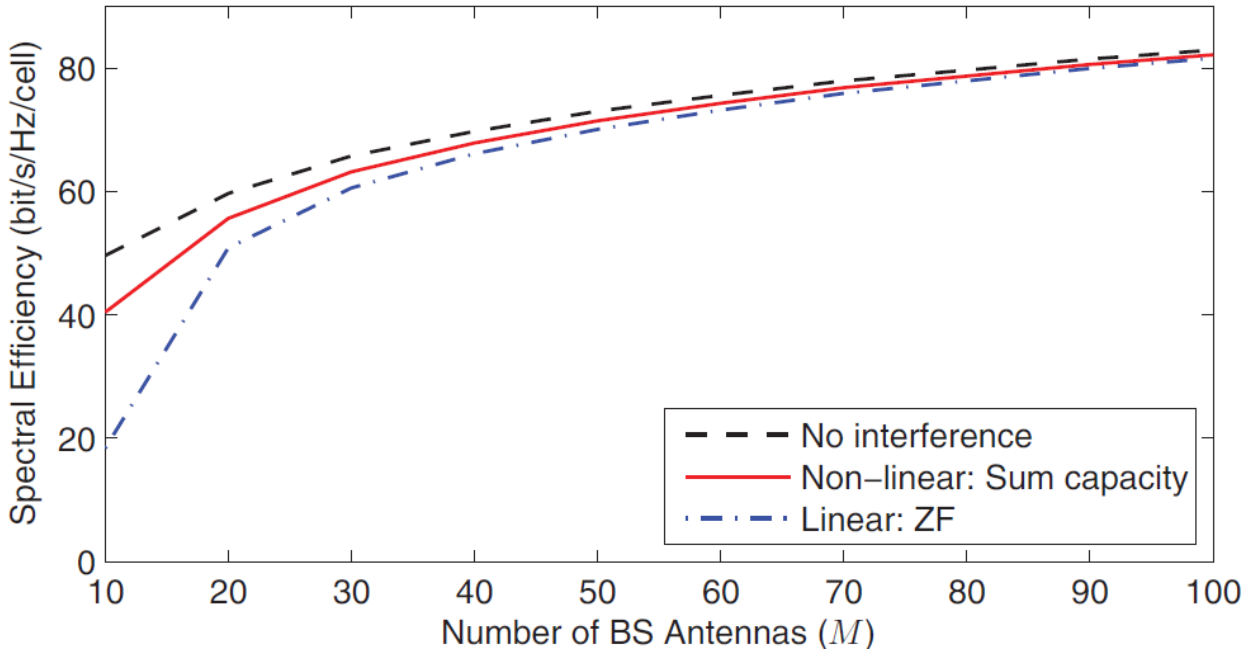

Figure 3.5.1 Spectral Efficiency Vs. Number of BS antennas showing the performance of ZF receiver with non-linear receivers [6]

Consider two channels $\boldsymbol{h}1, \boldsymbol{h}2 \in \mathbb{C}^M$ between the BS and two user terminals, and let s_1 and s_2 be two symbols transmitted by those users. If $\boldsymbol{h}1, \boldsymbol{h}2 \neq 0$ and $\boldsymbol{h}1^H\boldsymbol{h}2 = 0$, this means that the two channels are orthogonal and the base Station can easily separate their symbols by simply compute the inner product between $\boldsymbol{h}1^H\boldsymbol{y} = \boldsymbol{h}1^H\boldsymbol{h}1s_1 + \boldsymbol{h}1^H\boldsymbol{h}2s_2 = \|\boldsymbol{h}1\|^2 s_1$, where $\boldsymbol{y}$ is the received signal at the BS. The symbol s_2 of the second user terminal can be separated using the same way, $\boldsymbol{h}2^H\boldsymbol{y} = \boldsymbol{h}2^H\boldsymbol{h}1s_1 + \boldsymbol{h}2^H\boldsymbol{h}2s_2 = \|\boldsymbol{h}2\|^2 s_2$. This orthogonality property between the two channels is called favorable propagation where the BS can with linear receiver separate the signals without encountering interference.

Favorable propagation is not real case scenario due to its strict condition of orthogonality ($\boldsymbol{h}1^H\boldsymbol{h}2 = 0$). Unless with Non-Line-Of-Sight (NLOS) scenario with rich scattering environment, channels approach orthogonality. Supported with many antennas at the BS, $\lim_{a.s\ M\to\infty} \frac{\boldsymbol{h}1^H\boldsymbol{h}2}{M} = 0$.
The proof of this assumption is defined by the law of large numbers see [7].

The mentioned assumption can be declared as follows, as M increase, if the channels $\boldsymbol{h}1, \boldsymbol{h}2$ are normalized to M, then $\frac{\boldsymbol{h}1^H\boldsymbol{h}2}{M}$ goes asymptotically to zero. This phenomenon referred to it as *Asymptotic Favorable Propagation.* This also leads to the result in fig 3.5.1, where one can see that the ZF receiver almost converge to non-interference spectral efficiency as M increases.
Note that $\lim_{a.s\ M\to\infty} \frac{\boldsymbol{h}1^H\boldsymbol{h}2}{M} = 0$ does not means that $\lim_{a.s\ M\to\infty} \boldsymbol{h}1^H\boldsymbol{h}2 = 0$ unless, most wireless channels appear to maintain asymptotic favorable propagation. Even with small number of antennas at the BS, the channel correlation has a negligible impact due to the fact that Spectral efficiency (SE) depends on the normalized channel to M, which converge to zero even with small number of BS antennas.

6 Massive MIMO System Model

We consider a system of multi-user MIMO with K user terminals each holds one antenna served with a base station holding M antennas subjected to the constraint that $M >> K$ and working in a Time Division Duplexing (TDD) reciprocity scheme. This assumption can be deduced after the proposed concept in the seminal paper [8] and the patent [9].

The TDD reciprocity protocol used contains a part dedicated to channel training where orthogonal pilot sequence should be uploaded each coherence interval (See Fig 3.6.1).

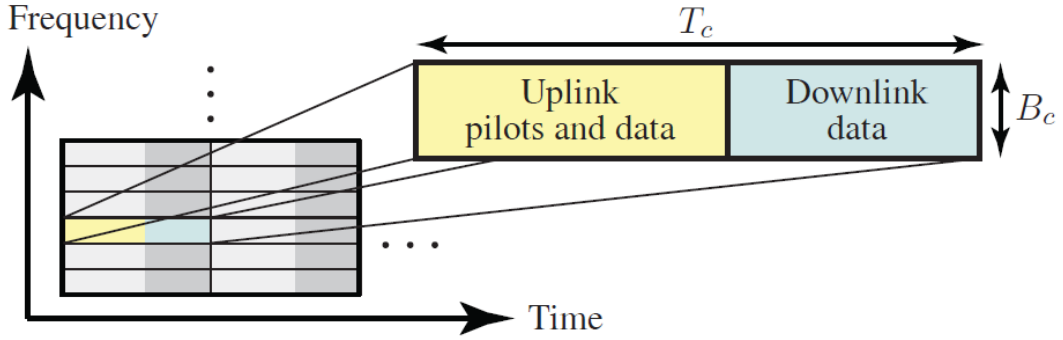

Figure 3.6.1 TDD scheme for Massive MIMO reciprocity protocol [6].

Considering this work, the coherence interval period is referred to it as T_c and B_c for the coherence bandwidth and $\tau_c = T_c B_c$ symbol in each coherence interval.
A basic MIMO system contains L cells each served with one BS holding M antennas and communicate with K UTs (see Fig 3.6.2). Due to the limited coherence interval length, training pilot sequences should be reused in adjacent cells and uplink pilot contamination considered can take place if considering the users in the adjacent cells are synchronized and uploading their pilots at the same time. Let the channel response vector between the j-th BS and the k-th UT in the l-th cell, denoted by $\boldsymbol{h_{jlk}} = [h_{jlk1}, \dots h_{jlkm}, \dots, h_{jlkM}]^T$, where subscript m stands for the m-th antenna and. Further, $\bar{\boldsymbol{h}}_{\boldsymbol{jlk}} = \mathbb{E}\{\boldsymbol{h_{jlk}}\}$ denotes the expectation of $\boldsymbol{h_{jlk}}$ and $\beta_{jlk} = \mathbb{V}\{h_{jlkm}\}$ denotes the variance of h_{jlkm} which is supposed to be independent of the antenna index m.

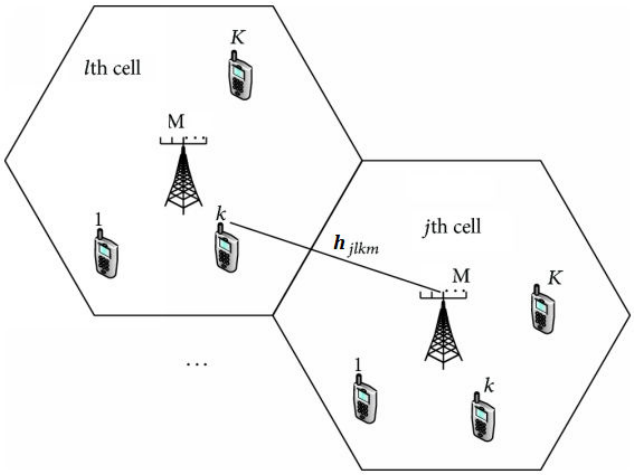

Figure 3.6.2 Massive MIMO system

These channel statistics are assumed to stay static for several coherence intervals, and the channel of UTs are assumed to be independent.

7 Linear Detection

This section will consider the uplink linear detection and channel estimate considering maximum Ratio Combination (MRC) receiver, Zero Forcing (ZF) receiver and Minimum Mean Square Error MMSE estimation.

7.1 Uplink Detection

The received signal at the j-th BS can be expressed as follows:

$$\boldsymbol{y_j} = \sum_{l=1}^{L} \sum_{k=1}^{K} \sqrt{P_{lk}} \boldsymbol{h_{jlk}} s_{lk} + \boldsymbol{w_j} \qquad (3.7.1)$$

$$= \sum_{l=1}^{L} \boldsymbol{H_{jl}} \boldsymbol{P_l^{1/2}} \boldsymbol{S_l} + \boldsymbol{w_j}$$

Where $\boldsymbol{y_j} \in \mathbb{C}^M$, s_{lk} is the normalized symbol transmitted by the *k*-th UT from the *l*-th cell and P_{lk} is its transmitted power with, $\mathbb{E}\{|s_{lk}|^2\} = 1$. $\boldsymbol{w_j} \in \mathbb{C}^M$ models the Additive White Gaussian Noise AWGN with distribution $\boldsymbol{w_j} \sim \mathbb{CN}(\boldsymbol{0}, \sigma_{UL}^2 \boldsymbol{I_M})$ and variance σ_{UL}^2.

In matrix notation $\boldsymbol{H_{jl}} = [\boldsymbol{h_{jl1}}, \dots \boldsymbol{h_{jlk}}, \dots, \boldsymbol{h_{jlK}}] \in \mathbb{C}^{M \times K}$, $\boldsymbol{P_l^{1/2}} = diag(\sqrt{P_{l1}}, \dots, \sqrt{P_{lk}}, \dots \sqrt{P_{lK}}) \in \mathbb{C}^{K \times K}$ and $\boldsymbol{S_l} = [s_{l1}, \dots, s_{lk}, \dots, s_{lK}]^T \in \mathbb{C}^K$.

7.1.1 Channel Estimation

Considering the training session, each UT needs to upload a pilot sequence of length τ_p symbol. We assume that the pilot sequences are reused according to the following factor, $\tau_p = fK$ where is a positive integer (e.g. $f = 1, 2 \dots$). This allows τ_p orthogonal sequence of pilot to take place within the *L* cells and to disjoint *L* into *f* sets to reduce interference. In this design, *L* cells are grouped into *f* different cell group.

The received pilot sequence during training session $\boldsymbol{Y_j^p} \in \mathbb{C}^{M \times \tau_p}$ can be expressed as,

$$\boldsymbol{Y_j^p} = \sum_{l=1}^{L} \boldsymbol{H_{jl}} \boldsymbol{P_l^{1/2}} \boldsymbol{\phi_l^H} + \boldsymbol{W_j^p} \quad (3.7.2)$$

with $\boldsymbol{\phi_l} = [\boldsymbol{\phi_{l1}}, \dots, \boldsymbol{\phi_{lk}}, \dots \boldsymbol{\phi_{lK}}] \in \mathbb{C}^{\tau_p \times K}$ denotes the pilot sequences that is used by UTs of the *l*-th cell where $\boldsymbol{\phi_{lk}} \in \mathbb{C}^{\tau_p}$ is the *k*-th user sequence. $\boldsymbol{W_j^p} \in \mathbb{C}^{M \times \tau_p}$ denotes the AWGN noise.

The pilot matrix is designed as follows,

$$\boldsymbol{\phi_l^H \phi_j} = \begin{cases} \tau_p \boldsymbol{I}_K & if\ l = j \\ \boldsymbol{0} & if\ l,j\ \in\ different\ cell\ group \\ \tau_p \boldsymbol{I}_K & if\ l,j\ \subset\ same\ cell\ group \end{cases}$$

The *j*-th BS can separate the signal received from the *l*-th cell using the statistical data gathered during previous sessions. Based on a technique developed by [10], where linear Minimum Mean Square Error is used to separate the signal of the k-th user in the *l*-th cell according to the following lemma.

Lemma 3.7.1: *considering the j-th BS need to separate the channel coefficient of the k-th user in the l-th cell using the MMSE receiver. The estimated channel can be estimated as:*

$$\widehat{\boldsymbol{h}}_{\boldsymbol{jlk}} = \overline{\boldsymbol{h}}_{\boldsymbol{jlk}} + \frac{\sqrt{P_{lk}} \tau_p \beta_{jlk}}{\sum_{i \in \int_l}^{L} P_{ik} \tau_p \beta_{ilk} + \sigma_{UL}^2} \left(\boldsymbol{Y_j^p} \boldsymbol{\phi_{lk}} - \sum_{i \in \int_l}^{L} \sqrt{P_{ik}} \tau_p \overline{\boldsymbol{h}}_{\boldsymbol{jlk}} \right) \quad (3.7.3)$$

The uncorrelated error [11] is expressed as $\boldsymbol{E_{jlk}} = \widehat{\boldsymbol{h}}_{\boldsymbol{jlk}} - \overline{\boldsymbol{h}}_{\boldsymbol{jlk}}$*, with zero mean and variance*

$$\mathrm{MSE}_{jlk} = \beta_{jlk} \left(1 - \frac{P_{lk} \tau_p \beta_{jlk}}{\sum_{i \in \int_l}^{L} P_{ik} \tau_p \beta_{ilk} + \sigma_{UL}^2} \right) \quad (3.7.4)$$

where $\int_l \subset \{1, \dots, L\}$ is the set off cell indices related to the same cell group as l, in other words, it is the set of cells that upload the same pilot reuse sequences.

The proof of Lemma 3.7.1 can be found in Appendix A.

In advance of this, the estimation error is independent of *M* which means that it is not affected by the increasing number of antennas at the BS. Note that the estimation quality will be improved with increasing the number of antennas if the channel correlation structure and distribution is known prior [12]. From equation (3.7.3), one can find that the computational complexity of estimating the channel depends on basic linear algebra operation which can be simply solved in linear time. The estimation

error expressed in equation (3.7.4) is only affected by the AWGN and the interfered signal from the user in the same pilot reuse cell group.

7.1.2 Channel detection

The estimated channel in (3.7.3) will be used to separate the *K* user terminal in the *j*-th cell, where other signals from adjacent cells will be considered as interfering noise.

The BS in the *j*-th cell separate the signal of the *k*-th UT by multiplying the received signal with a linear detector $\boldsymbol{v_{jk}} \in \mathbb{C}^M$ as follows,

$$\boldsymbol{v_{jk}^H y_j} = \sum_{l=1}^{L} \sum_{\boldsymbol{t=1}}^{\boldsymbol{K}} \sqrt{P_{lt}} \boldsymbol{v_{jk}^H h_{jlt}} s_{lt} + \boldsymbol{v_{jk}^H w_j}$$

$$= \underbrace{\sqrt{P_{lk}} \boldsymbol{v_{jk}^H h_{jjk}} s_{jk}}_{preferred\ signal} + \underbrace{\sum_{\boldsymbol{t \neq k}}^{\boldsymbol{K}} \sqrt{P_{lt}} \boldsymbol{v_{jk}^H h_{jjt}} s_{jt}}_{intra-cell\ interference} + \underbrace{\sum_{l \neq j}^{L} \sum_{\boldsymbol{t \neq k}}^{\boldsymbol{K}} \sqrt{P_{lt}} \boldsymbol{v_{jk}^H h_{jlt}} s_{lt}}_{inter-cell\ interference} + \underbrace{\boldsymbol{v_{jk}^H w_j}}_{AWGN\ noise} \qquad (3.7.5)$$

It is evident from (3.7.5) that the received signal is composed of 4 parts, the first part corresponds to the preferred signal while the other three sections model the inter and intracell interference and the AWGN respectively. The linear detection vector $\boldsymbol{v_{jk}}$ can be chosen to amplify the desired signal and reduce the interference and noise signal. Two most used detectors in Massive MIMO systems are Zero Forcing (ZF) and Maximum Ratio Combination (MRC) receivers which can be expressed in matrix form as follows,

$$\boldsymbol{V_j} = \begin{cases} \boldsymbol{\hat{H}_{jj}} & for\ MRC \\ \boldsymbol{\hat{H}_{jj}} \left((\boldsymbol{\hat{H}_{jj}}^H) \boldsymbol{\hat{H}_{jj}} \right)^{\boldsymbol{-1}} & for\ ZF \end{cases} \qquad (3.7.6)$$

The MRC receiver aims to maximize the ratio between the average signal gain and the norm of the estimated channel vector:

$$\mathbb{E}\left\{ \frac{\boldsymbol{v_{jk}}^H \boldsymbol{h_{lk}}}{\|\boldsymbol{v_{jj}}\|} \right\} = \frac{\boldsymbol{v_{jk}}^H \boldsymbol{\hat{h}_{jk}}}{\|\boldsymbol{v_{jj}}\|} \leq \|\boldsymbol{\hat{h}_{jk}}\| \qquad (3.7.7)$$

This inequality reach maximum value when $\boldsymbol{v_{jk}} = \boldsymbol{\hat{h}_{jk}}$, and thus $\boldsymbol{V_j} = \boldsymbol{H_{jj}}$.

The ZF receiver aims to minimize the intra-cell interference of the observed signal as,

$$\mathbb{E}\left\{ \boldsymbol{V_j}^H \boldsymbol{H_{jj}} \boldsymbol{P_{jj}^{1/2}} \boldsymbol{s_{jj}} \right\} = \boldsymbol{V_j}^H \boldsymbol{\hat{H}_{jj}} \boldsymbol{P_{jj}^{1/2}} \boldsymbol{S_{jj}} = \left((\boldsymbol{H_{jj}}^H) \boldsymbol{H_{jj}} \right)^{\boldsymbol{-1}} \left((\boldsymbol{H_{jj}}^H) \boldsymbol{H_{jj}} \right) \boldsymbol{P_{jj}^{1/2}} \boldsymbol{S_{jj}} = \boldsymbol{P_{jj}^{1/2}} \boldsymbol{S_{jj}}$$

When M ≥ K the inverse of $\left((\boldsymbol{H_{jj}}^H) \boldsymbol{H_{jj}} \right)$ can be found and the average received signal becomes $\boldsymbol{P_{jj}^{1/2}} \boldsymbol{S_{jj}}$, with no inter-cell interference.

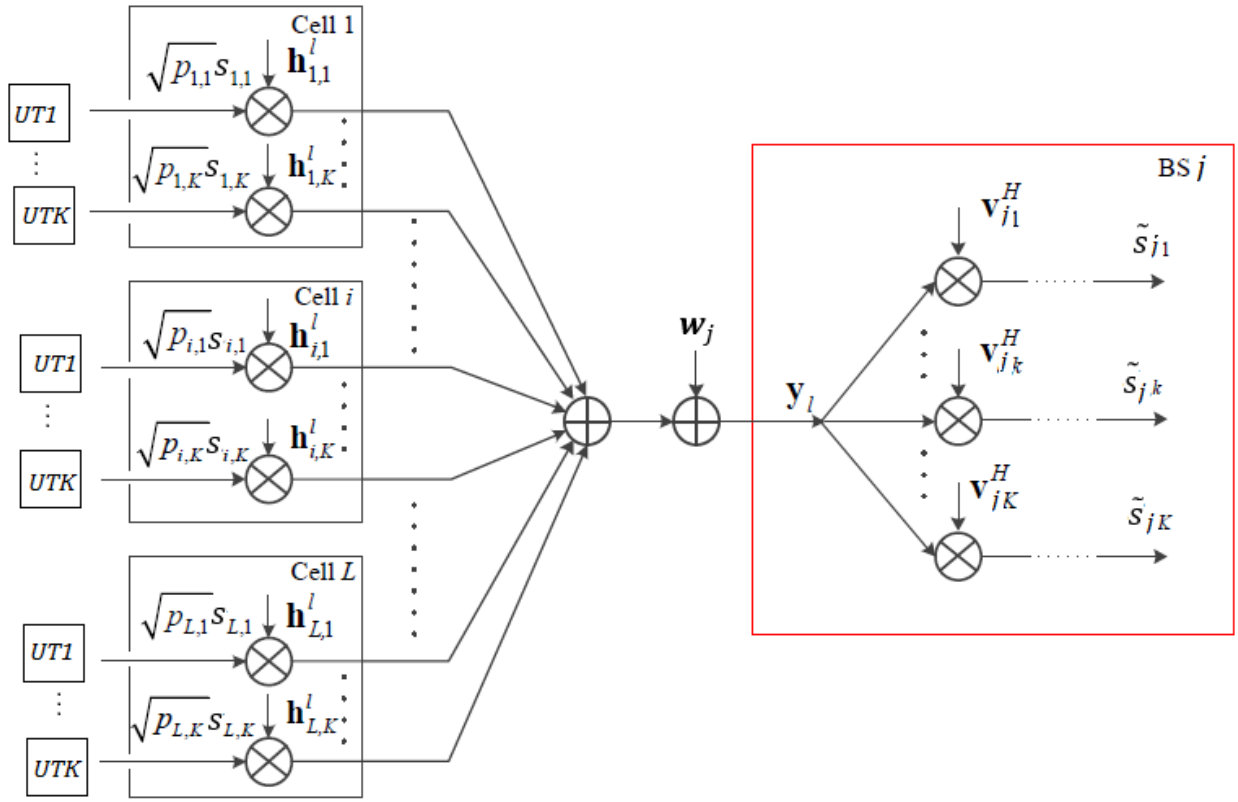

Figure 3.7.1 Block diagram showing multi-cell uplink scheme with linear detector

Since there always exists an additive noise to the detected symbols which limit the capacity of the link, the transmitted symbol is usually selected from a known constellation which restricts the probability of finding the true symbol to a finite set (e.g. QAM). Let symbol $s \in \mathbb{X}$, where $\mathbb{X}$ is a set of constellations which is known at the transmitter and the receiver, then $\tilde{s}_{jk}$ is chosen to be the minimum distance to the constellation element.

$$\tilde{s}_{jk} = \min_{s \in \mathbb{X}} \left| \boldsymbol{v}_{jk}^H \boldsymbol{y}_j - \boldsymbol{v}_{jk}^H \hat{\boldsymbol{h}}_{jjk} P_{jk} s \right|^2 \qquad (3.7.8)$$

8 Non-Linear Detection

Considering large-scale systems where $K = M$, linear detectors are not able to collect diversity in symmetric way, this is due to the loss of mutual information. Hence, non-linear techniques to cancel interference at various levels have been extensively studied in the literature. Most widespread techniques include Parallel Interference Cancellation (PIC) and Successive Interference Cancellation (SIC). Within this section, several non-linear detectors will be introduced.

8.1 Successive Interference Cancellation

SIC aim to successively decode the different layers of the signal, using either MMSE or ZF. It also cancels the consequence of the estimated symbol from the received signal. To enhance the performance, one possible method is to decode the symbol with the maximum SNR continuously. Consequently, the detector must sort the received symbols in an optimal detection order. This approach is often called "Ordered-SIC (O-SIC)" or "V-BLAST" [13]. Considering performance, the diversity gain achieved by V-BLAST in the *i-th* layer will be (M – K + i), leading to a better diversity gain in the low SNR regime. However, the outage probability is conquered by the first detected layer and diversity persist *(M –K +1)*

in the high SNR regime. Even so, there is a significant gain in the SNR, since at each iteration one interferer is suspended from the detection [14]. According to results studied in [14], the maximum expected SNR gain compared to the classical linear detectors is revealed to be about $10\log_{10} K \ dB$ (see fig 3.8.1)

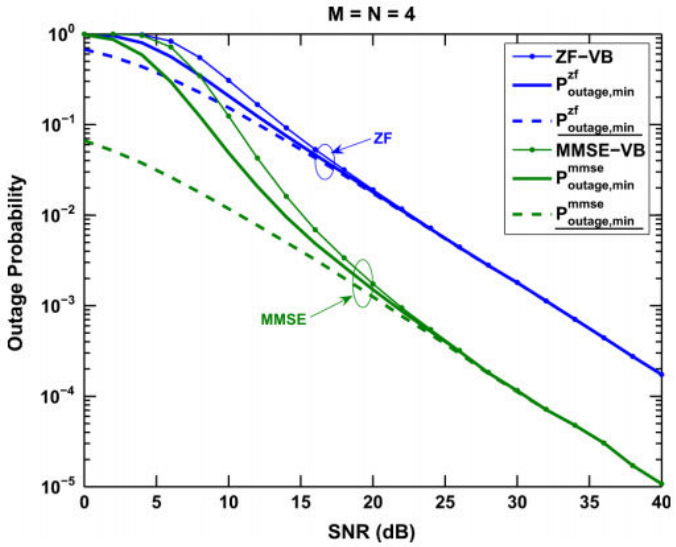

Figure 3.8.1 Outage probabilities of conventional ZF and MMSE vs. V-BLAST [14]

8.2 Lattice-Reduction-Aided Algorithms

An important limit to achieve Shannon channel capacity is the orthogonal high deficiency of the channel matrix $\mathrm{od}(\boldsymbol{H})$. To cope with this problem, one can think of transforming channel matrix $\boldsymbol{H}$ into more orthogonal basis $\tilde{\boldsymbol{H}} = \boldsymbol{HT}$ by means of a transform matrix $\boldsymbol{T}$. This is known in the literature as Lattice Reduction-Aided (LRA) methods [15].

Thus, $\boldsymbol{H}$ is interpreted as the basis of the lattice, where the transform matrix $\boldsymbol{T}$ is designed to reduce orthogonality deficiency and with a shortest length vector, which will lead to better detection performance. Before we proceed we shall define some important lattice theories.

Definition 1. Primal Lattice [16]

Let $\{\boldsymbol{h_1}, \boldsymbol{h_2}, , \dots, \boldsymbol{h_K}\} \in \mathbb{R}^M$ *be a real linear independent set of vectors with* $M \geq K$ *then,*

$$\boldsymbol{L} = \left\{ \boldsymbol{y} \in \mathbb{R}^M : \boldsymbol{y} = \sum_{i=1}^{K} \boldsymbol{h_i r_i}, \boldsymbol{r_i} \in \mathbb{z} \right\},$$

is called a lattice with basis $\{\boldsymbol{h_1}, \boldsymbol{h_2}, , \dots, \boldsymbol{h_K}\}$ *and dimension M.*

Follow this definition, any set of discrete points in $\mathbb{R}^M$ forms a Lattice. With the primal basis, dual lattice can be defined as follows.

Definition 2. Dual Lattice [17]

Given a primal Lattice $\boldsymbol{L}$ *with basis* $\boldsymbol{H}$*, a dual lattice will be unique and defined as follows,*

$$\boldsymbol{L_D} = \{\boldsymbol{z} \in \mathbb{R}^K : \langle \boldsymbol{z}, \boldsymbol{r} \rangle \in \mathbb{z}, \forall \boldsymbol{r} \in \boldsymbol{L}\}.$$

This means that, $\boldsymbol{L_D}$ is the set of points whose inner product with any point $\boldsymbol{r} \in \boldsymbol{L}$ is an integer. There are many LR algorithms in the literature includes, Seysen's algorithm (SA) [18], Hermite–Korkin-Zolotarev (HKZ) reduction [19], Minkowski reduction [20], Lenstra-Lenstra-Lovasz (LLL) [21] and Complex-LLL (CLLL). The most used LR algorithm in the literature is the LLL due to its bounded orthogonality deficiency and its polynomial complexity $O(M^4)$ [3]. Further, the Complex-LLL extend a significant contribution to LLL, where it enables LLL to work in the complex domain with half it

computational complexity. Lately, an Element-based LR (ELR) algorithm was developed to generate a low deficiency channel matrix to reduce the asymptotic error probability of the conventional detectors [22]. This is done by translating the diagonal of the noise covariance matrix after lattice reduction is applied which leads to low complexity algorithm compared to its performance.

9 DOWNLINK PRECODING

Precoding is a generalization of Beamforming, here the second aim to adjust the weight of the channel, (includes the amplitude and phase shift) at each antenna to constructively add the signal at the receiving antenna.

Precoding is the preprocessing coding of the symbols that are ready to be transmitted to the receiver. This is done to reduce complexity at the receiver which is supposed to be with limited resources (e.g. mobile phone). Consider the that the channel h between the transmit antenna and the receive antenna, and the transmitter aim to transmit a symbol s to the user terminal, the received signal at the user terminal will then be $y = hs + n$, with n the Gaussian additive noise. Due to the limited resources of the user terminal, it can only reduce the effect of additive noise by increasing the SNR, while the effect of channel persists. The transmitter, in this case the BS, is considered to have previously estimate the channel. The channel state information CSI a the transmitter make it possible to mitigate the channel effect at the receiver by simply send the symbol s with inverse properties of the estimated channel and hence, if the estimation is perfect, the received signal at the user terminal will be $\frac{y}{h^{est}} = \frac{h}{h^{est}}s + n$.

In Massive MIMO systems, Space-Division Multiple Access (SDMA) is implemented using a precoder. Two types of precoding algorithms are used linear and non-linear precoding. Non-linear precoding is capable of achieving Shannon capacity [23] but with high computational complexity while linear precoders (e.g. (Maximum Ratio Transmitter MRT), MMSE, ZF) prove their ability to approach near capacity with low computational complexity [24].

Non-linear precoding algorithms are mainly based on the concept that any known interference at the transmitter can be subtracted without any additional resources penalty. This is done by Dirty Paper Coding (DPC) [23], where channel capacity can be achieved with such algorithm.

10 LINEAR PRECODING

In this section, we will consider a linear precoding taking place in the downlink where the BS in the j-th cell transmit $\boldsymbol{x}_j \in \mathbb{C}^K$ vector to its K user terminals. This vector is computed by means of a linear precoder vector $\Lambda_{jt} \in \mathbb{C}^M$ as follows,

$$\boldsymbol{x}_j = \sum_{t=1}^{K} \sqrt{\rho_{jk}}\Lambda_{jt}s_{jt} \qquad (3.10.1)$$

Where s_{jt} corresponds to the symbol downloaded to the t-th user terminal in the j-th cell with normalized transmission power $\mathbb{E}\left\{\left|s_{jt}\right|^2\right\} = 1$, each user data signal is controlled by the power gain factor ρ_{jk}. The liner precoder Λ_{jt} determines the spatial directivity of the sent signal and is given here as a Maximum Ratio transmission (MRT) or ZF linear precoder.

We can model the received signal at the k-th user terminal in the j-th cell as,

$$y_{jk=}\sum_{i=1}^{L} \boldsymbol{h}_{jlk}{}^{H}\boldsymbol{x}_j + w_{jk} \qquad (3.10.2)$$

With w_{jk}~$\mathbb{C}\mathcal{N}(\mathbf{0}, \sigma_{DL}^2)$ models the Additive white Gaussian Noise (AWGN) with complex circular symmetric distribution of zero mean and σ_{DL}^2 variance. Due to the reciprocity principle, the channel vector $\boldsymbol{h}_{jlk}$ reserve the same characteristics within the same coherence interval.

In Massive MIMO, the downlink contains no pilots who may reduce the capacity in small MIMO system, but due to a large number of antennas at the base station make it easy for the precoder to reach

the mean value of the specific user. This is one advantage of Massive MIMO; another advantage is that a simple receiver at the user terminal is capable of detecting the signal efficiently without encountering complex computations. The detection at the user terminal is possible using just statistics about the Channel State Information (CSI).

$$\Lambda_{jk} = \begin{cases} \dfrac{\widehat{\boldsymbol{h}}_{jjk}}{\mathbb{E}\left\{\left\|\widehat{\boldsymbol{h}}_{jjk}\right\|^2\right\}} & for\ MRT \\ \dfrac{\widehat{\boldsymbol{H}}_{jj}\boldsymbol{r}_{jk}}{\sqrt{\mathbb{E}\left\{\left\|\widehat{\boldsymbol{H}}_{jj}\boldsymbol{r}_{jk}\right\|^2\right\}}} & for\ ZF \end{cases} \quad (3.10.3)$$

where $\boldsymbol{r}_{jk}$ is the k-th column of $\left(\widehat{\boldsymbol{H}}_{jj}{}^{H}\widehat{\boldsymbol{H}}_{jj}\right)^{-1}$. The channel estimation at the uplink session is affected with the pilot contamination and hence affect the downlink data according to the following relation $\widehat{\boldsymbol{h}}_{ijk} = \frac{\sqrt{P_{jk}}\,\beta_{ijk}}{\sqrt{P_{ik}}\,\beta_{iik}}\widehat{\boldsymbol{h}}_{iik}$ where $\widehat{\boldsymbol{h}}_{ijk}$and $\widehat{\boldsymbol{h}}_{iik}$ are the channel estimation at the j-th and i-th cell and $j \in \int_i$.
The block diagram that can express the downlink precoding scheme in multi-cell massive MIMO can be shown below.

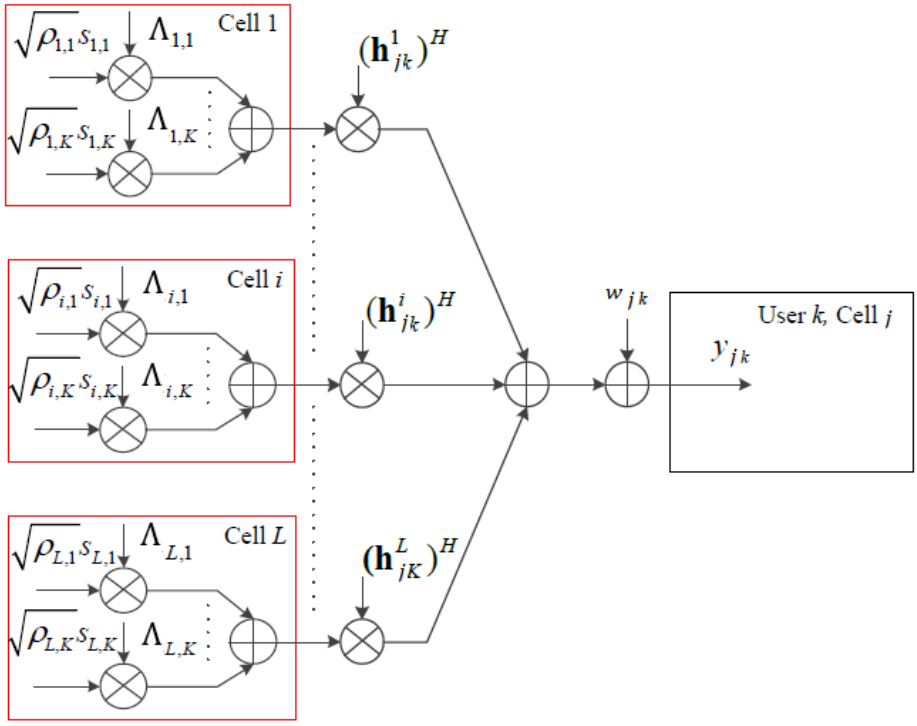

Figure 3.10.2 Precoding scheme in multi-cell massive MIMO

11 NON-LINEAR PRECODER

This section considers a brief overview of the non-linear precoding process. Let $\boldsymbol{x} = f(\boldsymbol{s})$ be a vector that result from mapping symbol vector $\boldsymbol{s} \in \chi$ with dimension B to $\boldsymbol{x}$ with dimension M by means of function $f(): \mathbb{C}^B \to \mathbb{C}^M$.
For instance, the constellation χ is an N-QAM alphabet,

$$\chi \triangleq \left\{\mathcal{K}(z_r + iz_i): z_r \in \left\{\frac{-\sqrt{N}+1}{2}, \dots, \frac{\sqrt{N}-1}{2}\right\}\right\}, \quad (3.10.1)$$

Where $\mathcal{K}$ normalize the average energy of χ to one.
The mapping we consider here is a nonlinear mapping that obtains a non-linear precoder. One known nonlinear precoding technique is the vector perturbation [25]–[27]. This technique perturbs the symbol vector $\boldsymbol{s}$ by another lattice vector $\boldsymbol{p}$ to reduce the transmitted energy. Let $s_i = [\boldsymbol{s}]_i$ belong to a bounded cube region in the complex plane $s_i \in \mathcal{K} = \{a: |Re\{s\}| < 0.5, |Im\{s\}| < 0.5\}$.
Let's construct a vector $\boldsymbol{a}$ such that,

$$\boldsymbol{a} = \boldsymbol{H}^{+}(\boldsymbol{s} + \boldsymbol{p}), \qquad (3.10.2)$$

with $(.)^{+}$ is the Moore-Penrose pseudo-inverse operation and $\boldsymbol{p}$ is the solution to the following minimization problem,

$$\boldsymbol{p} = \arg \min_{q \in \mathbb{Z}[i]^B} \|\boldsymbol{H}^{+}(\boldsymbol{s} + \boldsymbol{q})\|^2. \qquad (3.10.3)$$

where $\mathbb{Z}[i]^B$ is the set of Gaussian integer vector of dimension B.
The precoding function,

$$f(\boldsymbol{s}) = \sqrt{\frac{P}{\mathbb{E}\{\|\boldsymbol{a}\|^2\}}}\,\boldsymbol{a}\,.$$

with P be the transmitted power.
The transmitter will now be $\boldsymbol{x} = \sqrt{\frac{P}{\mathbb{E}\{\|\boldsymbol{a}\|^2\}}}\,\boldsymbol{a}$, and the received signal,

$$\boldsymbol{y} = \sqrt{\frac{P}{\mathbb{E}\{\|\boldsymbol{a}\|^2\}}}\,(\boldsymbol{s} + \boldsymbol{p}) + \boldsymbol{n}. \qquad (3.10.4)$$

The complexity of this precoding technique is high due to the computational cost of solving the minimization problem in Equation (3.10.3) which should take place every TDD session. This complexity may prevent some time sensitive payloads to take place.

12 CONCLUSION

By the conclusion, this chapter introduces different detection and precoding processing techniques while keeping the focus on the linear processing for its low complexity and good performance. First, an overview of some parameters on orthogonality was briefly discussed. Some detection fundamentals and definitions where introduced, including orthogonality deficiency, diversity order gain, spatial multiplexing gain and signal to noise ratio. Then, a brief representation of maximum likelihood detection and its limitation was introduced. Further, an overview on favorable propagation was presented followed with the system model. Considering the uplink scenario, the estimation process in multi-user multi-cell MIMO was discussed using reused training pilots. Considering TDD scheme, in the same coherence interval and using the estimated channel, linear detection includes (ZF, MRC) technique was presented and some algorithms related to non-linear detection was introduced. In the downlink session, precoding techniques with linear (ZF, MRT) as introduced and perform near capacity rate with moderate complexity while nonlinear precoding techniques can perform channel capacity but with additive complexity cost.
This lead us to appreciate the ability of massive MIMO to reach channel capacity with simple linear detectors and precoders.

13 REFERENCES

[1] X. Ma and W. Zhang, "Fundamental limits of linear equalizers: Diversity, capacity, and complexity," *IEEE Trans. Inf. Theory*, vol. 54, no. 8, pp. 3442–3456, 2008.
[2] L. Zheng and D. N. C. Tse, "Diversity and multiplexing: A fundamental tradeoff in multiple-antenna channels," *IEEE Trans. Inf. Theory*, vol. 49, no. 5, pp. 1073–1096, 2003.
[3] M. da Silva and F. Monteiro, *MIMO Processing for 4G and Beyond: Fundamentals and Evolution*. 2014.
[4] S. Verdú, "Computational complexity of optimum multiuser detection," *Algorithmica*, 1989.
[5] E. Agrell, T. Eriksson, A. Vardy, and K. Zeger, "Closest point search in lattices," *IEEE Trans.*

Inf. Theory, vol. 48, no. 8, pp. 2201–2214, 2002.
[6] T. Van Chien and E. Björnson, "Massive MIMO Communications," in *5G Mobile Communications*, Cham: Springer International Publishing, 2017, pp. 77–116.
[7] R. Couillet and M. Debbah, "Random Matrix Methods for Wireless Communications," in *Random Matrix Methods for Wireless Communications*, Cambridge University Press, 2011.
[8] T. L. Marzetta, "Noncooperative cellular wireless with unlimited numbers of base station antennas," *IEEE Trans. Wirel. Commun.*, vol. 9, no. 11, pp. 3590–3600, 2010.
[9] T. Marzetta and A. Ashikhmin, "MIMO system having a plurality of service antennas for data transmission thereof," *US Pat. 8,594,215*, 2013.
[10] N. Shariati, E. Bjornson, M. Bengtsson, and M. Debbah, "Low-complexity polynomial channel estimation in large-scale MIMO with arbitrary statistics," *IEEE J. Sel. Top. Signal Process.*, vol. 8, no. 5, pp. 815–830, 2014.
[11] S. M. Kay, "Fundamentals of statistical signal processing: estimation theory," *Prentice-Hall Signal Processing Series*. p. 595, 1993.
[12] E. Björnson and B. Ottersten, "A framework for training-based estimation in arbitrarily correlated Rician MIMO channels with Rician disturbance," *IEEE Trans. Signal Process.*, vol. 58, no. 3 PART 2, pp. 1807–1820, 2010.
[13] G. D. Golden, C. J. Foschini, R. a. Valenzuela, and P. W. Wolniansky, "Detection algorithm and initial laboratory results using V-BLAST space-time communication architecture," *Electron. Lett.*, vol. 35, no. 1, p. 14, 1999.
[14] Y. Jiang, M. K. Varanasi, and J. Li, "Performance analysis of ZF and MMSE equalizers for MIMO systems: An in-depth study of the high SNR regime," *IEEE Trans. Inf. Theory*, vol. 57, no. 4, pp. 2008–2026, 2011.
[15] D. Wubben, D. Seethaler, J. Jalden, and G. Matz, "Lattice reduction," *IEEE Signal Process. Mag.*, vol. 28, no. 3, pp. 70–91, 2011.
[16] F. Oggier and E. Viterbo, "Algebraic number theory and code design for Rayleigh fading channels," *Found. Trends®*, 2004.
[17] D. Aharonov and O. Regev, "Lattice problems in NP coNP," *Annu. Symp. Found. Comput.*, 2004.
[18] D. Seethaler, G. Matz, and F. Hlawatsch, "Low-complexity MIMO data detection using Seysen's lattice reduction algorithm," *Acoust. Speech*, 2007.
[19] C. Schnorr, "Block reduced lattice bases and successive minima," *Comb. Probab. Comput.*, 1994.
[20] B. Helfrich, "Algorithms to construct Minkowski reduced and Hermite reduced lattice bases," *Theor. Comput. Sci.*, 1985.
[21] M. Taherzadeh and A. Mobasher, "LLL reduction achieves the receive diversity in MIMO decoding," *IEEE Trans.*, 2007.
[22] Q. Zhou and X. Ma, "Element-based lattice reduction algorithms for large MIMO detection," *IEEE J. Sel. Areas*, 2013.
[23] H. Weingarten, Y. Steinberg, and S. Shamai, "The capacity region of the Gaussian multiple-input multiple-output broadcast channel," *IEEE Trans. Inf. Theory*, vol. 52, no. 9, pp. 3936–3964, 2006.
[24] F. Rusek *et al.*, "Scaling up MIMO : Opportunities and challenges with very large arrays," *IEEE Signal Process. Mag.*, vol. 30, no. 1, pp. 40–60, 2013.
[25] A. Razi, D. Ryan, and I. Collings, "Sum rates, rate allocation, and user scheduling for multi-user MIMO vector perturbation precoding," *IEEE Trans.*, 2010.
[26] D. Ryan, I. Collings, and I. Clarkson, "Performance of vector perturbation multiuser MIMO systems with limited feedback," *IEEE Trans.*, 2009.
[27] J. He and M. Salehi, "A new finger placement algorithm for the generalized RAKE receiver," *Sci. Syst. 2008. CISS 2008. ...*, 2008.

Chapter 4: Massive MIMO Interference

The only thing that interferes with my learning is my education~ Albert Einstein

This Chapter introduces interference challenge in 5G networks and mainly on massive MIMO networks. Also, a brief literature review of interference management techniques including multi-cell interference of different levels, advanced receivers and joint scheduling. Further, practical challenges were studied including receiver architecture, realistic interference conditions, channel state information reporting and backhaul links.
Uplink pilot contamination gets the most interest in this Chapter. Where a brief survey on pilot contamination sources, effect and mitigation technique, occupies most of this work.

1 INTRODUCTION

Since cellular system get more densify, interference effect arises to be more severe. The demand on the high dense cellular area is one of the primary issues by ongoing research on 5G networks. According to the 5G Infrastructure Public-Private Partnership, which is a joint initiative between the European Commission and the European ICT industry, demand on high-density network deployment that connects over 7 trillion wireless devices serving 7 billion people is needed [1]. Furthermore, the emergence of services like Machine-to-Machine (M2M) communication, Internet of the Things (IoT), e-learning, e-banking, cloud computing and e-health coped with the evolution of smartphones and tablets, have induced the urgent want for a new generation of cellular network. This network should be capable of offering higher capacity compared to the 4G cellular systems. For instance, mobile data traffic grew 69% in 2014 [2], which is due to the greedy use of smartphones, tablets with video streaming.
Currently, 4G cellular networks, identified by the International Telecommunication Union (ITU), (i.e. IEEE 802.16m and 3rd Generation Private Public Partnership 3GPP LTE-Advance), can support an average spectral efficiency of 2 bps/Hz and a maximum of 15 bps/Hz with ultra-low latency and bandwidth of approximately 100 MHz [3]. Nonetheless, the growth in data traffic, cell density and latency exceeds the capability of 4G. Thus there is a need for 5G cellular networks. New key technology components are expected to be introduced in the 5G networks, i.e. Massive MIMO, mmWave MIMO, device-to-device communication and large-scale machine communication. To meet the heightened demands [4], many ongoing types of research includes collaborative projects (i.e. 5GNOW and Mobile and Wireless Communications Enablers for the Twenty-twenty Information Society (METIS) [5]), have taken up the challenge.
One key technology that had been defined by METIS to require significant advancement under multi-node/multi-antenna is Massive MIMO [5]. Massive MIMO is expected to offer high data rate as well as enhanced coverage, link reliability, spectral and energy efficiency; thus, it attracts a lot of research interest. Many studies have been carried out to analyses its benefits as well as its limitations and challenges [6]–[12]. To achieve the promised gain in Massive MIMO, the base station should accurately estimate the channel matrix to each user, which can be done using pilot training that can take place in Frequency Division Duplexing (FDD) or Time Division Duplexing (TDD) scheme. In many types of research on channel estimation [6]–[12], TDD scheme is preferred over FDD, since in TDD we require channel estimation on the BS. However, FDD channel estimation should take place at the user terminal and feedback to the base station. Due to the massive number of antennas at the BS, which will lead to large channel matrix. Due to the limited resources computational and energy at the user terminal, it is suggested to use the TDD scheme over FDD.
Considering TDD architecture, channel reciprocity is the main principle, where the channel during the uplink session is supposed to be equal to the conjugate of that in the forward link within the same

coherence interval. The channel estimation obtained by pilot training is exploited for uplink data reception and downlink precoding within the same coherence interval. Due to the limited length of the coherence interval and due to a large number of user terminals in the same interference region, pilot reuse will cause severe interference problem, which will eventually degrade the system sum-rate. This type of interference resides under Inter-Cell Interference where in most cases users from across cell that reuse the same pilot get interfered during an uplink training session.
In the case of non-perfect Channel State Information (CSI) at the base station, downlink precoding will cause Intra-Cell Interference among users within the same cell. Intra-cell interference also can be due to imperfect hardware implementation and impairment between circuits. Imperfect receivers also can boost intra-and inter-cell interference intensively.

Another issue that will increase the effect of interference is the cell edge user terminals (UT's). This problem persists from the previous generation and gains much attention during the last two decades.
The term interference in this chapter is related to the inter-cell interference and intra-cell interference. The aim of this chapter is to focus on the inter-cell interference caused by users from distinct cells, mainly in Massive MIMO networks and especially the one related to pilot contamination at the uplink TDD session.

2 INTERFERENCE MANAGEMENT TECHNIQUES

The most two factors that limit the performance of mobile networks are Interference and fading. While the first limit the coverage and reliability of wireless links, the second boundary is the reusability of the resources (i.e. frequency, codes, time slots, pilots, etc.). Fading can be easily overcome by compensating the decayed signal at the transmitter leaving interference as the primary challenge facing mobile system designers. One attempt to overcome interference is by implementing cooperation in the wireless network. Two scenarios are envisioned for cooperation, the first is by considering a virtual MIMO network and the second is by implement additional relay layers. Considering virtual MIMO, physical base stations are equipped with an array of antennas that may be a member of a virtual base station based on an interference mitigation clustering technique. In such scenario, even geographical cell area will be considered dynamic and shaped based on the coverage area of the virtual antenna array (i.e. [13]–[15]).

Non-cooperative approaches to mitigate interference, prevent spatial resources reuse (i.e. frequency within a certain cluster of cells). In such scenarios, frequency reuse factor lags unity. Thus the co-channel interference level is low. Hence, interference is managed at the base station by controlling the frequency reuse and maximizing spectral efficiency. Techniques like Code Division Multiple Access (CDMA) and Frequency Hopping, allow the full reuse of frequency resources unless this leads to severe interference at the cell edge and lack of fairness among cell user terminals.
Inter-cell coordination is introduced to mitigate interference in some studies unless such technique is not welcome with user scheduling mechanisms (e.g. cell breathing) and soft handover mechanisms. At the receiver side, inter-cell interference is considered as noise and handled by resorting to improve the link between the user terminal and base station [16].
Ongoing research on network design, recruit interference-aware multi-cell coordination techniques on the base station side to treat interference. Such techniques can be done using a coordination protocol that takes into consideration the coordination of physical and MAC layer resources (e.g. time slots, power level, beamforming coefficient, subcarrier usage). A global channel information and resources management information should be shared over backhaul links, an example of existing link technologies (e.g., 4G LTE, 802.16 WiMax). The complexity of the coordination protocol varies widely from one proposition to another, keeping a tradeoff between performance, overhead backhaul data and over-the-air feedback channels. The table below shows several interference mitigation techniques, their benefit, and their prospects.

Technique	Benefit	Key shortcomings	Prospects
Frequency reuse	Reduces OCI very simply and effectively	Low spectral efficiency, frequency planning	Not promising as a long-term solution
Maximum likelihood MUD	Optimum co-reception of signal and interference	Very high complexity, OCI awareness	Moore's law will help complexity, but prohibitive in near future
MMSE MUD	Suppresses OCI with much lower complexity than ML	Requires awareness of OCI, many mobile antennas; simpler versions have only modest performance gain	Requires instantaneous OCI knowledge, under present investigation by industry
OCI-blind MMSE	Like ZF spatial receiver with lower noise enhancement	Enhances OCI rather than suppressing it: very poor performance	Will provide only incremental gain (10–25%), but likely to be implemented
Other-cell interference cancellation	Good performance vs. complexity	Complexity still high, awareness and accuracy of OCI knowledge crucial	Promising in long- to provide additional gain over OCI-blind receivers
Stream control	Reduces OCI; increases robustness	Lowers the data rate	Adaptive stream control is feasible and useful
Multiuser diversity	Decreases required transmit power or increases data rate	Competes with other forms of diversity like frequency diversity; log log *N* growth (i.e., rapidly diminishing returns)	Like to be useful in terms of scheduling, but not very effective for OCI reduction
Cooperative encoding, i.e., dirty paper coding	Optimal performance in theory	Requires very accurate channel knowledge and realtime intercell coordination	Unlikely to be practical in foreseeable future, if ever.
Closed-loop MIMO diversity	Achieves optimum diversity performance	Sacrifices spatial dimensions for multiplexing, channels known at Tx	Likely to be implemented, can lower OCI somewhat.
Beamforming	Reduces OCI	Sacrifices spatial dimensions, channels known at Tx	Has important merits, but implementation difficulties
Cooperative transmission	Reduces OCI, multiuser diversity gain relative to frequency reuse	Requires simple cooperation between base stations	Feasible in the short-term
Distributed antenna systems	Reduces OCI through lowered transmit power; better coverage; ease of maintenance	Requires new infrastructure deployment paradigm	Feasible in the short-term with large infrastructure investment

Table 4.2.1 Interference mitigation techniques [17]

2.1 Multi-cell Interference

Base station cooperation is an old technique in mobile networks, where mobile terminal used to communicate with the neighbor base station to overcome the effect of short-term and long-term fading (e.g., hand-off). In conventional mobile networks, such as CDMA, the mobile station communicates with several base stations for the decision of the next connection as a soft-handoff approach. The diversity selection aims to increase both capacity and coverage [18], and when coped with power control it will allow for frequency reuse in each cell.

2.2 The different levels of multi-cell cooperation

In this part, we will discuss the various levels of multi-cell cooperation that are most used in the literature.

2.2.1 Interference coordination

Interference coordination is since the channel state information is shared via a feedback link. By using channel state information, base stations can manage the direction of beamforming, power allocation and user scheduling in time and frequency. With a modest amount of backhaul data, base stations can reach good performance especially if many users exist in the system [19]. Since no sharing of signal level synchronization or transmission data between base stations, this interference management technique is referred to it as, *interference-coordination.* Base stations follow this

interference management scheme, handles the transmission data corresponds only for their *K* user terminals.

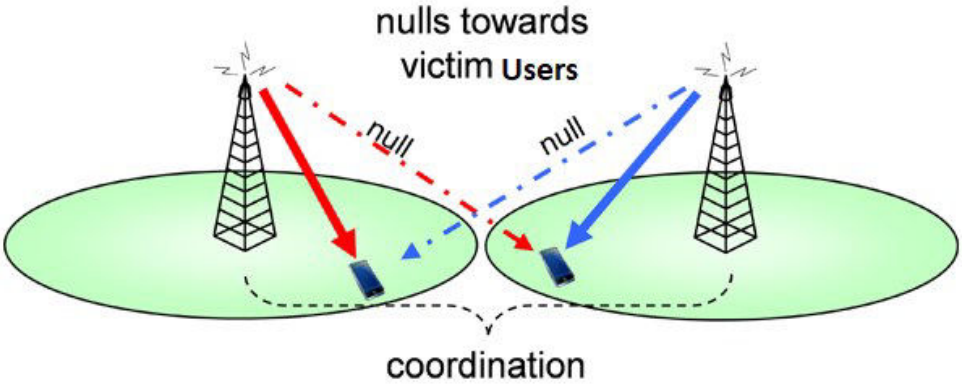

Figure 4.2.1 Specific coordinated beamforming [20]

2.2.2 *MIMO cooperation:*

If both channel state information and transmission data are shared between base stations, cooperative beamforming can be achieved. In such scheme, each user terminal can be served by a combination of antennas belong to different bases stations having the maximum SNR over this channel. Considering this cooperation, multi-cell MIMO will act as a multi-user MIMO and a virtual base station consist of antennas belong to different physical bases station will exist. This type of cooperation cannot be achieved unless a low delay with high capacity links occurs between base stations. Otherwise backhaul overhead will limit the system capacity.

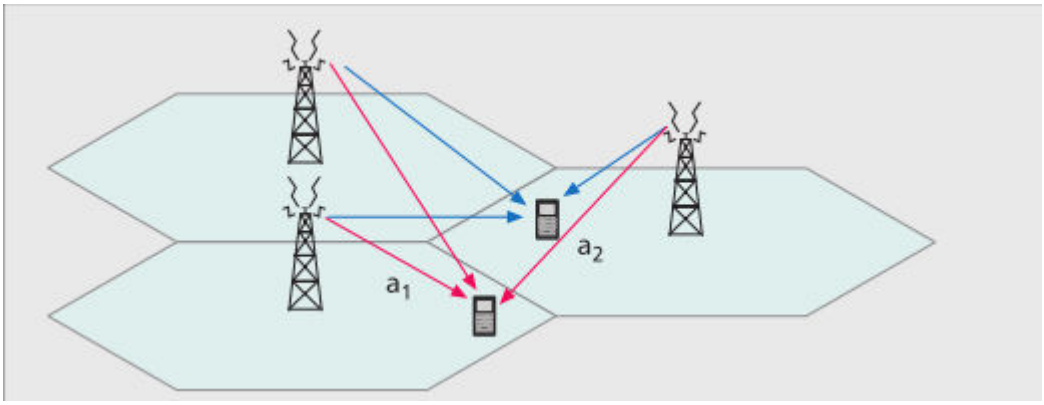

Figure 4.2.2 MIMO cooperation [21].

Cooperative MIMO channel models studied extensively in the literature, but the WINNER II channel model is the most comprehensive one [22], which includes 13 scenarios presented in (Table 4.2.1).

- A1: indoor (small office/residential), A2: indoor to outdoor
- B1: urban microcell, B2: bad urban micro- cell, B3: indoor hotspot, B4: outdoor to indoor, B5: stationary feeder
- C1: suburban macrocell, C2: urban macro- cell, C3: bad urban macrocell, C4: urban macrocell outdoor to indoor
- D1: rural macro-cell, D2: moving networks.

The above scenarios can be used to describe most of the MIMO channel links. For instance, four scenarios on relay models were studied in [23], includes (in-building coverage, fixed infrastructure, temporary coverage and mobile vehicle coverage). By comparison, cooperative MIMO channel model can selectively apply using the 13 scenarios defined in the WINNER II channel model.

Cooperative MIMO scheme	Link type	Description	Recommended scenario
CoMP	BS-MS	MS indoor	C2 (NLoS)
		MS outdoor	C2 (LoS)
Fixed relay	BS-MS	Indoor or outdoor	C2
	BS-RS	Various RS locations	B5 (LoS/NLoS)
	RS-RS	Various RS locations	B5 (LoS/NLoS)
	RS-MS	Indoor-to-indoor	A1 (LoS/NLoS)
		Indoor-to-outdoor	A2 (NLoS)
		Outdoor-to-outdoor	B1 (LoS/NLoS)
Moving network	BS-MS	Indoor	C2 (NLoS)
	BS-RS	LoS for RS	C2 (LoS)
	RS-MS	Indoor	B3 (LoS/NLoS)
Mobile user relay	BS-MS	Indoor or outdoor	C2
	MS-MS	LoS	B5b (*not aN M2M scenario*

Table 4.2.2 A cooperative MIMO channel model based on the WINNER II channel model [21].

For more information on cooperative MIMO channel models, see [21].

2.2.3 Rate-limited MIMO cooperation:

Considering a limited backhaul link between base stations, one can think of quantizing user data and share it between cooperative base stations. First the channel state information must be shared, then the requested sub-stream of user data will be quantized and shared. Such a hybrid technique is referred as *Rate-limited MIMO cooperation*.

2.2.4 Relay-assisted cooperation:

Cooperation can be done between an assistant relay and the base station. This cooperation will save the backhaul links between base stations from data overhead. The assisted relays can decrease the area of the interference regions and strengthen the link between the base station and the user terminal. Thus the resources reuse factor will increase and more accurate coverage in the cell.

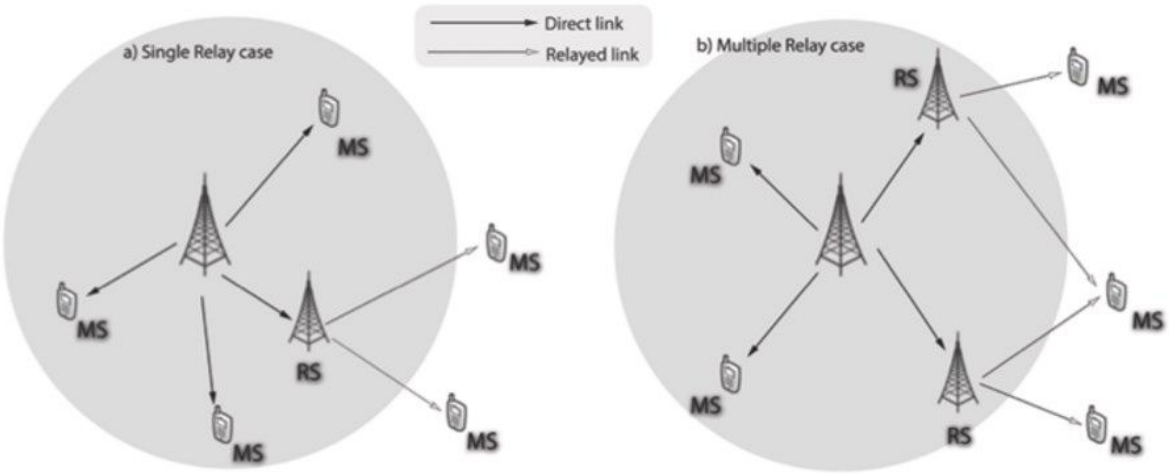

Figure 4.2.3 Single and multiple relay case [24]

2.3 Advanced Receiver

Normally, classical receivers assume a moderate noise scenario. This noise can be mitigated using an optimal receiving technique such as Maximum Aposterior Probability (MAP) and Maximum Likelihood (ML) receiver, or by a sub-optimal receiving technique such as Zero Forcing (ZF), Maximum Combinational (MC) and Minimum Mean Square Error (MMSE) receivers. Such a classical approach deal with interference as noise. However, in real scenarios, noise and interference are of a different structure regarding statistical distribution and correlation with transmitted data. For instance, interference is like the preferred signal, where it is generated using similar modulation technique, similar coding and selected from the similar constellation, since they should be the desired signal in other cells. For this reason and more, noise and interference signals must be considered separately. Due to the severe loss in performance, interference randomization techniques are employed to treat the interfered signal as noise-like. However, these techniques are not suitable for high interference scenarios, where the severe loss in performance can arise.

For the 5G mobile network, an advanced technique should be added to the receivers, and a new generation of interference management should take place. Advanced Interference Management (AIM) techniques go beyond the standard receivers to access interference signal structure including, coding scheme, modulation constellation, and resource allocation. This added authority can be exploited to decode the interference signal and separate the signal in higher layers rather than a physical layer. Advance receiving techniques thus can help improve the system performance even with partial decoding/detection of the interference signal.

In the 5G networks, a large number of antennas at the base station is possible, which allows for a new type of transmission scheme, for example, multi-user MIMO, superposed transmission and spatial multiplexing due to spatial beamforming. Thus, not only inter-cell interference mitigation is possible, but also intra-cell interference can be mitigated using the same advanced receiver. Also, within an interference-free region, advanced receivers are capable by decoding to increase the spatial layer of the signal and thus increase the capacity of the system.

In the 4G and before, receivers issue had been considered an implementation issue and advanced receiving at the mobile side was not considered attracted study, due to the low computational capabilities at the user terminal. However, advanced interference mitigation at both sides (user terminal and the base station) will boost the performance of the system and considered an attractive field especially with the new generation of smartphones that implements a moderate computational resource. This leads to a more mature form of advanced receivers that will be included in the next 5G networks.

2.4 Joint Scheduling

Advanced co-channel interference management does not appear in the earlier LTE standard releases (release 8, 9), outside of interference randomization that was introduced in release 9. By the release of

3GPP, LTE-Advanced releases 10,11, an improvement on the cell edge was presented by a coordinated transmission which takes place among multiple transmitters distributed in different adjacent cells. This fact leads to the initiation of Coordinated Multiple Point (CoMP) transmission, which was the core of Release 11. Another scheme, including coordinated scheduling (CS), dynamic point selection (DPS), coordinated beamforming (CB), and joint transmission (JT), were mentioned in the standardization course of CoMP. Unless, they were not implemented in Release 11, except for some new devices like new reference and control signals. For the next generation, and to obtain interoperability with rapid deployment, advanced interfere management should be studied and specified in details. Furthermore, interference management on user terminal side should be taken into consideration to optimize the system performance.

3 PRACTICAL CHALLENGES

For the real implementation, several issues should be considered. For instance, receiver architecture, realistic interference condition and channel state information reporting for advanced interference management can lead to ever loss in system performance if they are not considered.

3.1 Receiver Architecture

Optimal coding schemes such as Dirty-Paper Coding (DPC) and Gaussian Random Coding (GRC) are far from practical implementation due to their high computational complexity. However, practical systems used to implement coding schemes such as, bit-interleaved coded modulation (BICM) that use quadrature amplitude modulation (QAM), space-time precoding and turbo/low-density parity check (LDPC) codes. At the receiver side, optimal joint decoding is also impractical due to its high complexity. Instead, when code block length and modulation order are large enough, a turbo iterative receivers provides suboptimum performance [25]. Such a receiver aim to detect the interfered and the preferred signal jointly. A block diagram of the advance iterative receiver is illustrated in Fig. 4.3.1. As can be seen from the figure, an iterative exchange between the detection and decoding blocks take place in the middle using Log-Likelihood-Ratio (LLR), while at the end only the decoded preferred signal exists.

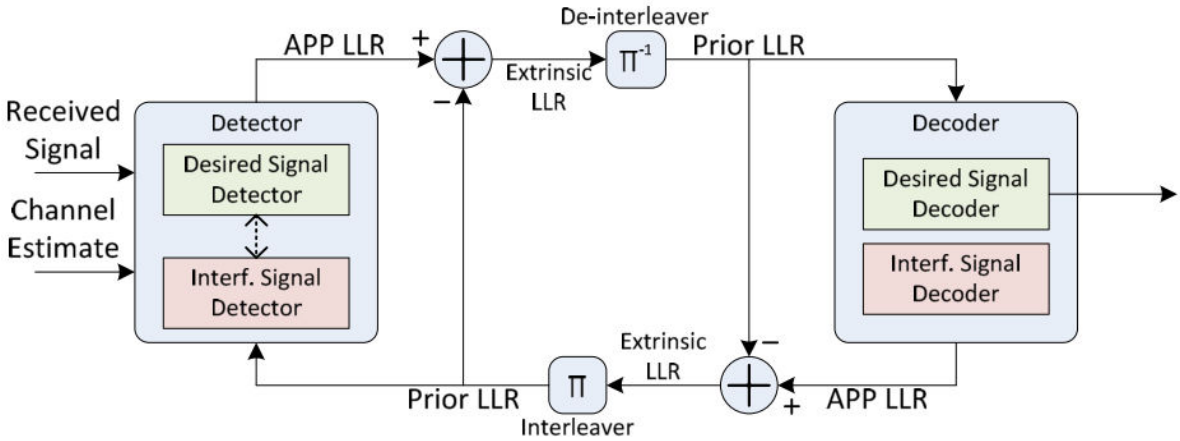

Figure 4.3.1 Iterative Receiver [26]

As not to increase the complexity of the receiver, some optimal decoding and detection schemes, such as, maximum a posteriori probability (MAP) detector that perform optimal performance, can be replaced with a successive interference cancellation (SIC) based detector with a negligible performance loss. In a high SNR regime scenario, decoding of the interference signal can be ignored, and direct signal detection can be done.

3.2 Realistic Interference Condition

Many interference signals represent practically interference, but dealing with all these signals is technically oppressive. Thus, only interference signals that are beyond the noise level and at the edge of the preferred signal are considered. Consequently, dealing with only dominant interference signals is sufficient to reach sub-optimal receivers. As previously mentioned, part of the interference signal should be known at the receiver. For instance, interference channel information should be known at the receiver to detect and decode the signal. Also, control signaling between network base stations should afford a comfort sharing media to transfer resources allocation, coding, and modulation schemes. Other extra information about the interference signal can be blindly estimated to avoid backhaul signaling overhead. Nevertheless, this will add extra computational complexity to the receiver especially if the estimate was inaccurate.

3.3 Channel State Information Reporting

Considering the transmitter should be aware of the channel characteristics and interference information. In LTE, this was implemented by a single feedback report of the CSI from the user terminal. Single CSI feedback report is not sufficient to address the interference characteristics at the user terminal, thus for the next generation network, multiple reports will take place. This framework had already supported by CoMP LTE Release 11. The multi-point multi-report feedback allows the transmitter to have a wide look on interference to apply advanced interference management techniques. Worth to mention, that even with the multiple-CSI-feedback framework, the transmitter can suffer from inaccurate CSI information which is practically due to the imperfect CSI acquisition.

3.4 Practical Joint Scheduling

The main issue that takes place in joint scheduling is the clustering optimization that is characterized by selecting the best transmitting and receiving group of terminals. This clustering mechanism can be done in a centralized or distributed scheme. Considering the centralized scheme, the selection is made by a centralized controller that is responsible for taking the decision on which transmitting point should serve another selected set of user terminals. This scheme considered dominating over distributed one. However, it is more computationally expensive and overloads the network backhaul with control signaling. Considering the distributed scheme, each transmitter will do its calculation to optimize an objective function of a belief propagation to select the best set of user terminals to be served and share a small amount of information with other transmission points for coordination issue [27].
In large cluster scenario, distributed scheme is desirable due to its limited information exchange and low complexity, unless it also grieves from the severe delay.
In view of joint scheduling coped with multiple CSI feedback, the receiver channel characteristic curve is constructed based on the inaccurate CSI information. Look for example at the discrete curve in the illustration (Fig. 4.3.2).

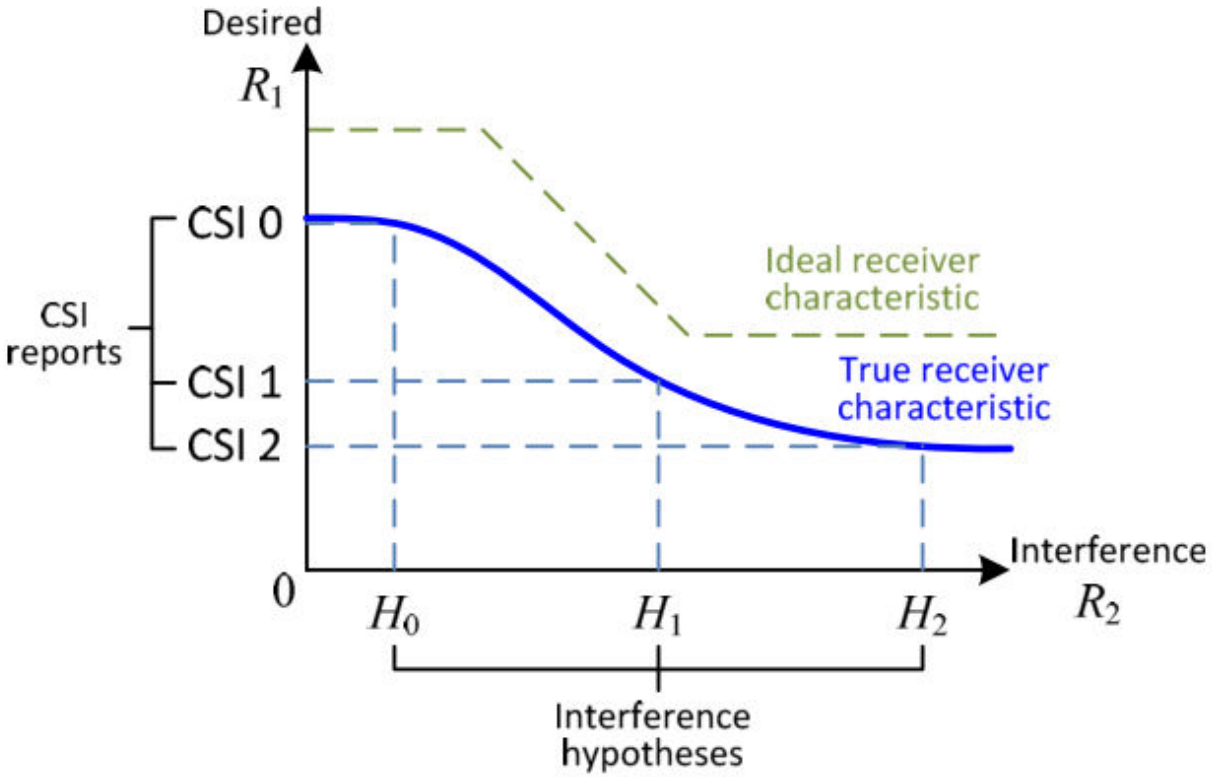

Figure 4.3.2 Channel Characteristic Curve vs. interference hypotheses [26]

The lake of accuracy in the feedback report and thus in the hypothesis will result in a bad scheduling scheme. To compensate the inaccurate hypothesis of the curve, some techniques such as outer loop link adaptation can be used. It can be done by controlling the feedback request strategy. For instance, if consecutive acknowledgment takes place the scheduler, will be less conservative. In contrast, if acknowledgment message was missed, the scheduler will be more conservative.

3.5 Backhaul Links

In the previous sub-section, both centralized and distributed scheme inexorably need to use the backhaul of the network to exchange coordination information. However, backhaul links are practically non-ideal and can be easily overflood. For this reason and more, network backhaul gets much concern in the 5G architecture. Thus, a need for more reliable backhaul links with high capacity is an urgent matter. Consequently, the backhaul message units of joint scheduling should be concisely studied in the standard for the interoperability of different base station developers.

4 PILOT CONTAMINATION

To achieve Massive MIMO capacity, accurate CSI should be estimated. Unless several challenges face channel acquisition. For instance, pilot contamination is one of the main difficulties that countenance performing accurate estimation.

Channel estimation through training takes place in two states, either by feedback or by reciprocity scheme. Thus, channel training can be done via Frequency Division Duplexing (FDD) scheme, where CSI feedback will take place, or via Time Division Duplexing (TDD) scheme, where channel reciprocity will be considered. TDD scheme is preferred in the literature since it only needs channel estimation while FDD needs estimation and feedback. Also, as the number of antennas grows, the feedback information size will eventually increase [6], [8], [28].

METIS suggest the use of TDD for massive MIMO [5] since it efficiently exploits the radio resources. However, some studies suggest the use of FDD scheme [29]–[31].

In TDD scheme, channel reciprocity should be considered, where the channel at the uplink is supposed to be approximately equal to the transpose of that at the downlink session [32]. Hence, at the uplink session, all user terminals should upload their pilots, as to have the channel being estimated. Supposing each terminal is uploading an orthogonal pilot sequence, the number of pilot symbols that should be uploaded should be greater than or equal to the number of user terminals that uploads their frams at the same time slot [30]. This constraint will lead to a limited number of users per cell and pilot reuse in adjacent cells. Consequently, users belong to distinct cells may upload the same pilot sequence which will lead to uplink pilot contamination (see figure 4.4.1). This phenomenon will lead to a severe reduction in spectral efficiency [33] and an increase in the inter-cell interference ratio, which is proportional to the number of antennas [34].

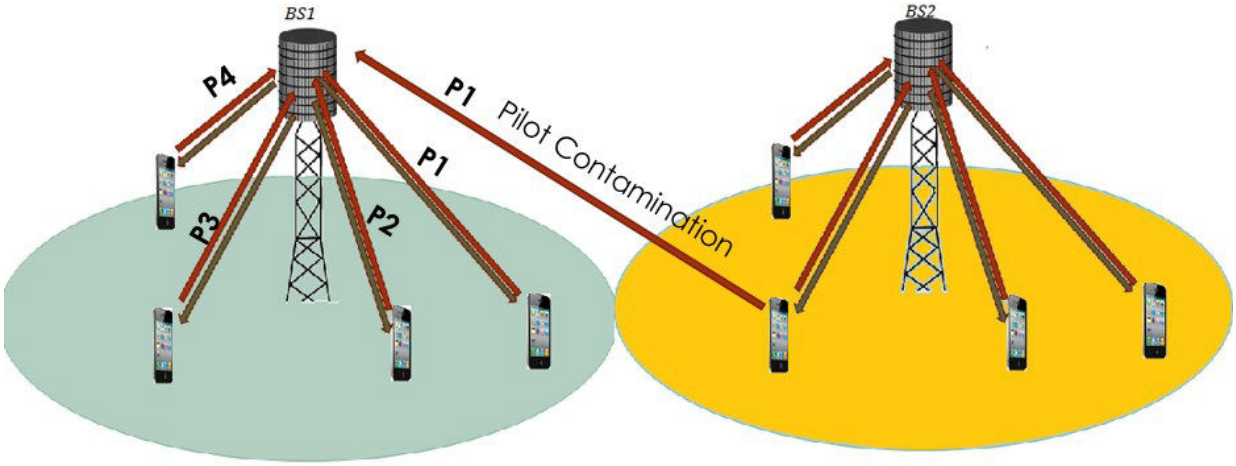

Figure 4.4.1 Uplink Pilot Contamination in a multi cell scenario where BS1 receive pilots from adjacent cell.

4.1 Channel State Information Acquisition

One of the main tasks in Massive MIMO system is the acquisition of accurate CSI, which is also considered a special issue in many 4G and 5G wireless communication systems [35]. When the CSI is more precise, it helps increase the accuracy of focusing the beam in downlink and collecting data with higher power during the uplink session. This fact, made searching the best channel estimation methods, an urgent need. The effect of channel estimation on system performance was studied widely in the literature (see [36], [37]). Channel estimation can be driven by one of the following three techniques, training sequence [36], blind estimation [38] and semi-blind estimation [39]. Considering training sequence, training overhead decrease system performance by reducing the spectral efficiency and resource reuse. However, blind based estimation need higher computational complexity to be achieved. In what follows, we will focus on the training based estimation using pilots as the training sequence.

4.2 Training Methods

Using training based estimation, a pilot sequence which is known at both the receiver and the transmitter is used to estimate the channel between the user terminal and the base station [40]. Two different schemes do this, the first usual one is the standard time division multiplexing scheme, and the second scheme is called superimposed pilots. Considering classical pilot training, each frame contains a dedicated part for sending pilots. However, using superimposed pilot scheme, the pilots are superimposed over the data during the training session [41]. A study in [42], [43], shows the performance analysis of classical and superimposed schemes. Classical pilot training estimation scheme is classified based on mutual information and signal processing parameters [42].

A key question that could be asked in this manner is, “how much training time is required for a given number of antennas?” [32]. There is always a tradeoff between the accuracy of the channel estimate, and

the consumed resources include (spectral, computational and financial). This tradeoff plays the key role of how to choose the optimal estimator.
Since Massive MIMO uses many antennas at the base station, it is necessary to use low computational complexity estimator scheme. Linear estimator such as maximal Ration Combination (MRC), Minimum Mean Square Error (MMSE) and Zero-Forcing (ZF) estimators was considered best choice in massive MIMO especially for their linear complexity compared to blind estimation and semi-blind schemes.
The following table (Table 4.4.1) shows different estimation schemes and their performance.

Reference	Scheme	Estimation Methods	Performance	outcomes
[44]	Semi-orthogonal pilot	Successive Interference Cancellation	Throughput, Mutual information	The proposed scheme overcome the conventional scheme at high and low SNR
[45]	Semi-Blind	Least Square, Semi-Blind Maximum-a-posteriori (MAP)	Subspace estimation error, sum-rate	Semi-Blind Maximum-a-posteriori (MAP) surpass Least Square even with dwindling number of antennas at the BS
[46]	Zhadoff Chu Sequence-based pilots	Chu sequence is used to allocate different phase shift on pilot sequences in the near cells	Signal to Interference Noise Ratio (SINR)	Chu sequence pilot surpass conventional pilots on the dimension of SINR and eliminate partial interference
[47]	Conventional TDD pilots	Diagonalized Estimator, coined Polynomial Expansion Channel (PEACH), the Bayesian channel estimator	Computational complexity, Minimum Square Error (MSE)	The lowest complexity is done by PEACH estimator compared to MMSE and W-PEACH
[48]	Zhadoff Chu, conventional sequence pilots	Joint channel estimation using improved MMSE	Computational cost	Improved MMSE overcome conventional MMSE with a ratio of 61%

Table 4.4.1 Estimation Methods and Performance Analysis

4.3 TDD Based Training

Based on the reciprocity principle, where the forward channel is assumed to be equal to the backward, Time Division Duplexing (TDD) considered a satisfactory solution [32]. Furthermore, TDD uses the same frequency resources in the uplink and downlink, which makes it favorable in congested systems.

In advance of this, CSI feedback will be eliminated, and uplink training is sufficient for CSI acquisition [49]. However, the limitation of coherence interval should be taken into consideration. Thus, orthogonal pilot sequences are constrained by the length of the coherence interval. TDD works well with Massive MIMO; this is because system performance can be scaled up with the number of the antenna to a specific extent [35] since channel estimation takes place completely at the base station with no CSI feedback.
TDD scheme works in two phases; first user terminals should send their pilot sequences during the

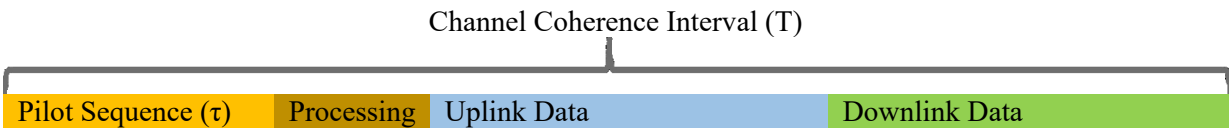

Figure 4.4.2 Conventional TDD Frame

uplink session while the BS estimates the channel matrix and prepare the precoding matrix. At the second phase, the BS uses the precoding matrix to estimate the uplink data from user terminal send then use it to precode the downlink data to user terminals. An illustration of the TDD frame is presented in the figure 4.4.2 below.

4.4 FDD Based Training

In this chapter, we will briefly discuss FDD scheme to focus on the scope of this thesis. Frequency Division Duplexing FDD is another scheme for pilot based training where a dedicated channel is assigned for downlink and another for uplink. Channel estimation under FDD scheme has been studied widely in the literature (see [50], [51]). Since the precoding and the detection in downlink and uplink use different frequency bands, CSI feedback is required. The CSI is obtained after the base station sends its pilot in the downlink to the user terminals, where the user terminals had to estimate a partial or a complete version of the CSI and feed it back to the base station. Considering a Massive MIMO system, the substantial number of antennas at the base station and the limited computation; resources at the user terminal, makes FDD scheme hard to be implemented. Where the computational complexity scales up with the increase in the number of antennas at the base station [52]. Comparing to TDD systems, FDD is not preferred in Massive MIMO systems in the sense that TDD complexity scales only with the number of user terminal antennas. Regarding pilot contamination, FDD works better than TDD unless more resources are required.

4.5 Channel Model

This section presents two type of channel models, independent and spatial correlated model. Where the first is a statistical model that assumes each user has an independent channel, which is far from realistic scenario but simple to implement, while the other take into consideration the special location of the user terminal and base station antennas.

4.5.1 Independent channel

Considering a system with L cells each holding one base station equipped with M antennas and serving K single-antenna user terminal, where $K \ll M$. Denotes by $h_{jlkm} = \sqrt{d_{jlk}}\, g_{jlkm}$ (4.4.1) the independent channel propagation factor between the *m-th* antenna of the *j-th* base station and the *k-th* user in the *l-th* cell. Where we denote by g_{jlkm}, the small-scale fading coefficient which is independent and identically distributed circularly-symmetric complex Gaussian with zero mean and unit variance $\mathbb{CN}(\mathbf{0}, 1)$, random variable and d_{jlk} represents the large-scale fading coefficient.
This channel model is introduced in many studies in the literature includes, [7], [32], [53], [54].
The matrix form of the channel modeling the relation between the K user terminals in the *l-th* cell to the M antennas of the *j-th* base station can be represented as follows:

$$\boldsymbol{H_{lj}} = \boldsymbol{D}_{lj}^{1/2}\boldsymbol{G}_{lj} = \begin{bmatrix} h_{jl11} & \dots & h_{jlK1} \\ \vdots & \ddots & \vdots \\ h_{jl1M} & \dots & h_{jlKM} \end{bmatrix},$$

Where,

$$\boldsymbol{G}_{lj} = \begin{bmatrix} g_{jl11} & \cdots & g_{jlK1} \\ \vdots & \ddots & \vdots \\ g_{jl1M} & \cdots & g_{jlKM} \end{bmatrix},$$

and

$$\boldsymbol{D}_{lj} = \begin{bmatrix} d_{jl1} & & \\ & \ddots & \\ & & d_{jlK} \end{bmatrix}.$$

This model assumes a different small-scale fading at each antenna of the base station and the user terminals while assuming the same large-scale fading at the different antenna of the same base station.

4.5.2 Spatial correlation channel model

Spatial correlation channel model was used in many studies in the literature, (e.g. [55]–[57]), and it is represented by the statistical correlation between channel matrix entries. Considering this model, the correlation between antenna elements at the base station and the user terminal is presented.

Let represent by $\boldsymbol{h}_l$ the $M\times 1$ channel vector between the user in the *l-th* cell and the responsible base station. Then, $\boldsymbol{h}_l = \boldsymbol{R}_l^{\mathbf{1/2}}\check{\boldsymbol{h}}_l$ (4.4.2), with $l=1, 2,\ldots,L$ and $\check{\boldsymbol{h}}_l \sim \mathbb{CN}(\mathbf{0}, \boldsymbol{I}_M)$, denotes the white spatial $M\times 1$ SIMO channel vector with zero mean and identity covariance $\boldsymbol{I}_M$. The spatial statistics is described by the covariance channel matrix $\boldsymbol{R}_l \triangleq \mathbb{E}\{\boldsymbol{h}_l \boldsymbol{h}_l^H\}$.

4.6 Pilot contamination in uplink and downlink

The two-way communication scheme during TDD frame includes uplink and downlink, where training pilots are uploaded during the uplink session. In this sub-section, a brief discussion about the Uplink session and the downlink session will be introduced, shed the lights on the uplink pilot contamination in what follows.

4.6.1 Uplink performance

During the uplink session, each user terminal uploads a training pilot sequence of length τ to the base station. However, due to the limited channel coherence interval, limited orthogonal pilot sequence pool is not sufficient for all user terminal. Hence, pilot sequence reuse may take place, especially in cross cells.

Considering the worst-case scenario, we assume that all user terminals among the L cells are synchronized, so they upload their pilots at the same time. This issue will contaminate the signal at each base station and leads to pilot interference. Due to the lack of orthogonality between the received signal at the base station, channel estimation will be the main challenge, and an inaccurate CSI will be estimated.

Let's denote by $\boldsymbol{\phi}_j = (\boldsymbol{\phi}_{j1}, \ldots, \boldsymbol{\phi}_{jk})$ of dimension $l \times K$, the pilot matrix that holds orthogonal pilot sequences of all K users of the *j-th* cell and satisfy $\boldsymbol{\phi}_j^T \boldsymbol{\phi}_j = \tau \boldsymbol{I}_K$.

The received signal at the base station can be found in equation (3.7.2), where the estimated CSI in equation (3.7.3), will also be used at the uplink session to separate the received signals at the receiver. Therefore, noisy received data will be obtained at the receiver.

A common metric to evaluate the performance of 5G network in the literature is the ergodic channel capacity. Worth to mention that it is hard to obtain particular channel capacity for a user terminal, due to channel change over time and imperfect CSI. However, lower bound on uplink ergodic capacity can represent by the following theorem.

Theorem 4.4.1 [58] *The lower bound on uplink ergodic channel capacity of the k-th user in the l-th cell can be given as:*

$$C_{lk}^{UL} = \gamma^{UL}\left(1 - \frac{\tau_p}{\tau_c}\right)\log_2(1 + SINR_{lk}^{UL}) \qquad (4.4.3)$$

where,

$$SINR_{lk}^{UL} = \frac{p_{lk}|\mathbb{E}\{\boldsymbol{v}_{lk}{}^{H}\boldsymbol{h}_{llk}\}|^2}{\sum_{i=1}^{L}\sum_{t=1}^{K} p_{it}\mathbb{E}\{|\boldsymbol{v}_{lk}{}^{H}\boldsymbol{h}_{lit}|^2\} - p_{lk}|\mathbb{E}\{\boldsymbol{v}_{lk}{}^{H}\boldsymbol{h}_{llk}\}|^2 + \sigma_{UL}^2\mathbb{E}\{\|\boldsymbol{v}_{lk}\|^2\}} \quad (4.4.4)$$

With $\boldsymbol{v}_{lk}$ denote the receiving vector and $\boldsymbol{h}_{llk}$denotes the channel between the user in the *l-th* cell and the BS.

The proof of Theorem 4.4.1 can be found in Appendix A

Based on equation (4.4.4), the achievable spectral efficiency rate of the *k-th* user terminal in the *l-th* cell can be described by $SINR_{lk}^{UL}$ which is related to the expectation of the small-scale fading.

The gain of the preferred signal is characterized by the numerator, while the average power of all the signal, the decoding signal power, and the effective noise power characterize the three denominator terms sequentially. The factor $\left(1-\frac{\tau_p}{\tau_c}\right)$ in equation (4.4.3) characterize the payload data, where $\frac{\tau_p}{\tau_c}$ is the pilot sequence symbol length over the total frame length, and γ^{UL} is the fraction of the uplink data from the TDD fram. Considering the detection scheme, it clear that Maximal Ratio (MR) receiver aim to maximize the numerator, while Zero Forcing (ZF) detection aim to minimize the intra cell interference at the denominator of $SINR_{lk}^{UL}$. Since the numerator $|\mathbb{E}\{\boldsymbol{v}_{lk}{}^{H}\boldsymbol{h}_{llk}\}|^2$, grows as M^2 and the noise power $\sigma_{UL}^2\mathbb{E}\{\|\boldsymbol{v}_{lk}\|^2\}$ grows as M with the increase of the number of antennas, the last term become less significant. This is known in the literature as coherent detect *array gain.*

The inter-cell interference in a multi-user scenario depends on the channel distribution, and it scales as M. Considering the worst-case scenario where all users in all cells upload their pilots at the same time, inter-cell interference will become harmful and will scale faster. This phenomenon is referred to it as *pilot contamination*.

Considering an uncorrelated Rayleigh fading channel between the *l-th* base station and the *k-th* user in the *i-th* cell, as follows:

$$\boldsymbol{h}_{lik} \sim \mathcal{CN}(\boldsymbol{0}, \beta_{lik}\boldsymbol{I}_M) \quad (4.4.5)$$

Thus, $\bar{\boldsymbol{h}}_{lik} = \mathbb{E}\{\boldsymbol{h}_{lik}\} = \boldsymbol{0}$, which indicates a rich scattering environment with no Line-of-Sight (LOS) with no dominant channel directivity.

The estimation in (Lemma 3.7.1) can be simplified to,

$\widehat{\boldsymbol{h}}_{\boldsymbol{ljk}} = \frac{\sqrt{P_{jk}}\tau_p\beta_{ljk}}{\sum_{i\in\int_j}^{L} P_{ik}\tau_p\beta_{lik}+\sigma_{UL}^2}\left(\boldsymbol{Y}_{\boldsymbol{l}}^{\boldsymbol{p}}\boldsymbol{\phi}_{\boldsymbol{jk}}\right)$ (4.4.6),

moreover, defined as,

$$\widehat{\boldsymbol{h}}_{\boldsymbol{ljk}} \sim \mathcal{CN}\left(\boldsymbol{0}, \left(\beta_{lik} - MSE_{ljk}\right)\boldsymbol{I}_M\right) \quad (4.4.7)$$

The relation between the two estimated channel $\widehat{\boldsymbol{h}}_{\boldsymbol{lik}}$ and $\widehat{\boldsymbol{h}}_{\boldsymbol{llk}}$, where $i \in \int_l$ expressed as

$$\widehat{\boldsymbol{h}}_{\boldsymbol{lik}} = \frac{\sqrt{P_{ik}}\beta_{lik}}{\sqrt{P_{lk}}\beta_{llk}}\widehat{\boldsymbol{h}}_{\boldsymbol{llk}} \quad (4.4.8)$$

From equation (4.4.8) we can deduce that the estimation of the *l-th* base station is contaminated with the channels of the *i-th* cell, where they are the same up to a scaling factor. This is the key cause of pilot contamination that will degrade the system performance.

Note that the LMMSE estimation and MMSE estimation are the same in a special case where channels are Gaussian distributed Rayleigh fading [59]. By exploiting this property, a closed form for ZF and MR detection of the Spectral Efficiency in Theorem 4.4.1 can be expressed as in the following Corollary.

Corollary 4.4.1 [58]**.** *A lower bound on the uplink ergodic capacity, with uncorrelated Rayleigh fading, can be expressed as follows:*

$$C_{lk}^{UL} = \gamma^{UL}\left(1-\frac{\tau_p}{\tau_c}\right)\log_2(1+SINR_{lk}^{UL}) \quad (4.4.9)$$

where,

$$SINR_{lk}^{UL} = \frac{G p_{lk}\beta_{llk} \dfrac{p_{lk}\tau_p\beta_{llk}}{\sum_{i\prime\in\int_l} p_{i\prime k}\tau_p\beta_{li\prime k} + \sigma_{UL}^2}}{G\sum_{i\in\int_l\setminus\{l\}} p_{lk}\beta_{lik}\dfrac{p_{lk}\tau_p\beta_{llk}}{\sum_{i\prime\in\int_l} p_{i\prime k}\tau_p\beta_{li\prime k} + \sigma_{UL}^2} + \sum_{i=1}^{L}\sum_{t=1}^{K} p_{it}Z_{lit} + \sigma_{UL}^2} \quad (4.4.10)$$

Considering MR detection scheme, $G = M$ and $Z_{lit} = \beta_{lit}$, while considering ZF detection scheme, $G = M - K$ and

$$Z_{lit} = \begin{cases} MSE_{lit}, & for\ i \in \int_l \\ \beta_{lit}, & otherwise \end{cases}$$

Knowing that MSE_{lit} was previously defined in equation (3.7.4).

The proof of Corollary 4.4.1 can be found in Appendix A.

The pilot contamination in equation (4.4.10) is represented by the first term of the denominator, which also has a similar structure to the preferred signal. This term is amplified at the same rate with the preferred signal; this fact is due to the limitation of the BS to separate reused pilot sequences. The SINR will be degraded by adding interference signals which scale as *M* with MR detector and as *M-K* with ZF detector.
Looking to the ratio of pilot contamination to the signal term in equation (4.4.10), the relative strength is preferred to be small.

$$\frac{\sum_{i\in\int_l\setminus\{l\}} p_{lk}\beta_{lik}\dfrac{p_{lk}\tau_p\beta_{llk}}{\sum_{i\prime\in\int_l} p_{i\prime k}\tau_p\beta_{li\prime k} + \sigma_{UL}^2}}{G p_{lk}\beta_{llk}\dfrac{p_{lk}\tau_p\beta_{llk}}{\sum_{i\prime\in\int_l} p_{i\prime k}\tau_p\beta_{li\prime k} + \sigma_{UL}^2}} = \sum_{i\in}\left(\frac{p_{ik}\beta_{lik}}{p_{lk}\beta_{llk}}\right)^2 \quad (4.4.11)$$

When the k-th UT in the *i-th* cell is close to the serving *l-th* BS, analytically β_{lik}/β_{llk} decreases when β_{llk}increases or β_{lik} decreases due to moving away from the interfering cell.

Worth to mention, that pilot contamination effect will persist even when the number of the antenna at the base station increases without limits. This will be shown in the performance results in the next sections.

4.6.2 Downlink session

After estimating the CSI from the training session during upload, BS can use the estimated CSI to precode data to each user. However, if the CSI is imperfect, the precoded signal quality can be degraded. This is due to many factors, where we are interested in presenting the pilot contamination effect as a key challenge.
Based on the received signal expression at the k-th user terminal, equation (3.10.2), a lower bound on the capacity between the *k-th* user terminal in the *l-th* cell and its serving BS is presented in the following theorem.

Theorem 4.4.2 [58]**.**
The ergodic rate of the k-th user terminal in the l-th cell during downlink session is expressed as follows.

$$\boldsymbol{C}_{l,k}^{DL} = \gamma^{DL}\left(1 - \frac{\tau_p}{\tau_c}\right)\log_2\left(1 + SINR_{l,k}^{DL}\right) \quad (4.4.12)$$

with

$$SINR_{l,k}^{DL} = \frac{\rho_{lk}\left|\mathbb{E}\{\boldsymbol{h}_{llk}{}^H\boldsymbol{w}_{lk}\}\right|^2}{\sum_{i=1}^{L}\sum_{t=1}^{K}\rho_{it}\mathbb{E}\left\{\left|\boldsymbol{h}_{ilk}{}^H\boldsymbol{w}_{it}\right|^2\right\} - \rho_{lk}\left|\mathbb{E}\{\boldsymbol{h}_{llk}{}^H\boldsymbol{w}_{llk}\}\right|^2 + \sigma_{DL}^2} \quad (4.4.13)$$

The proof is available in Appendix A.

Theorem 4.4.2 provides a spectral efficiency expression which is independent of any distributed choice of a precoding vector. It is also evident that the expressions in ***Theorem 4.4.2*** and ***Theorem 4.4.1*** looks similar which is since downlink and uplink channels are reciprocal. However, the detection vector is replaced with the precoding one. Considering the interference term the, it also has a similar structure unless the indices between the channel vector and the processing vector are swapped. Following this observation, an uplink-downlink duality is expressed in [12] that corresponds to the following assumption.
Given a downlink precoding vector as

$$\boldsymbol{w}_{lk} = \frac{\boldsymbol{v}_{lk}}{\sqrt{\mathbb{E}\{\|\boldsymbol{v}_{lk}\|^2\}}} \quad (4.4.14)$$

For any distribution of uplink power p_{it} there exist a set of corresponding downlink power ρ_{it} such that

$$SINR_{l,k}^{UL} = SINR_{l,k}^{DL} \quad (4.4.15)$$

and

$$\frac{\sum_{i=1}^{L}\sum_{t=1}^{K}\rho_{it}}{\sigma_{DL}^2} = \frac{\sum_{i=1}^{L}\sum_{t=1}^{K}p_{it}}{\sigma_{UL}^2},$$

holds for all *l,k.*
Based on this duality principle, MR and ZF precoding can be defined as

$$\boldsymbol{w}_{lk} = \begin{cases} \dfrac{\widehat{\boldsymbol{h}}_{llk}}{\mathbb{E}\{\|\widehat{\boldsymbol{h}}_{llk}\|^2\}}, & for\ MR \\ \dfrac{\widehat{\boldsymbol{H}}_{ll}\boldsymbol{r}_{lk}}{\mathbb{E}\{\|\widehat{\boldsymbol{H}}_{ll}\boldsymbol{r}_{lk}\|^2\}}, & for\ ZF \end{cases} \quad (4.4.16)$$

With $\boldsymbol{r}_{lk}$ is the *k-th* column of $((\widehat{\boldsymbol{H}}_{ll})^H \widehat{\boldsymbol{H}}_{ll})^{-1}$.

Since we assume a channel reciprocity, the estimated channel during the uplink will be exploited for precoding in the downlink, where the channel estimates $\widehat{\boldsymbol{h}}_{iik}$ and $\widehat{\boldsymbol{h}}_{ilk}$ with $l \in \int_i$ are related according to the following expression

$$\widehat{\boldsymbol{h}}_{ilk} = \frac{\sqrt{p_{lk}}\beta_{ilk}}{p_{ik}\beta_{iik}}\widehat{\boldsymbol{h}}_{iik} \quad (4.4.17).$$

By this expression, the pilot contamination effect also persists in downlink, where the *i-th* BS cannot precode the signal toward its *k-th* UT, without precode the same signal toward users belong to the same group that reuses the pilot sequences.
In the same way, as in the analysis of the uplink, we will consider ***Theorem 4.4.2***, with a particular case of uncorrelated Rayleigh fading. A lower bound on the ergodic capacity of the k-th UT is stated in the following corollary.

Corollary 4.4.2.
A lower bound on the downlink ergodic capacity in Theorem 4.4.2 of the k-th UT in the l-th cell, given an uncorrelated Rayleigh fading channel, is stated below.

$$\boldsymbol{C}_{l,k}^{DL} = \gamma^{DL}\left(1 - \frac{\tau_p}{\tau_c}\right)\log_2\left(1 + SINR_{l,k}^{DL}\right) \quad (4.4.18)$$

With

$$SINR_{lk}^{DL} = \frac{G\rho_{lk}\beta_{llk}\dfrac{p_{lk}\tau_p\beta_{llk}}{\sum_{i\prime\in\int_l}p_{i\prime k}\tau_p\beta_{li\prime k} + \sigma_{UL}^2}}{G\sum_{i\in\int_l\setminus\{l\}}\rho_{ik}\beta_{ilk}\dfrac{p_{lk}\tau_p\beta_{ilk}}{\sum_{i\prime\in\int_l}p_{i\prime k}\tau_p\beta_{ii\prime k} + \sigma_{UL}^2} + \sum_{i=1}^{L}\sum_{t=1}^{K}\rho_{it}Z_{ilt} + \sigma_{DL}^2} \quad (4.4.19)$$

Considering MR precoding scheme, $G = M$ *and* $Z_{lit} = \beta_{lit}$*, while considering ZF detection scheme,* $G = M - K$ *and*

$$Z_{ilt} = \begin{cases} MSE_{ilt}, & for\ i \in \mathfrak{J}_l \\ \beta_{ilk}, & otherwise \end{cases}$$

The proof of ***Corollary 4.4.2*** is available in Appendix A.

Referring to **Corollary 4.4.2**, one can see that the pilot contamination and all other attributes of ZF and MR precoding are similarly presented in the uplink counterpart.

By the conclusion, it is evident from the uplink-downlink duality, that the same performance can be achieved in the uplink and the downlink.

4.7 Impact of pilot Contamination

To have an insight about the effect of pilot contamination, illustration from [58], presents the spectral efficiency taking into consideration number of users and pilot reuse factor for both MR and ZF detection scheme.
Figure 4.4.3 and Figure 4.4.4, shows how the spectral efficiency of the system degrades with the increase of the number of users and pilot reuse factor.

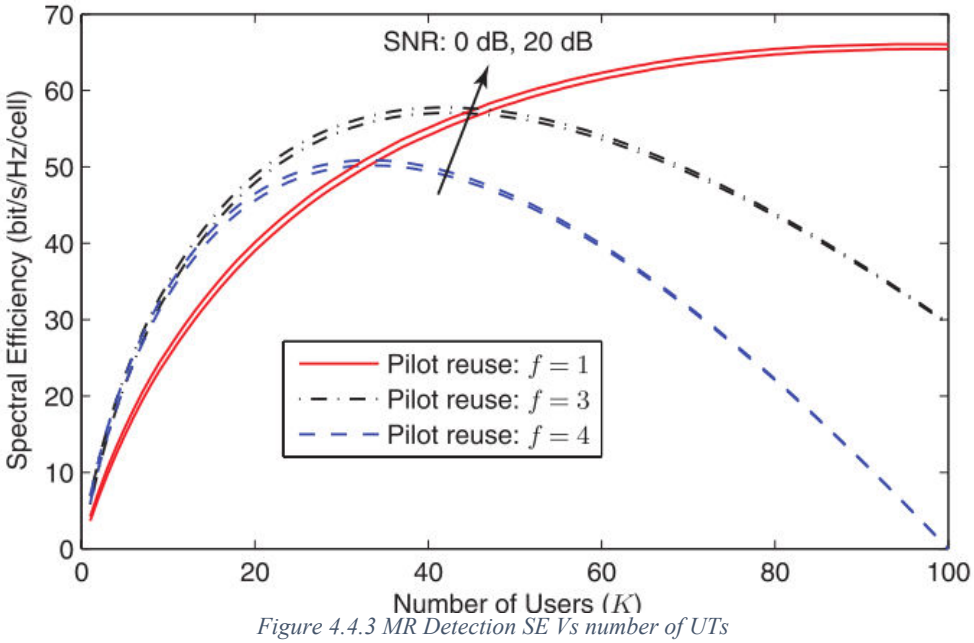

Figure 4.4.3 MR Detection SE Vs number of UTs

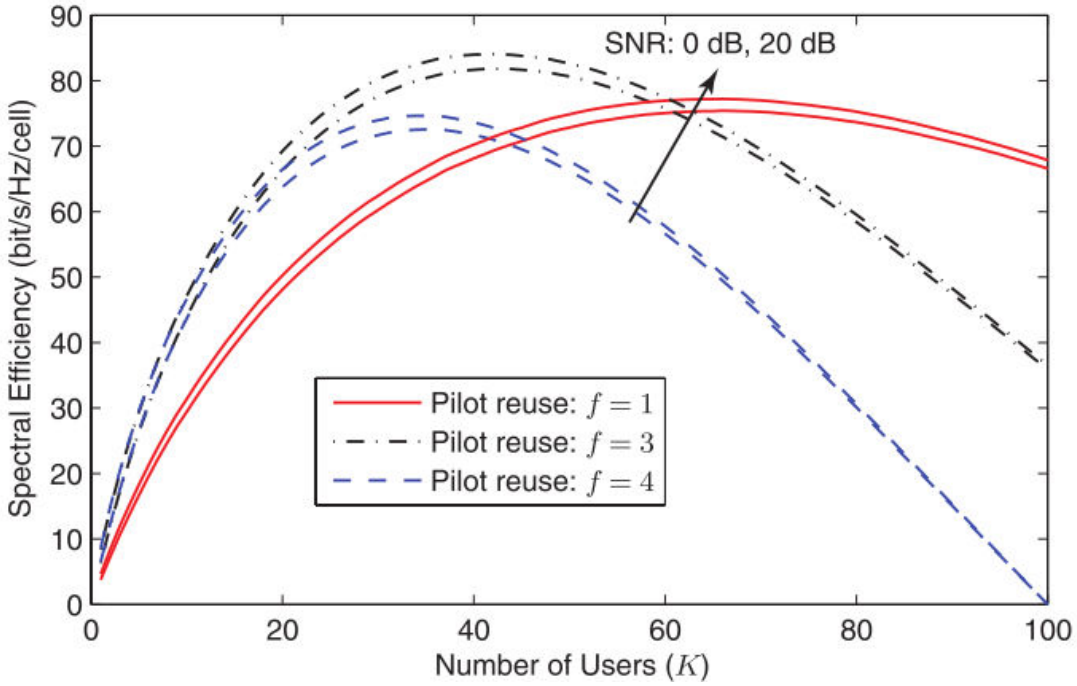

Figure 4.4.4 ZF Detection SE Vs number of UTs

In Figure 4.4.5 the reuse factor is fixed to 3, and a ZF precoding is used in the sense of increasing the number of antennas with 0 dB SNR. It is clear that the average spectral efficiency increase with the increase in the number of antennas at the BS where the increasing number of users were also shown.

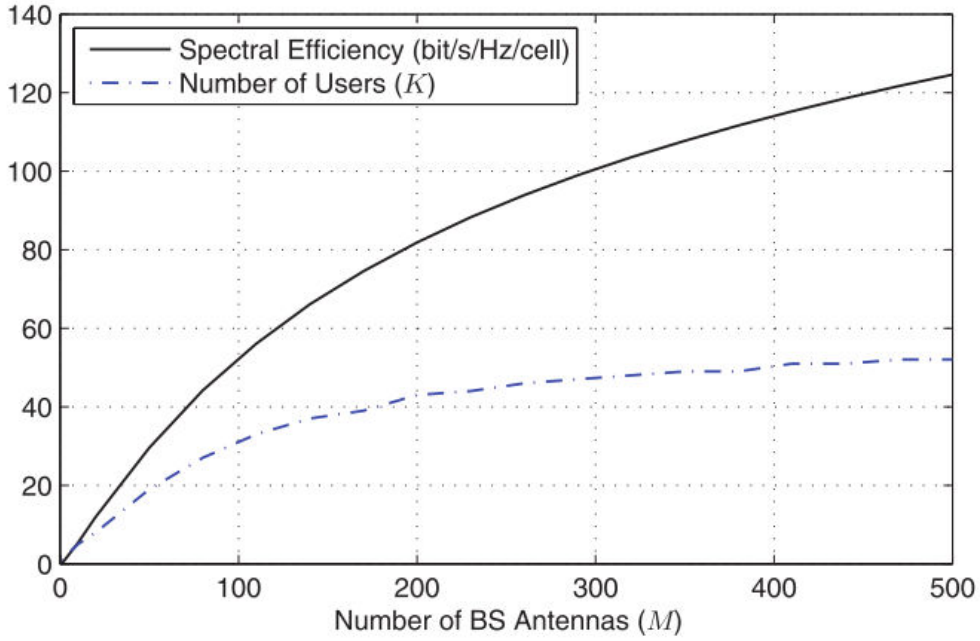

Figure 4.4.5 Average Spectral Efficiency and number of UTs Vs increase number of BS antennas M with f=3, SNR=0db

5 Pilot Contamination Sources

In this section, we consider main sources of pilot contamination, starting by the reuse of non-orthogonal pilots and passing through hardware impairment and non-reciprocity in the transceiver.

5.1 Non-orthogonal pilot reuse:

Assuming an L cell, where a frequency band is shared among all cells, the intra-cell interference is considered negligible due to the orthogonality of pilots within the same cell. However, since adjacent cells may encounter the same pilot sequences, inter-cell interference may occur.
The reuse factor will directly scale up the contamination effect leading to severe performance degradation. This is starts in the uplink session, while BS is trying to separate pilot signals. However, due to the lack of pilot sequence orthogonality between several users, the BS will fail to separate user signals. Hence, an inaccurate CSI estimation will be trained.
The received pilot sequence during training session $\boldsymbol{Y_j^p} \in \mathbb{C}^{M\times\tau_p}$ can be expressed as (3.7.2),

$$\boldsymbol{Y_l^p} = \sum_{j=1}^{L} \boldsymbol{H_{lj}} \boldsymbol{P_j^{1/2}} \boldsymbol{\phi_j^H} + \boldsymbol{W_l^p}$$

with $\boldsymbol{\phi_j} = [\boldsymbol{\phi_{j1}}, \dots, \boldsymbol{\phi_{jk}}, \dots \boldsymbol{\phi_{jK}}] \in \mathbb{C}^{\tau_p \times K}$ denotes the pilot sequences that is used by UTs of the j-th cell where $\boldsymbol{\phi_{jk}} \in \mathbb{C}^{\tau_p}$ is the k-th user sequence. $\boldsymbol{W_l^p} \in \mathbb{C}^{M\times\tau_p}$ denotes the AWGN noise.
The pilot matrix is designed as follows,

$$\boldsymbol{\phi_j^H \phi_l} = \begin{cases} \tau_p \boldsymbol{I}_K & if\ l = j \\ \boldsymbol{0} & if\ l,j\ \in\ different\ cell\ group \\ \tau_p \boldsymbol{I}_K & if\ l,j\ \subset\ same\ cell\ group \end{cases}$$

Chapter 1: Where it is evident from the third term, the effect of pilot contamination in the detection expression of equation (3.7.5).

$$\boldsymbol{v_{jk}^H y_j} = \underbrace{\sqrt{P_{lk}}\boldsymbol{v_{jk}^H h_{jjk}} s_{jk}}_{preferred\ signal} + \underbrace{\sum_{\boldsymbol{t\neq k}}^{\boldsymbol{K}} \sqrt{P_{lt}}\boldsymbol{v_{jk}^H h_{jjt}} s_{jt}}_{intra-cell\ interference} + \underbrace{\sum_{l\neq j}^{L}\sum_{\boldsymbol{t\neq k}}^{\boldsymbol{K}} \sqrt{P_{lt}}\boldsymbol{v_{jk}^H h_{jlt}} s_{lt}}_{inter-cell\ interference} + \underbrace{\boldsymbol{v_{jk}^H w_j}}_{AWGN\ noise}$$

5.2 Hardware Impairment

Several studies had been done on the effect of hardware impairment on Massive MIMO includes [60], [61]. According to studies on experimental systems,[62], [63], they declare that the hardware components in radio frequency are prone to hardware impairments such as quadrature imbalance, quantization error, phase noise and amplifier non-linearity. Lately, a study by [64], shows how hardware impairment leads to a mismatch between the generated signal and the intended transmitted signal. This impairment affects the accuracy of the channel estimation and thus leads to pilot contamination and performance degrades in massive MIMO systems.

5.3 Non-Reciprocal Transceiver

Considering TDD massive MIMO System, the forward and backward channels are assumed to be reciprocal since they operate at the same frequency.
The point-to-point reciprocity model in figure 4.5.1 was adopted from *[65]*, where two scenarios may take place. If the system considered ideal, then the low noise amplifiers (R1 and R2), the effective electromagnetic channel C(t) and the power amplifiers (T1 and T2) are considered identical. In the case

of a non-ideal system, the channel reciprocity will be affected by residual offset frequency [66]. Even a small offset in few Hz will cause the forward and the backward channels non-reciprocal.

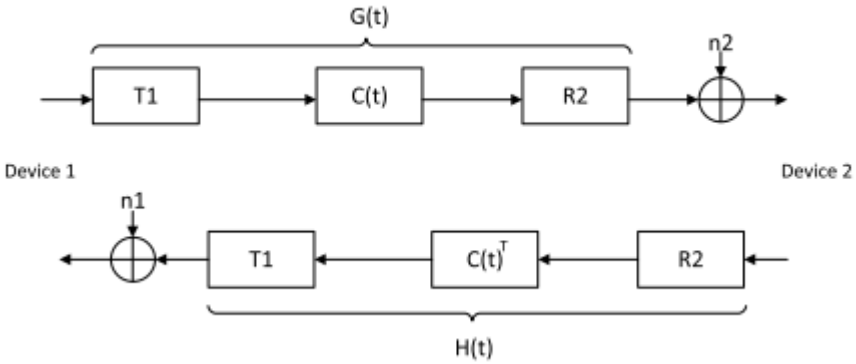

Figure 4.5.1 Point-to-Point case reciprocal model [65]

The imperfect CSI calibration, due to the presence of residual offset frequency, will play a major role in pilot contamination during channel estimation session.

6 PILOT CONTAMINATION MITIGATION

This section Considers the methods proposed to either eliminate or mitigate pilot contamination in multi-cell TDD massive MIMO systems. Two types of approaches are deemed to deal with pilot contamination problem. The first type is pilot-based estimation approach, where this category uses full pilot for channel estimation. The second type is subspace-based estimation where proposals in this category, estimate channel with a limited pilot or without pilots.

6.1 Pilot-Based Estimation

1- Time-Shifted Pilots
Time-Shifted pilot was introduced in several studies to mitigate pilot contamination [33], [67]. This technique allocates the transmission of non-orthogonal pilots between cross cells to different time shifts. In other words, the pilot position is shifted across the TDD frame for each cell that reuses the same pilot pool. Considering this scheme, pilot contamination was shown to be eliminated if the pilots do not overlap in time.

2- Power Allocation Algorithm
Power allocation algorithm coped with time shifted pilots was introduced in [67], the result obtained was promising where this method provides a significant gain in overall system performance. However, a significant challenge is the control mechanism which is needed to synchronize the pilots across different cells.

3- Covariance-Aided Channel Estimation
By exploiting the channel estimation of the desired and the interfered signals, covariance aided channel estimation can vanish the contamination. This method was proposed by [68], [69], it was shown that the pilot contamination effect with large antenna array system, can be vanished when the interfering users and the desired users are located in distinct subspaces. For instance, they show that users with different Angle of Arrival (AoA) can hardly contaminate each other. Follows this finding a coordinated pilot allocation was proposed to allocate similar pilots to a selected group of users. The outcome of this method is promising where it shows a significant increase in downlink and uplink SINR with a reduction in inter-cell interference. However, it is practically difficult to implement due to the second order statistics required for uplink channels.

4- Spatial Domain Based Method

Motivated by the fact that temporal and spatial characteristics different user channels are distinguishable, [70] proposed a spatial domain based method. Further, the channel coefficient of the largest power is selected as the downlink beamformer. Based on the assumption that AoA of interfering signals is not overlapping, and an offline codebook to receive the uplink path and then exploited as a downlink vector. Nonetheless, the channel coherence interval should be taken into consideration when searching for the best steering vector for the downlink precoding. However, the cost of training is high and can go toward infinity.

5- Precoding based Method

A multi-cell MMSE precoding scheme is developed by [54], which take into account all UTs when allocating pilot sequences. The method uses an optimization technique to minimize the MMSE while choosing the best precoding parameters. The proposed method reduces the inter-cell and intra-cell interference and increases the overall system capacity compared to conventional single cell precoding techniques. However, this approach deals with all user channels the same regarding their spatial and temporal characteristics.

Another precoding based method was proposed by [71], where pilot contamination precoding (PCP) need limited cooperation between BSs. Using this method each BS share the estimated slow fading channel coefficient with other BS's or with a network hub that is capable of computing the PCP precoding matrices. Then each BS will receive a specific precoded matrix corresponding for the computation of its transmitted vector. A key challenge in this method is the accuracy of the shared information from each BS.

6.2 Subspace-Based Estimation

Due to a minimum or no pilot symbol needed, subspace-based estimation had been proposed as an attractive technique in the literature [72]. Considering this approach variety of channel characteristics can be exploited for channel estimation, includes fixed symbol rate, high order statistical properties, constant modulus, independence and finite alphabet structure. This approach had been adopted to deal with uplink pilot contamination in multi-cell TDD systems to eliminate pilot contamination.

6.2.1 EVD Based Method

In [73] eigenvalue decomposition (EVD) was applied to the covariance matrices of the received samples with a short orthogonal pilot in all the L cells. However, EVD-based estimation is prone to error since, with an enormous number of antennas at the BS, the channels between UTs and the BS tends to be orthogonal. EVD is also combined with iterative least square and a projection algorithm [74] to overcome the error of channel orthogonality. By result, the EVD-based method shows a significant performance compared to pilot based estimation techniques, but on the cost of complex algorithms and large sampling data within the coherence interval.

6.2.2 Non-linear Channel Estimation

Non-linear channel estimation or blind estimation was proposed by [75], [76] to eliminate pilot contamination by controlling the power and subspace projection. The intuition behind this idea can be summarized by finding the Singular Value Decomposition (SVD) of the received signal then match the subspace to the appropriate signal parameter based on random analysis from random matrix theory. This method shows the ability of this algorithm to determine the subspace of the preferred signal.

7 CONCLUSION

In this chapter, we introduce a general overview on interference management in Massive MIMO systems. For instance, multi-cell interference, multi-cell cooperation, advanced receivers and joint scheduling as briefly discussed. Further, Practical challenges facing massive MIMO was introduced, including Receiver architecture, realistic interference conditions, channel state interference reporting,

practical joint scheduling and backhaul links. We focus on the uplink pilot contamination in multi-cell TDD systems. Considering this phenomenon, the SE expression were derived in the uplink and downlink and the effect of increasing the number of users and the reuse factor was introduced. Also, training methods were briefly discussed including TDD and FDD schemes on the basis of independent and spatial correlated channel models. Further discussion on the pilot contamination sources including hardware impairment and non-reciprocal transceiver was briefly discussed. At last, the method used to mitigate pilot contamination was considered including pilot based estimation and subspace-based estimation. In the next chapters, our novel proposed techniques will be introduced to mitigate pilot contamination based on artificial intelligence and graph theory.

8 REFERENCES

[1] "5G-PPP," 2016. [Online]. Available: https://5g-ppp.eu/.

[2] C. Cisco, "Global mobile data traffic forecast update, 2013–2018," *white Pap.*, 2014.

[3] N. Prasad, H. Zhang, and H. Zhu, "Multi-user MIMO scheduling in the fourth generation cellular uplink," *IEEE Trans. Wirel. Commun.*, 2013.

[4] J. Andrews, S. Buzzi, W. Choi, and S. Hanly, "What will 5G be?," *IEEE J.*, 2014.

[5] A. Osseiran *et al.*, "Scenarios for 5G mobile and wireless communications: The vision of the METIS project," *IEEE Commun. Mag.*, vol. 52, no. 5, pp. 26–35, 2014.

[6] E. Larsson, O. Edfors, F. Tufvesson, and T. Marzetta, "Massive MIMO for next generation wireless systems," *Commun. Mag. IEEE*, vol. 52, no. 2, pp. 186–195, 2014.

[7] T. L. Marzetta, "Noncooperative cellular wireless with unlimited numbers of base station antennas," *IEEE Trans. Wirel. Commun.*, vol. 9, no. 11, pp. 3590–3600, 2010.

[8] F. Rusek *et al.*, "Scaling up MIMO : Opportunities and challenges with very large arrays," *IEEE Signal Process. Mag.*, vol. 30, no. 1, pp. 40–60, 2013.

[9] H. Q. Ngo, E. G. Larsson, and T. L. Marzetta, "Energy and spectral efficiency of very large multiuser MIMO systems," *IEEE Trans. Commun.*, vol. 61, no. 4, pp. 1436–1449, 2013.

[10] W. Liu, S. Han, and C. Yang, "Is massive mimo Energy Efficiency," *arXiv.org*, pp. 1–30, 2015.

[11] J. Hoydis, S. Ten Brink, and M. Debbah, "Massive MIMO in the UL/DL of cellular networks: How many antennas do we need?," *IEEE J. Sel. Areas Commun.*, vol. 31, no. 2, pp. 160–171, 2013.

[12] E. Björnson, E. G. Larsson, and M. Debbah, "Massive MIMO for Maximal Spectral Efficiency: How Many Users and Pilots Should Be Allocated?," in *IEEE Transactions on Wireless Communications*, 2016, vol. 15, no. 2, pp. 1293–1308.

[13] M. Dohler, "Virtual antenna arrays," *Thesis*, no. November, pp. 1–208, 2004.

[14] S. K. Jayaweera, "Virtual MIMO-based cooperative communication for energy-constrained wireless sensor networks," *IEEE Trans. Wirel. Commun.*, vol. 5, no. 5, pp. 984–989, 2006.

[15] W. Tong, J. Ma, P. Zhu, M. Jia, and D. Yu, "Virtual mimo communication system," *US Pat. 7,508,798*, 2009.

[16] D. Gesbert *et al.*, "From theory to practice: An overview of space-time coded MIMO wireless systems," *IEEE J. Sel. Areas Commun.*, vol. 21, no. 3, pp. 281–302, 2003.

[17] J. Andrews, W. Choi, and R. Heath, "Overcoming interference in spatial multiplexing MIMO cellular networks," *IEEE Wirel.*, 2007.

[18] A. M. A. J. Viterbi, A. M. A. J. Viterbi, K. S. Gilhousen, and E. Zehavi, "Soft handoff extends CDMA cell coverage and increases reverse link capacity," *IEEE J. Sel. Areas Commun.*, vol. 12, no. 8, pp. 1281–1288, 1994.

[19] D. Gesbert, S. G. Kiani, A. Gjendemsj, and G. E. Ien, "Adaptation, coordination, and distributed resource allocation in interference-limited wireless networks," *Proc. IEEE*, vol. 95, no. 12, pp. 2393–2409, 2007.

[20] G. Jöngren, "Multi-antennas for improved LTE performance | Ericsson Research Blog." [Online]. Available: https://www.ericsson.com/research-blog/lte/multi-antennas-improved-lte-performance/. [Accessed: 02-Apr-2017].

[21] C.-X. W. C.-X. Wang, X. H. X. Hong, X. G. X. Ge, X. C. X. Cheng, G. Z. G. Zhang, and J. Thompson, "Cooperative MIMO channel models: A survey," *IEEE Commun. Mag.*, vol. 48, no.

2, pp. 80–87, 2010.
[22] J. Meinilä, P. Kyösti, and T. Jämsä, “WINNER II channel models,” *Radio Technol.*, 2009.
[23] G. Senarath *et al.*, “Multi-hop Relay System Evaluation Methodology (Channel Model and Performance Metric),” *Response*, pp. 1–46, 2007.
[24] “Link asymmetry problem (LAP) in relay assisted cellular network | SAN.” [Online]. Available: http://celtic-san.com/2015/06/11/link-asymmetry-problem-lap-in-relay-assisted-cellular-network/. [Accessed: 02-Apr-2017].
[25] S. Ten Brink, J. Speidel, and R. Yan, “Iterative demapping and decoding for multilevel modulation,” *, 1998. GLOBECOM 1998*.
[26] W. Nam, D. Bai, J. Lee, and I. Kang, “Advanced interference management for 5G cellular networks,” *IEEE Commun. Mag.*, vol. 52, no. 5, pp. 52–60, 2014.
[27] V. Abdrashitov, W. Nam, and D. Bai, “Rate and UE selection algorithms for interference-aware receivers,” *Technol. Conf. (VTC …*, 2014.
[28] L. Lu, S. Member, G. Y. Li, and A. L. Swindlehurst, “An Overview of Massive MIMO : Benefits and Challenges,” *IEEE J. Sel. Top. Signal Process.*, vol. 8, no. 5, pp. 742–758, 2014.
[29] J. Nam, J. Y. Ahn, A. Adhikary, and G. Caire, “Joint spatial division and multiplexing: Realizing massive MIMO gains with limited channel state information,” *2012 46th Annu. Conf. Inf. Sci. Syst. CISS 2012*, vol. 1, no. 1, pp. 1–6, 2012.
[30] S. L. H. Nguyen and A. Ghrayeb, “Compressive sensing-based channel estimation for massive multiuser MIMO systems,” in *IEEE Wireless Communications and Networking Conference, WCNC*, 2013, pp. 2890–2895.
[31] J. Choi, D. J. Love, and T. Kim, “Trellis-extended codebooks and successive phase adjustment: A path from LTE-advanced to FDD massive MIMO systems,” *IEEE Trans. Wirel. Commun.*, vol. 14, no. 4, pp. 2007–2016, 2015.
[32] T. L. Marzetta, “How much training is required for multiuser MIMO?,” *Conf. Rec. - Asilomar Conf. Signals, Syst. Comput.*, pp. 359–363, 2006.
[33] K. Appaiah, A. Ashikhmin, and T. L. Marzetta, “Pilot contamination reduction in multi-user TDD systems,” *IEEE Int. Conf. Commun.*, 2010.
[34] A. Ashikhmin, T. Marzetta, and L. Li, “Interference Reduction in Multi-Cell Massive MIMO Systems I: Large-Scale Fading Precoding and Decoding,” *arXiv Prepr. arXiv1411.4182*, pp. 1–18, 2014.
[35] T. L. Marzetta, G. Caire, M. Debbah, I. Chih-Lin, and S. K. Mohammed, “Special issue on massive MIMO,” *Journal of Communications and Networks*, vol. 15, no. 4, pp. 333–337, 2013.
[36] M. Biguesh and A. B. Gershman, “Training-based MIMO channel estimation: A study of estimator tradeoffs and optimal training signals,” *IEEE Trans. Signal Process.*, vol. 54, no. 3, pp. 884–893, 2006.
[37] C. Wang, E. K. S. Au, R. D. Murch, W. H. Mow, R. S. Cheng, and V. Lau, “On the performance of the MIMO zero-forcing receiver in the presence of channel estimation error,” *IEEE Trans. Wirel. Commun.*, vol. 6, no. 3, pp. 805–810, 2007.
[38] H. Bölcskei, R. W. Heath, and A. J. Paulraj, “Blind channel identification and equalization in OFDM-based multiantenna systems,” *IEEE Trans. Signal Process.*, vol. 50, no. 1, pp. 96–109, 2002.
[39] B. Muquet, M. De Courville, and P. Duhamel, “Subspace-based blind and semi-blind channel estimation for OFDM systems,” *IEEE Trans. Signal Process.*, vol. 50, no. 7, pp. 1699–1712, 2002.
[40] G. Taricco and E. Biglieri, “Space-time decoding with imperfect channel estimation,” *IEEE Trans. Wirel.*, 2005.
[41] S. A. Vorobyov, “Superimposed pilots: An alternative pilot structure to mitigate pilot contamination in massive MIMO,” *Icassp 2016*, pp. 3366–3370, 2016.
[42] M. Coldrey and P. Bohlin, “Training-based MIMO systems - Part I: Performance comparison,” *IEEE Trans. Signal Process.*, vol. 55, no. 11, pp. 5464–5476, 2007.
[43] M. Coldrey and P. Bohlin, “Training-based MIMO systems: Part II - Improvements using detected symbol information,” *IEEE Trans. Signal Process.*, vol. 56, no. 1, pp. 296–303, 2008.
[44] H. Zhang, X. Zheng, W. Xu, and X. You, “On massive MIMO performance with semi-orthogonal pilot-assisted channel estimation,” *EURASIP J. Wirel. Commun. Netw.*, vol. 2014, pp. 1–14,

2014.
[45] D. Neumann, M. Joham, and W. Utschick, “Channel Estimation in Massive MIMO Systems,” pp. 1–24.
[46] A. Hu, T. Lv, H. Gao, Y. Lu, and E. Liu, “Pilot design for large-scale multi-cell multiuser MIMO systems,” *Commun. (ICC), 2013*, 2013.
[47] N. Shariati, E. Bjornson, M. Bengtsson, and M. Debbah, “Low-complexity polynomial channel estimation in large-scale MIMO with arbitrary statistics,” *IEEE J. Sel. Top. Signal Process.*, vol. 8, no. 5, pp. 815–830, 2014.
[48] K. Li, X. Song, M. Omair Ahmad, and M. N. S. Swamy, “An improved multicell MMSE channel estimation in a massive MIMO system,” *Int. J. Antennas Propag.*, vol. 2014, 2014.
[49] T. L. Marzetta and B. M. Hochwald, “Fast transfer of channel state information in wireless systems,” *IEEE Trans. Signal Process.*, vol. 54, no. 4, pp. 1268–1278, 2006.
[50] Y. Yu and D. Gu, “Enhanced MU-MIMO downlink transmission in the FDD-based distributed antennas system,” *IEEE Commun. Lett.*, 2012.
[51] Z. Gao, L. Dai, Z. Wang, and S. Chen, “Spatially common sparsity based adaptive channel estimation and feedback for FDD massive MIMO,” *IEEE Trans. Signal*, 2015.
[52] Z. Jiang, A. F. Molisch, G. Caire, and Z. Niu, “Achievable rates of FDD massive MIMO systems with spatial channel correlation,” *IEEE Trans. Wirel. Commun.*, vol. 14, no. 5, pp. 2868–2882, 2015.
[53] J. Jose, A. Ashikhmin, and T. Marzetta, “Pilot contamination problem in multi-cell TDD systems,” *Theory, 2009. ISIT …*, vol. 10, no. 8, pp. 2640–2651, 2009.
[54] J. Jose, A. Ashikhmin, T. L. Marzetta, and S. Vishwanath, “Pilot Contamination and Precoding in Multi-Cell TDD Systems,” pp. 1–23, 2009.
[55] A. Adhikary, J. Nam, and J. Ahn, “Joint spatial division and multiplexing—The large-scale array regime,” *IEEE Trans.*, 2013.
[56] H. Yin, D. Gesbert, M. Filippou, and Y. Liu, “A coordinated approach to channel estimation in large-scale multiple-antenna systems,” *IEEE J. Sel. Areas Commun.*, vol. 31, no. 2, pp. 264–273, 2013.
[57] M. Filippou, D. Gesbert, and H. Yin, “Decontaminating pilots in cognitive massive MIMO networks,” in *Proceedings of the International Symposium on Wireless Communication Systems*, 2012, pp. 816–820.
[58] T. Van Chien and E. Björnson, “Massive MIMO Communications,” in *5G Mobile Communications*, Cham: Springer International Publishing, 2017, pp. 77–116.
[59] S. M. Kay, “Fundamentals of statistical signal processing: estimation theory,” *Prentice-Hall Signal Processing Series*. p. 595, 1993.
[60] E. Bjornson, P. Zetterberg, and M. Bengtsson, “Optimal coordinated beamforming in the multicell downlink with transceiver impairments,” in *GLOBECOM - IEEE Global Telecommunications Conference*, 2012, pp. 4775–4780.
[61] A. Pitarokoilis, S. K. Mohammed, and E. G. Larsson, “Uplink performance of time-reversal MRC in Massive MIMO systems subject to phase noise,” *IEEE Trans. Wirel. Commun.*, vol. 14, no. 2, pp. 711–723, 2014.
[62] B. Goransson, S. Grant, and E. Larsson, “Effect of transmitter and receiver impairments on the performance of MIMO in HSDPA,” *Process. Adv. …*, 2008.
[63] P. Zetterberg, “Experimental investigation of TDD reciprocity-based zero-forcing transmit precoding,” *EURASIP J. Adv. Signal Process.*, 2011.
[64] E. Björnson, J. Hoydis, and M. Kountouris, “Massive MIMO Systems With Non-Ideal Hardware : Energy Efficiency , Estimation , and Capacity Limits,” vol. 60, no. 11, pp. 7112–7139, 2014.
[65] M. Guillaud and F. Kaltenberger, “Towards practical channel reciprocity exploitation: Relative calibration in the presence of frequency offset,” *Wirel. Commun.*, 2013.
[66] E. Björnson, “Optimal Resource Allocation in Coordinated Multi-Cell Systems,” *Found. Trends® Commun. Inf. Theory*, vol. 9, no. 2–3, pp. 113–381, 2013.
[67] F. Fernandes, A. Ashikhmin, and T. L. Marzetta, “Inter-cell interference in noncooperative TDD large scale antenna systems,” *IEEE J. Sel. Areas Commun.*, vol. 31, no. 2, pp. 192–201, 2013.
[68] and Y. L. Haifan Yin, David Gesbert Fellow, IEEE, Miltiades Filippou, “A Coordinated

Approach to Channel Estimation in Large-scale Multiple-antenna Systems," *IEEE J. Sel. Top. Signal Process.*, vol. 4553, no. c, pp. 1–1, 2012.
[69] H. Yin, D. Gesbert, M. C. Filippou, and Y. Liu, "Decontaminating Pilots in Massive MIMO Systems," in *IEEE International Conference on Communications*, 2013, pp. 3170–3175.
[70] H. Wang, Z. Pan, J. Ni, and I. Chih-Lin, "A spatial domain based method against pilot contamination for multi-cell massive MIMO systems," *Netw. China (…*, 2013.
[71] A. Ashikhmin and T. Marzetta, "Pilot contamination precoding in multi-cell large scale antenna systems," in *IEEE International Symposium on Information Theory - Proceedings*, 2012, pp. 1137–1141.
[72] A. J. van der Veen, S. Talwar, and A. Paulraj, "A subspace approach to blind space-time signal processing for wireless communication systems," *Signal Process. IEEE Trans.*, vol. 45, no. 1, pp. 173–190, 1997.
[73] H. Q. Ngo and E. G. Larsson, "EVD-based channel estimation in multicell multiuser MIMO systems with very large antenna arrays," in *2012 IEEE International Conference on Acoustics, Speech and Signal Processing (ICASSP)*, 2012, no. 1, pp. 3249–3252.
[74] S. Talwar, M. Viberg, and A. Paulraj, "Blind separation of synchronous co-channel digital signals using an antenna array. I. Algorithms," *IEEE Trans. Signal Process.*, vol. 44, no. 5, pp. 1184–1197, 1996.
[75] R. R. Müller, L. Cottatellucci, and M. Vehkaperä, "Blind pilot decontamination," *IEEE J. Sel. Top. Signal Process.*, vol. 8, no. 5, pp. 773–786, 2014.
[76] L. Cottatellucci, R. R. Müller, and M. Vehkaperä, "Analysis of pilot decontamination based on power control," in *IEEE Vehicular Technology Conference*, 2013, pp. 1550–2252.

Chapter 5: Channel State Information Map

Our brain is mapping the world. Often that map is distorted, but it's a map with constant immediate sensory input. ~ E. O. Wilson

By enforcing a huge number of antenna on the base station (BS) the performance of MIMO system will increase significantly in the dimension of (capacity per unit area, energy efficiency, spectral efficiency). Unless thinking about multi-cell multi-user MIMO or Massive MIMO with division duplexing (TDD) wireless system, best channel estimation all through the uplink session will end up a challenge due to the limited quantity of orthogonal pilot sequences that can be generated in short coherence interval. This trouble leads to pilot reuse throughout cells, and as a result, this will lead to uplink pilot contamination. This Chapter considers an indoor scheme of Massive MIMO systems and proposes an Artificial Intelligence (AI) method to mitigate uplink pilot contamination and expand system spectral efficacy, power efficiency, and sum-rate. The proposed technique exploits the first stage of classical channel estimation to search a memory Map of Quantized Channel State Information (QCSI) data. The realized CSI Map will be utilized in the second stage to predict the next UT's channel as an alternative of estimating it. We introduce a machine learning algorithm to create and replace the CSI Map and two modified TDD format for learning stage and prediction stage.
Simulation outcomes promise a significant increase in the overall performance compared to conventional Massive MIMO systems, in the dimension of sum-rate, spectral and energy efficiency.

1 INTRODUCTION

Massive MIMO brings many motivations for the subsequent fifth era cellular technology. It presents a significant acquisition in the achievable sum-rate, energy efficiency, and spectral efficiency [1], [2]. However, thinking about Multi-cell situation the overall performance of Massive MIMO will degrade due to uplink pilot contamination from neighbor cells [3]. As the number of antennas M on the BS increases barring limits, the impact of Additive White Gaussian Noise (AWGN) and the fast fading will vanish, whilst the pilot contamination impact persists [4], [5]. Considering the indoor scenario, Massive MIMO can face the same challenges, except the limited coverage area coped with low mobility velocity UT's and scattering objects allow to think in machine learning options to mitigate such challenge. Also, by measuring the entropy of every UT trajectory, one can find that UT mobility is predictable for high degree [6], [7].

1.1 State of Art

In this Chapter, we introduce a novel technique to predict CSI instead than estimating it; this can be completed in two stages. In the first stage, BS begins to analyze the CSI matrices using classical linear estimation methods (MRC, ZF, MMSE) and stores a quantized version of the realized CSI into a graph of nodes which we name the CSI Map. The CSI should be quantized to reduce the storage space. Thus, the CSI Map translates the geographical coverage map into a directive-connected graph by exploiting a

specific learning algorithm. The nodes of the graph characterize the quantized CSI value where the edges characterize the transition from one CSI to another. In the 2nd stage and after quite a few learning epochs, the CSI Map will be regarded matured to reveal UT mobility and to predict the subsequent most possible CSI matrix to be precoded. To gain from this prediction, we introduce a new format of TDD structure known as predictive format that does no longer consist of pilots. The use of predictive format reduces the energy transmission as properly as the pilot contamination and increase the spectral efficiency (SE), energy efficiency (EE) and the sum-rate of the system. To effortlessly save and retrieve quantized CSI (QCSI) from the map, we use a codebook of two parameters. At last, a Garbage Collection Algorithm (GCA) is additionally introduced to minimize the quantity of CSI nodes in the map through removing weakly connected nodes. The use of GCA will enable focusing on a highly-activated region on the map. Simulation results show the added value of the CSI Map on the overall performance of EE, SE and system sum-rate.

1.2 Related Works

Up to our knowledge, CSI Map had by no means been used in the literature to solve uplink pilot contamination in Massive MIMO. However, numerous tools used in our method had been substantially studied.

Uplink pilot contamination had been investigated using numerous studies [8]–[12]. In [13] authors tend to coordinate the use of pilots or adaptively allocate pilot sequences to distinct terminals in the network. This method requires a cooperative BS scheme where each BS should be aware of pilot allocations in neighbor cells. The author in [14] deals with the hassle of uplink pilot contamination using proposing a new channel estimation scheme that exploits interference cancellation and joint processing. Highly interfering terminals in neighboring cells are recognized based totally on the estimation of large-scale fading and then included in the joint channel processing. For additional information to mitigate uplink pilot mitigation, please see chapter 4 or read [15].

Quantized channel state information was introduced by [16], the authors propose a vector-quantization method to channel state information encoding that needs modest feedback bit rate. Another patent by the same authors was published on quantized channel information prediction in multiple antenna systems [17]. Regarding this work, we use a quantized CSI (QCSI) based on vector quantization of geometric attenuation and shadow fading parameters.

CSI prediction is of two types, model-based (e.g. [18]) or non-model based (e.g. [19] using stochastic channel model). Authors in [19], introduce a decision-directed channel predictors for orthogonal frequency division multiplexing (OFDM) scheme over time-varying channels. An adaptive codebook geodesic based channel prediction was proposed by [20], where the simulation results prove that the proposed scheme effectively reduce the feedback delay and clustering, even with only a 4-bit codebook. CSI prediction had been recently introduced by [21] to mitigate training overhead; the authors exploit the temporal correlation of UT channels to classify users into two groups. In each channel block, the BS select part of the UT's for training, while prediction determines the other UT CSI matrices. Nonetheless, our proposed technique allows the UT to decide either to send its pilot or not. Further, it allows the BS to predict the next position of the UT channel within the CSI Map. Furthermore, mobility and trajectory of users can be easily predicted using CSI Map, which also can be recruited for resources management (Frequency, Time and Pilot) within the network. The scope of this chapter includes the performance on the dimension of spectral and energy efficiency.

2 SYSTEM MODEL

Considering the uplink TDD session in a Massive MIMO system with L cells each contains one BS equipped with M antennas and serving K UT's equipped with one antenna each. Assuming a perfect synchronization among uplink session in all the L cells as in [4],[22] knowing that they share the same frequency band. Hence, following equation (3.7.1) the $M \times 1$ received vector at the *l-th* BS is given by:

$$\boldsymbol{y}_l = \sum_{j=1}^{L} \sum_{\boldsymbol{k=1}}^{\boldsymbol{K}} \sqrt{P_{jk}} \boldsymbol{h}_{ljk} s_{ljk} + \boldsymbol{w}_l \qquad (5.2.1)$$

$$= \sum_{j=1}^{L} \boldsymbol{H}_{lj} \boldsymbol{P}_j^{1/2} \boldsymbol{S}_j + \boldsymbol{w}_l$$

With $\left[\boldsymbol{H}_{lj} \in \mathbb{C}^{M\times K}\right]_k = \boldsymbol{h}_{ljk}$, $[\boldsymbol{P}_j^{\frac{1}{2}}] \in \mathbb{C}^{K\times 1}]_k = \sqrt{P_{jk}}$ being the SNR, $\left[\boldsymbol{S}_j \in \mathbb{C}^{1\times K}\right]_k = s_{ljk}$ being the symbol vector and $\boldsymbol{w}_l \in \mathbb{C}^{M\times 1}$ denote the AWGN noise with zero mean and unit variance.

2.1 Uplink Training

During training session of length τ_p, the received signal at the *l-th* BS in the *j-th* cell will be presented as follows:

$$\boldsymbol{Y}_{\boldsymbol{l}}^{\boldsymbol{p}} = \sum_{j=1}^{L} \boldsymbol{H}_{lj} \boldsymbol{P}_{\boldsymbol{j}}^{1/2} \boldsymbol{\phi}'^{H}_{j} + \boldsymbol{w}_l \qquad (5.2.2)$$

with $\boldsymbol{\phi}'_j{}^{\boldsymbol{p}} = \left[\boldsymbol{\phi}_j^P \odot \boldsymbol{q}_j\right]$, where $\boldsymbol{q}_j$ is a $K \times 1$ binary matrix of the *j-th* cell with elements$[\boldsymbol{q}]_k \in \{0,1\}$ as follows:

$$[\boldsymbol{q}]_k = \begin{cases} 1 & if\ the\ k^{th}\ user\ sends\ an\ initiative\ frame \\ 0 & if\ the\ k^{th}\ user\ sends\ a\ predictive\ frame \end{cases}$$

Let $K = K' + K"$, where K' represents the number of UT's that sends initiative frame and $K"$ the number of UT's that sends predictive frame in one cell, then the ratio to encounter pilot upload in any cell will be $\alpha = \frac{K'}{OP}$ where OP denotes the number of orthogonal pilot sequences in the system of L cells. Following this assumption $\int_j \subset \{1, \dots, L\}$ is the set of cell indices related to the same reused cell pilots as j, and $\int'_j \subset \int_j$ is the set of indices with cardinality $L' = r(L \times \alpha)$ and where $r(.)$ is a function that rounds to the nearest integer.

Since we assumed that every pilot sequence is used once per cell, L' represents the approximate number of contaminated cell. This means that $\frac{L'}{L} \propto \frac{K'}{K}$ by reducing the number of users transmits their pilot in each cell is proportional to reducing the number of interfered cells. Using this proportionality, we can represent $\mathbf{Y}_l^{\boldsymbol{p}}$ statistically as:

$$\boldsymbol{y}_l{}^{\boldsymbol{p}} = \sum_{j=1}^{L} \sum_{\boldsymbol{k=1}}^{\boldsymbol{K}} \sqrt{P_{jk}} \boldsymbol{h}_{ljk} \boldsymbol{\phi}'_{ljk} + \boldsymbol{w}_l \qquad (5.2.3)$$

$$= \sum_{j=1}^{L} \left[\sum_{\boldsymbol{k=1}}^{\boldsymbol{K'}} \sqrt{P_{jk'}} \boldsymbol{h}_{ljk'} \boldsymbol{\phi}'_{ljk'} + \sum_{\boldsymbol{k=1}}^{\boldsymbol{K"}} \sqrt{P_{jk"}} \boldsymbol{h}_{ljk"} \boldsymbol{\phi}'_{ljk"} \right] + \boldsymbol{w}_l$$

$$= \sum_{j=1}^{L} \sum_{\boldsymbol{k=1}}^{\boldsymbol{K'}} \sqrt{P_{jk'}} \boldsymbol{h}_{ljk'} \boldsymbol{\phi}'_{ljk'} + \boldsymbol{w}_l$$

$$\propto \underbrace{\sqrt{P_{lk}} \boldsymbol{h}_{llk'} \boldsymbol{\phi}'_{llk'}}_{Desired\ Signal} + \underbrace{\sum_{i=1}^{L'} \sum_{\boldsymbol{k=1}}^{\boldsymbol{K}} \sqrt{P_{ik}} \boldsymbol{h}_{lik} \boldsymbol{\phi}'_{lik}}_{reused\ pilots} + \underbrace{\sum_{i=L'}^{L} \sum_{\boldsymbol{k=1}}^{\boldsymbol{K}} \sqrt{P_{ik}} \boldsymbol{h}_{lik'} \boldsymbol{\phi}'_{lik}}_{Orthogonal\ pilots} + \underbrace{\boldsymbol{w}_l}_{noise}$$

$$= \underbrace{\sqrt{P_{lk}} \boldsymbol{h}_{llk'} \boldsymbol{\phi}'_{llk}}_{Desired\ Signal} + \underbrace{\sum_{i \in \int'_l \setminus \{l\}}^{L} \sum_{\boldsymbol{k=1}}^{\boldsymbol{K}} \sqrt{P_{ik}} \boldsymbol{h}_{lik'} \boldsymbol{\phi}'_{lik}}_{reused\ pilots} + \underbrace{\sum_{i \notin \int'_l}^{L} \sum_{\boldsymbol{k=1}}^{\boldsymbol{K}} \sqrt{P_{ik'}} \boldsymbol{h}_{lik} \boldsymbol{\phi}'_{lik}}_{Orthogonal\ pilots} + \underbrace{\boldsymbol{w}_l}_{noise}$$

The last expression of equation (5.2.3) is calculated based on the assumption that the pilot reuse is distributed equally on all the L cells and the expression before the last one can be computed based on the assumption of proportionality $\frac{L'}{L} \propto \frac{K'}{K}$.

2.2 Channel Estimation

The *l-th* BS can separate the signal received from the *j*-th cell using the statistical data gathered during previous sessions. In this subsection, linear Minimum Mean Square Error (MMSE) is used to separate the signal of the *k-th* user in the *l*-th cell according to *Lemma 3.7.1*.

The estimated channel can be expressed as:

$$\widehat{\boldsymbol{h}}_{\boldsymbol{ljk}} = \overline{\boldsymbol{h}}_{\boldsymbol{ljk}} + \frac{\sqrt{P_{jk}}\tau_p \beta_{ljk}}{\sum_{i\in\int_j}^{L} P_{ik}\tau_p \beta_{lik} + \sigma_{UL}^2}\left(\boldsymbol{Y}_{\boldsymbol{l}}^{\boldsymbol{p}}\boldsymbol{\phi}_{\boldsymbol{jk}} - \sum_{i\in\int_j}^{L}\sqrt{P_{ik}}\tau_p \overline{\boldsymbol{h}}_{\boldsymbol{lik}}\right) \quad (5.2.4)$$

The uncorrelated error is expressed as $\boldsymbol{e}_{\boldsymbol{ljk}} = \widehat{\boldsymbol{h}}_{\boldsymbol{ljk}} - \overline{\boldsymbol{h}}_{\boldsymbol{ljk}}$, with zero mean and variance

$$\mathrm{MSE}_{ljk} = \beta_{ljk}\left(1 - \frac{P_{lk}\tau_p \beta_{ljk}}{\sum_{i\in\int_j}^{L} P_{ik}\tau_p \beta_{ljk} + \sigma_{UL}^2}\right) \quad (5.2.5)$$

Recall that $\beta_{jlk} = \mathbb{V}\{h_{ljkm}\}$ denotes the variance of h_{ljkm}.

2.3 Uplink Detection

As the normal scenario in TDD scheme, the estimated channel will be exploited for detection during uplink and then for precoding during downlink. Following equation (3.7.5), the BS in the *l*-th cell separate the signal of the *k*-th UT by multiplying the received signal with a linear detector $\boldsymbol{v}_{\boldsymbol{lk}} \in \mathbb{C}^M$ as follows,

$$\boldsymbol{v}_{\boldsymbol{lk}}^H \boldsymbol{y}_{\boldsymbol{l}} = \sum_{i=1}^{L}\sum_{\boldsymbol{t=1}}^{\boldsymbol{K}}\sqrt{P_{it}}\boldsymbol{v}_{\boldsymbol{lk}}^H \boldsymbol{h}_{\boldsymbol{lit}} s_{it} + \boldsymbol{v}_{\boldsymbol{lk}}^H \boldsymbol{w}_l \quad (5.2.6)$$

$$= \underbrace{\sqrt{P_{lk}}\boldsymbol{v}_{\boldsymbol{ik}}^H \boldsymbol{h}_{\boldsymbol{jjk}} s_{jk}}_{preferred\ signal} + \underbrace{\sum_{\boldsymbol{t\neq k}}^{\boldsymbol{K}}\sqrt{P_{lt}}\boldsymbol{v}_{\boldsymbol{lk}}^H \boldsymbol{h}_{\boldsymbol{llt}} s_{it}}_{intra-cell\ interference} + \underbrace{\sum_{\boldsymbol{l\neq i}}^{\boldsymbol{L'}}\sum_{\boldsymbol{t\neq k}}^{\boldsymbol{K}}\sqrt{P_{lt}}\boldsymbol{v}_{\boldsymbol{ik}}^H \boldsymbol{h}_{\boldsymbol{ilt}} s_{lt}}_{inter-cell\ interference} + \underbrace{\boldsymbol{v}_{\boldsymbol{lk}}^H \boldsymbol{w}_l}_{AWGN\ noise} \quad (5.2.6)$$

The third term of the second expression of Equation (5.2.6) was indexed with L'.

The Zero Forcing (ZF), MMSE and Maximum Ratio Combination (MRC) receivers which can be expressed in matrix form as follows,

$$\boldsymbol{V}_{\boldsymbol{j}} = \begin{cases} \widehat{\boldsymbol{H}}_{\boldsymbol{jj}} & for\ MRC \\ \widehat{\boldsymbol{H}}_{\boldsymbol{jj}}\left(\left(\widehat{\boldsymbol{H}}_{\boldsymbol{jj}}{}^{H}\right)\widehat{\boldsymbol{H}}_{\boldsymbol{jj}}\right)^{-1} & for\ ZF \\ \widehat{\boldsymbol{H}}_{\boldsymbol{jj}}\left(\widehat{\boldsymbol{H}}_{\boldsymbol{jj}}{}^{\boldsymbol{H}}\widehat{\boldsymbol{H}}_{\boldsymbol{jj}} + \frac{1}{P_{lk}}\boldsymbol{I}_K\right)^{-1} & for\ MMSE \end{cases} \quad (5.2.7)$$

The received symbol at the *l-th* base station can be found by minimizing the value between the received signals and the expected symbol from a constellation $\mathcal{X}$.

$$\tilde{s}_{lk} = \min_{s\in\mathcal{X}}\left|\boldsymbol{v}_{\boldsymbol{lk}}^H \boldsymbol{y}_l - \boldsymbol{v}_{\boldsymbol{lk}}^H \widehat{\boldsymbol{h}}_{llk} P_{lk} s\right|^2 \quad (5.2.8)$$

2.4 Uplink Spectral and Energy Efficiency

According to *Theorem 4.4.1*, the lower bound on uplink ergodic channel capacity of the *k-th* user in the *l-th* cell can be given as:

$$C_{lk}^{UL} = \gamma^{UL}\left(1 - \frac{\tau_p}{\tau_c}\right)\log_2(1 + SINR_{lk}^{UL}) \quad (5.2.9)$$

where,

$$SINR_{lk}^{UL} = \frac{p_{lk}|\mathbb{E}\{\boldsymbol{v}_{lk}{}^H \boldsymbol{h}_{llk}\}|^2}{\sum_{i=1}^{L'}\sum_{t=1}^{K} p_{it}\mathbb{E}\{|\boldsymbol{v}_{lk}{}^H \boldsymbol{h}_{lit}|^2\} - p_{lk}|\mathbb{E}\{\boldsymbol{v}_{lk}{}^H \boldsymbol{h}_{llk}\}|^2 + \sigma_{UL}^2\mathbb{E}\{\|\boldsymbol{v}_{lk}\|^2\}} \quad (5.2.10)$$

Recall that, the factor $\left(1-\frac{\tau_p}{\tau_c}\right)$ characterize the payload data, where $\frac{\tau_p}{\tau_c}$ is the pilot sequence symbol length over the total frame length, and γ^{UL} is the fraction of the uplink data.

Considering an uncorrelated Rayleigh fading channel between the *l-th* base station and the *k-th* user in the *i-th* cell, as follows:

$$\boldsymbol{h}_{lik} \sim \mathcal{CN}(\mathbf{0}, \beta_{lik}\boldsymbol{I}_M) \quad (5.2.11)$$

Thus, equation (5.2.4) can be written as,

$$\widehat{\boldsymbol{h}}_{\boldsymbol{ljk}} = \frac{\sqrt{P_{jk}}\tau_p \beta_{ljk}}{\sum_{i\in\int_j}^{L} P_{ik}\tau_p \beta_{lik} + \sigma_{UL}^2}\left(\boldsymbol{Y}_{\boldsymbol{l}}^{\boldsymbol{p}}\boldsymbol{\phi}_{\boldsymbol{jk}}\right) \quad (5.2.12)$$

With circularly-symmetric complex Gaussian distributed,

$$\widehat{\boldsymbol{h}}_{\boldsymbol{ljk}} \sim \mathcal{CN}\left(\mathbf{0}, \left(\beta_{lik} - MSE_{ljk}\right)\boldsymbol{I}_M\right) \quad (5.2.13)$$

The spectral efficiency of equation (5.2.9) will become,

$$SE_{lk}^{UL} = \gamma^{UL}\left(1-\frac{\tau_p}{\tau_c}\right)\log_2(1+SINR_{lk}^{UL}) \quad (5.2.14)$$

where,

$$SINR_{lk}^{UL} = \frac{G p_{lk}\beta_{llk}\dfrac{p_{lk}\tau_p\beta_{llk}}{\sum_{i\prime\in\int_l} p_{i\prime k}\tau_p\beta_{li\prime k} + \sigma_{UL}^2}}{G\sum_{i\in\int_l\setminus\{l\}} p_{lk}\beta_{lik}\dfrac{p_{lk}\tau_p\beta_{llk}}{\sum_{i\prime\in\int_l} p_{i\prime k}\tau_p\beta_{li\prime k} + \sigma_{UL}^2} + \sum_{i=1}^{L\prime}\sum_{t=1}^{K} p_{it}U_{lit} + \sigma_{UL}^2} \quad (5.2.15)$$

Considering MRC detection scheme, $G = M$ *and* $U_{lit} = \beta_{lit}$, while considering ZF detection scheme, $G = M - K$ and

$$U_{lit} = \begin{cases} MSE_{lit}, & for\ i\in\int_l \\ \beta_{lit}, & otherwise \end{cases}$$

A lower bound on the uplink energy efficiency can be computed as,

$$EE_{lk}^{UL} = \left(\gamma^{UL}\left(1-\frac{\tau_p}{\tau_c}\right)K' + K"\right)\log_2(1+SINR_{lk}^{UL}) \quad (5.2.16)$$

3 PROPOSED TDD FRAME

User terminals are classified into two groups according to the type of TDD format they use, which directly depends on their previous SNR on the reverse link (see Figure 5.3.1). We introduce two TDD formats the Initiative and the Predictive format. Initiative TDD format, used by *K'* UT's encounters low SNR or initially transmit their pilots, and it is supposed to be a conventional format to enable training for channel estimation at the BS. Predictive TDD format, used by *K"* UT's that encounters high SNR at last forward link and UT's belong to this group will skip sending their pilots where channel prediction at the BS will take place during processing duration. Each TDD format contains three parts within a time slot of sample duration *T,* (Reverse link, Processing period and Forward link) which will be discussed separately as follows:

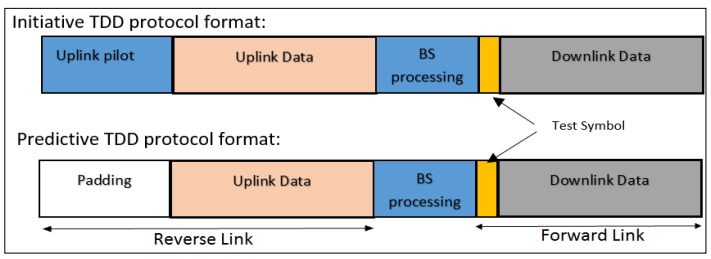

Figure 5.3.1. TDD protocol format

3.1 At the forward link

The BS will precode the downlink data and the test symbol using linear precoder (e.g. MRT, MMSE or ZF) using a composite channel matrix with estimated and predicted elements. Each downlink field is tagged with a test symbol (known at both BS and UT's) to allow UT's easy compute their SNR and decide whether to use predictive or initiative format (referring to a specific threshold) at the next transmission session. Both initiative and predictive TDD formats use the same structure for the forward link.

3.2 At the reverse link

UT's will either use predictive or initiative formats based on the measurement of the SNR of the test symbols from the previous forward link. The group of user terminals that use the predictive format is those who encounter high SNR according to a given threshold Θ, and all other UT's encounters test symbols SNR below Θ will send an initiative formats (see Figure.5.3.2).

$$Switch = \begin{cases} Predictive & if\ SNR \geq \Theta \\ Initiative & if\ SNR < \Theta \end{cases}$$

The predictive format at reverse link starts with a padding of zeros, which supposed to be orthogonal to all pilot sequences occupying the same spectral period. The second part of the predictive TDD format is intended to be the same structure and spectral period with the initiative format, and it is exploited to send uplink data symbols. The initiative format at the reverse link is considered as classical training massive MIMO frame [11],[23] with an orthogonal sequence of pilots of length τ at the header of the data symbols.

3.3 At the processing period

After BS receive the reverse TDD, it will estimate the channels using linear channel estimation (e.g. MRC, MMSE, ZF) for UT'S that upload an initiative format. Furthermore, the BS will update the CSI Map by the new estimated CSI after quantization (learning algorithm will be discussed later in this chapter). For UT's uploading predictive format, the BS will use a special algorithm to retrieve the next possible channel information from the CSI Map.

In both cases (prediction and learning), the BS will use a codebook to access the CSI Map for simplification and storage reduction issue.

The BS can exploit the test symbol as a control flag to force UT's to send their pilots, which is useful to increase the maturity of the CSI Map. This task can easily be done by reducing the transmission power of the test symbols.

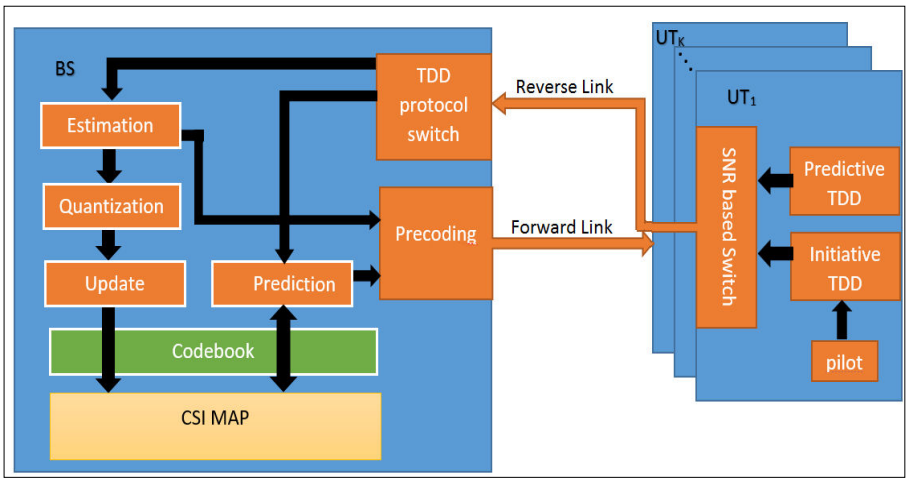

Figure.5.3.2 Block diagram shows different UTs and BS reciprocity operations

4 CHANNEL STATE INFORMATION MAP

CSI Map is a database of previously estimated QCSI represented by a directed graph with weighted edges. The weight of the edges is proportional to the frequency of directed transition between the two connected nodes. In other words, an edge $E_{x,y}$ issued from node N_x to node N_y means that there exist at least one transition from x to y. As a communication issue, this means that the CSI of one UT or more exhibit consecutive changes from CSI x to CSI y where CSI x and CSI y are the quantized versions of the CSI stored in the nodes (see Figure 5.4.1 (a,b)).

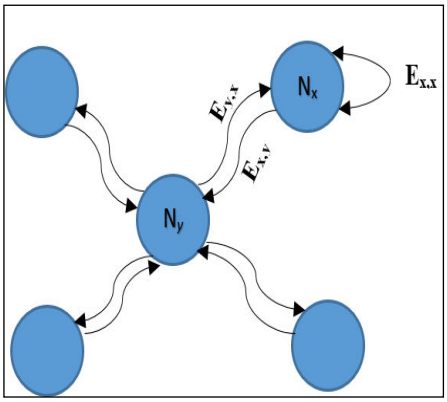

Figure 5.4.1(a) CSI map

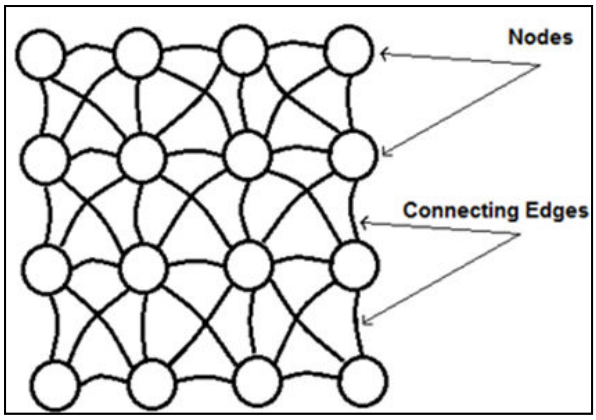

Figure 5.4.1 (b) Map connection overview

The intuition behind this map is to monitor the change in the CSI related to each position in the geographical map of the cell. Based on hypothesis one in [24], which was used for localization and proved by real measurements, CSI values maintain stability at a stationary location but exhibit variability between adjacent positions. The weight of $E_{x,y}$ will increase in essence with the transition from N_x to N_y. If there is no transition for several TDD sessions, an edge will be created from the current node to itself e.g. $E_{x,x}$ and will be updated as much as there is no transition. The creation and update of the graph is done by applying a special learning algorithm that will be explained later in this paper.
After CSI Map get enough matured or converged (no updates for many learning epochs), it can be used to monitor UT's CSI transitions in the cell and predict a possible next node to be visited given the current node (see Figure 5.4.2).

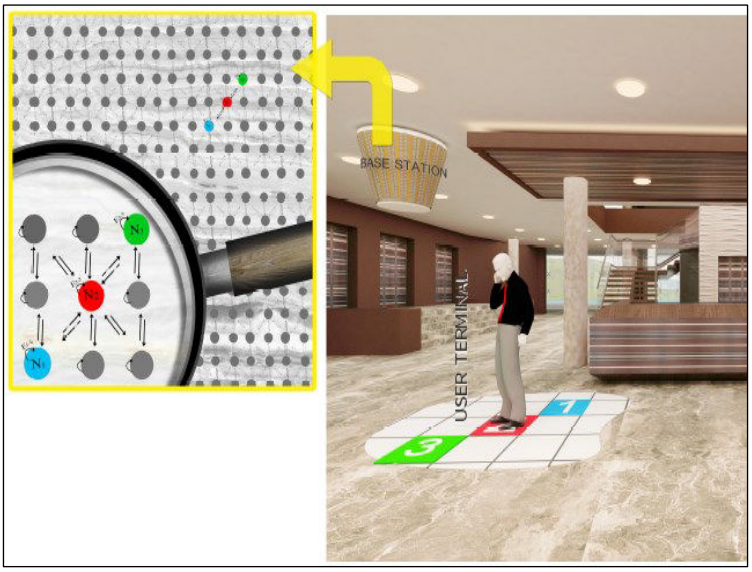

Figure 5.4.2 Conception of CSI Map representing an indoor scenario

5 CSI MAP LEARNING ALGORITHM

To create and update the CSI Map we propose CSI learning algorithm represented by the flowchart of Figure 5.5.1. The learning algorithm will run on each CSI estimation of each UT and will decide either to update an existing edge weight or to add a new node and connect it to the CSI Map.

After a finite number of learning iterations, the CSI Map will reach convergence. This convergence can be defined by a specific large number of iterations done without encountering any update to the CSI Map. Touching on the flowchart of Fig. 5.5.1, steps 7 and 8 will be executed if there exists a previously visited node. We denote the previous node as the QCSI that was stored in the CSI Map and previously visited by the user. One can look for the edge weights as the transition probability between two neighbor nodes.

The weight of the edges is updated using a modified version of the Erev and Roth algorithm [25].

Let denote by x the index of the last visited node and by y the index of the currently visited node and let denote by $E_{x,y}$ the edge issued from node N_x to N_y with weight $W_{x,y}>0$. After the transition from N_x to N_y, the weight update of $E_{x,y}$ is given by:

$$W_{x,y\ (new)} = W_{x,y}(old) + \Theta \qquad (5.5.1)$$

$$Subjected\ to\ \Theta + W_c \leq 1$$

with W_c denotes the sum of all edge weight issued from a node.

set F denotes the set of all node indices connected to N_x by edges issued from N_x. For each edge $E_{x,c'}$, the weight update will be as follows:

$$W_{x,c'\ (new)} = W_{x,c'}(old) - \left(\frac{W_{x,c'}(old)}{\sum_{c'=1,c'\neq c}^{F} W_{x,c'}(old)}\right)\Theta \qquad (5.5.2)$$

$$Subjected\ to\ W_{x,c'\ (new)} \geq 0$$

where $c' \in F$ and $c' \neq y$.

We initiate the weight of the first issued edge from each node to one, and we conserve this value for all future issued edges such that $\sum_{c'=1}^{F} W_{x,c'} = 1$.

The factor $0 < \Theta < 1$ is used to control the learning speed where assigning $\Theta = 0$ will stop the learning and $\Theta = 1$ will disconnect all issued edges except the last transition edge.

After convergence, the BS can predict the next possible QCSI of any monitored UT from the CSI Map.

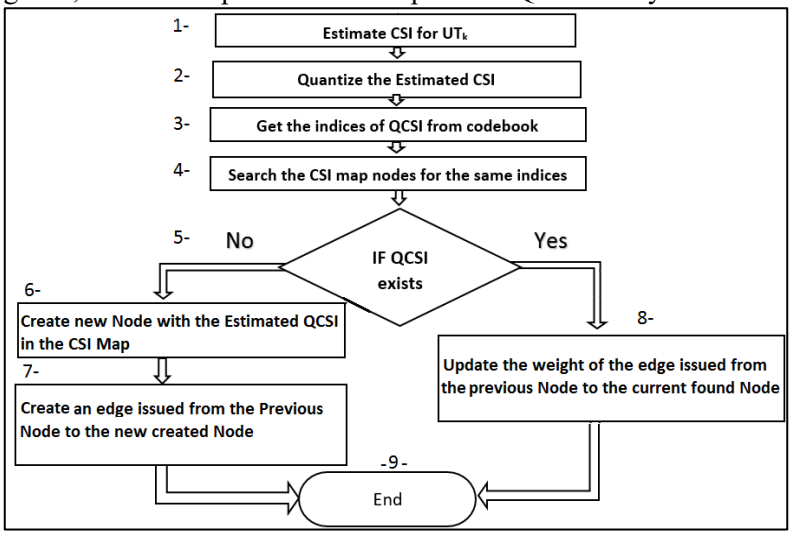

Figure 5.5.1 Flowchart of CSI Learning Algorithm

Given the place of any UT at node N_x, the next possible visited node N_y can be found by $N_y = \underset{y}{\text{argmax}}\, W_{x,y}$, where y ∈ F.

The predicted QCSI stored by N_y can be exploited in the next time-slot data receiving and precoding.

6 CSI QUANTIZATION

The parameters of QCSI are stored in a two-part codebook Z and R , where the first part stores a finite set of shadow fading parameters and the second part stores a finite set of distances between BS and each UT. The channel between the *l-th* BS and the *k-th* UT of the *j-th* cell are modeled as $h_{ljmk} = \sqrt{d_{jlk}}\, g_{ljmk}$.

Denotes by $\boldsymbol{G}_{lj}$ of dimension $M \times K$, the matrix of fast fading coefficients between the K users of cell j and the M antennas of the *l-th* BS, i.e. $g_{ljmk} \triangleq [\boldsymbol{G}_{lj}]_{m,k}$ and $\boldsymbol{D}_{lj}$ is the $K \times K$ diagonal matrix, i.e. $d_{ljk} \triangleq [\boldsymbol{D}_{lj}]_{k,k}$ presents the large-scale fading between the *l-th* BS and the k^{th} user terminal of cell the *j-th* cell. We assume a collocated antennas on the BS, where large-scale fading coefficient is independent of m as in [1],[2]. We can write the channel coefficient as:

$h_{mk} = g_{mk}\sqrt{d_k}$ m=1, 2,…,M (5.6.1)

The $\sqrt{d_k}$ models the geometric attenuation and shadow fading which is assumed to be constant over many coherent time intervals and known prior. Not to lose generality, the channel matrix can be represented as: $\boldsymbol{H} = \boldsymbol{G}\boldsymbol{D}^{1/2}$

According to [1] as $M \gg K$ the following relation holds

$$\left(\frac{\boldsymbol{H}_{lj}^{H}\boldsymbol{H}_{lj}}{M}\right)_{M\gg K} = \boldsymbol{D}_{lj}^{1/2}\left(\frac{\mathbf{G}_{lj}^{H}\mathbf{G}_{lj}}{M}\right)_{M\gg K}\boldsymbol{D}_{lj}^{1/2} \approx \boldsymbol{D}_{lj}^{\frac{1}{2}} \qquad (5.6.2)$$

and $\frac{1}{M}\boldsymbol{G}_{lj}^{T}\boldsymbol{G}_{lj}^{*} = \boldsymbol{I}_K\delta_{jl}$, where $\boldsymbol{I}_K$ is the $K \times K$ identity matrix and δ_{jl} corresponds to the covariance factor of $\mathbf{G}_{jl}$.

Based on (5.6.2), as $M >> K$ we can ignore the effect of fast fading and simply write.

$$h_{ljk} \cong \sqrt{d_{jlk}}$$

The large-scale fading $d_{ljk} = \frac{z_{ljk}}{r_{ljk}^{\delta}}$, where z_{ljk} represents the shadow fading with lognormal distribution with standard deviation σ_{Shadow} and δ is the path loss exponent with r representing the distance to the k^{th} UT.

Followed a technique used in [16], [26], the space of all possible channel realization of Z and R could be divided into V, W vector length respectively.

Let $\hat{z}_v = \{Z: |{z_v}^2 - Z| < |{z_j}^2 - Z|\ for\ all\ j \neq v\}$ and z_v is a scalar representing region $\hat{z}_v$, and let

$$\hat{r}_w = \{R: |{r_w}^2 - R| < |{r_j}^2 - R|\ for\ all\ j \neq w\}$$

where r_w scalar representing region $\hat{r}_w$.

We use the classical non-uniform quantizer algorithm found in [16] to design Z and R.

The parameters of Z and R are acquired from the estimated CSI by minimizing the root mean square error as follows:

$$\arg min_{z_v, r_w}\left[\frac{1}{VW}\sum_{v=1,w=1}^{V,W}\sqrt{{\hat{h}_{ljk}}^2 - \frac{z_v}{r_w^{\delta}}}\right] \qquad (5.6.3)$$

Where the *v-th* and the *w-th* elements of Z and R respectively are z_v, r_w and $\hat{h}_{ljk}$ is the estimated version of CSI related to user k.

7 GARBAGE COLLECTION ALGORITHM

The huge amount of nodes in the CSI map after convergence can be controlled by applying the next Garbage Collection Algorithm:

where *C"* is the index of the edges pointed towered N_i and *E* is the number of those edges.

For each Node N_i in the Graph
    If ($\sum_{c"=1}^{E} W_{c",i} < Th$) Then
    Delete (N_i)
Next

GCA works periodically to delete nodes that have weakly connected edges. In other words, all rarely visited nodes will be removed from the map. Consider increasing the threshold Th, CSI Map will shrink to represent most frequent visited positions in the Map.

8 System Performance

Considering the parameters in (Table 5.8.1), we simulate a scenario to show the performance of CSI Map over conventional Massive MIMO with increasing the number of antennas *M* at the BS. We assume that the user terminals are distributed uniformly in the cells, and they share the same time slot and bandwidth. This assumption brings a worst-case scenario to focus on the spatial multiplexing performance of the system.

Referring to Figure 5.8.1, it is evident that the performance of CSI Map with prediction increases the sum-rate dramatically with both MRC and ZF receivers among increasing the number of antennas. The increase in sum-rate is due to the reduction in uplink pilot contamination.

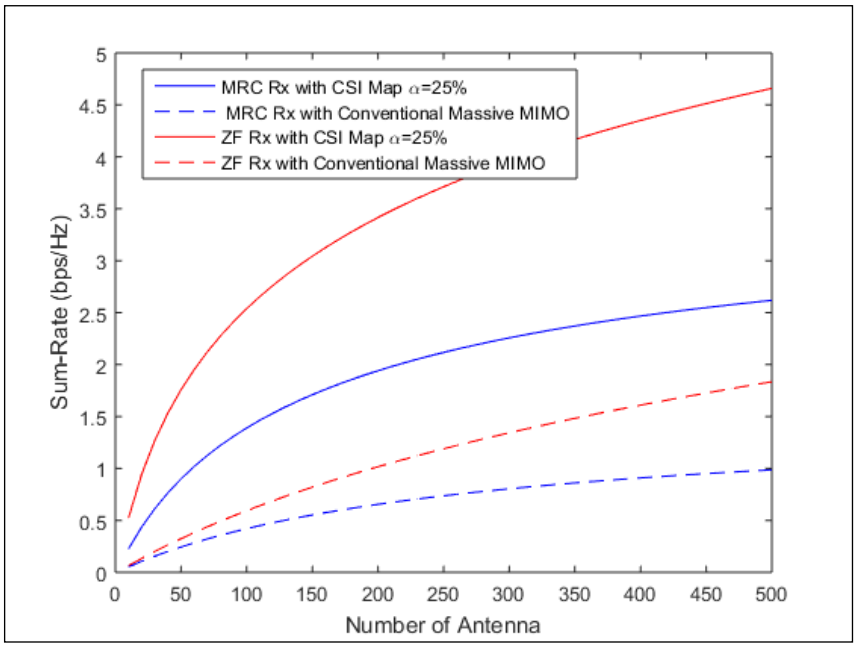

Figure 5.8.1. Sum-rate Vs Number of antennas

Table 5.8.1 Parameters

Parameter	Value
L	7
$K = \tau_p$	30
α	0.25
γ	0.3
T	92
P_u in dB	0.1

Figure. 5.8.2 and 5.8.3 show the performance of prediction using CSI Map in spectral and energy efficiency respectively. We increase the number of antennas and keep on using the parameters in Table 5.8.1, where it is evident from Figure 5.8.2 that the performance in spectral efficiency can be scaled up by a factor of three with MRC and ZF receiver even with *M=60*.

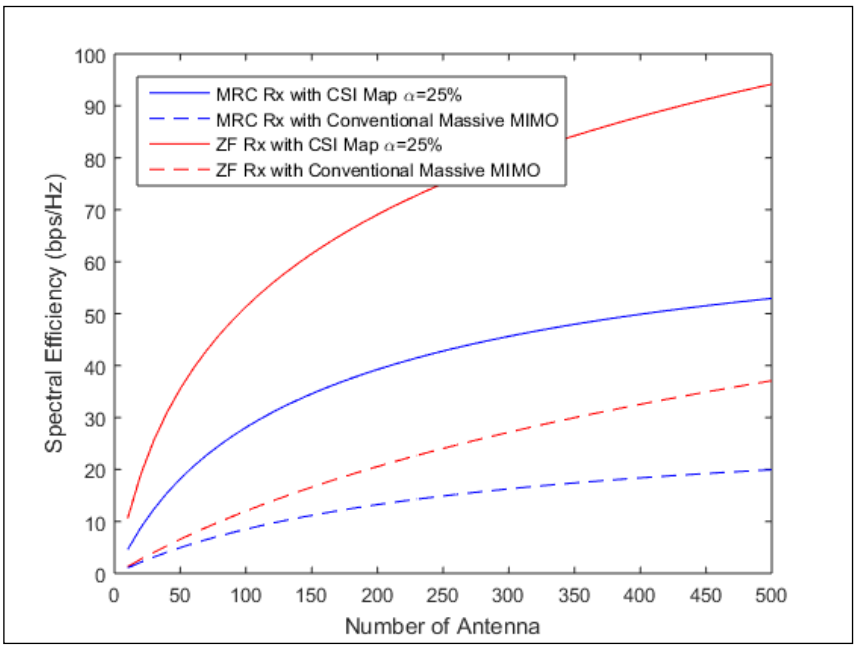

Figure. 5.8.2. Spectral Efficiency Vs. Number of antennas

The performance in energy efficiency compared to the conventional technique is more interesting, where with the same parameters the performance scaled up by a factor of four with ZF receiver and $M > 100$ (see Figure 5.8.3).

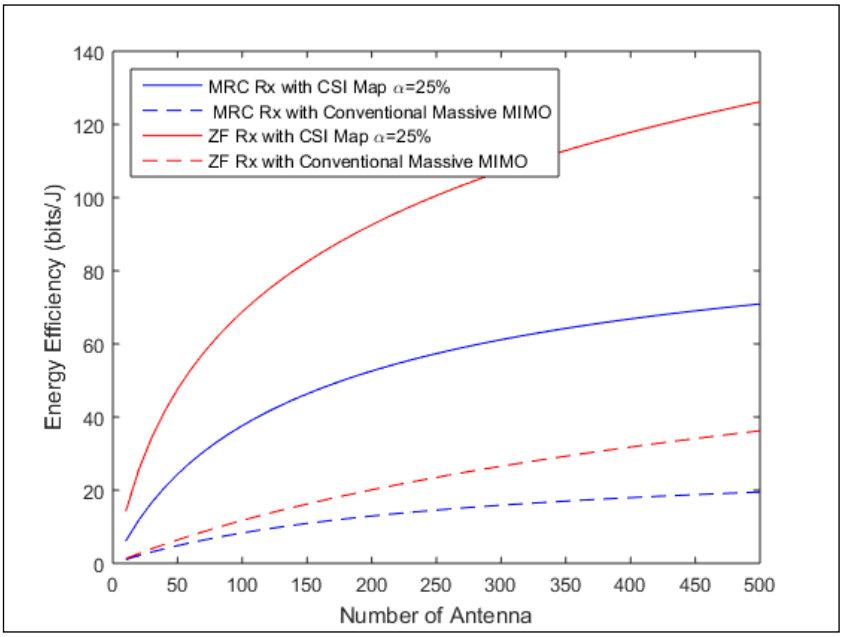

Figure. 5.8.3. Energy Efficiency Vs. Number of antennas

In order to validate the performance of CSI map algorithm, we develop a simulation software, which can create and update CSI map at the BS. Our results consider a system with six cells each including one BS equipped with 420 antennas. The six cells cover an indoor area of 300 m^2, representing a floor in a hotel.

Each cell serves 30 UTs and shares an interference area of 15% of its cell area with neighbor cells. UTs are initially uniform normal distributed and moves randomly in the area. At each TDD session, the new CSI estimated from UTs, are used to update the CSI map. The results presented in this chapter ignores the error results from false CSI prediction.
The progression of the hit ratio will increase and goes toward stability as TDD sessions between BS and UTs increases. Where the hit ratio is defined by the probability to find an estimated CSI in the graph. It is evident from Figure 5.8.4 that the hit ratio is not stable before 50000 TDD sessions, which is due to the lack of CSI of new positions in the cell and it goes toward stability as much as the CSI map get more matured after several learning epochs.
The increase in the hit ratio is directly proportional to the amount of uploaded predictive TDD formats, which leads to less uploaded pilots or initiative TDD formats and thus, less uplink pilot contamination.

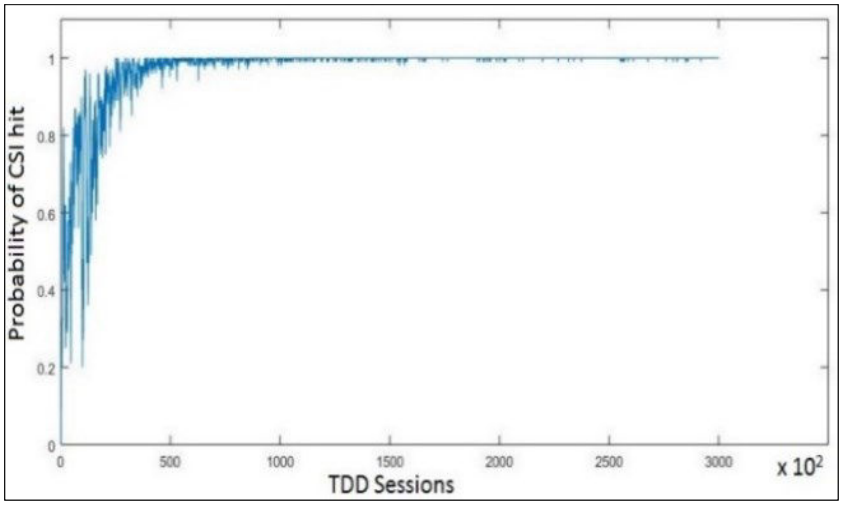

Figure 5.8.4. Hit ratio with respect to the number of TDD sessions

9 Conclusion

This chapter introduces a novel technique to map the CSI in an indoor cell region, independently from user terminals, to a bidirectional graph of weighted connected nodes. We introduce an algorithm to build and update the CSI Map and another Garbage Collection Algorithm to control the number of nodes in the CSI Map. We also introduce a simple algorithm to predict the next possible CSI of any UT given his current CSI. The stored CSI in the map was quantized based on well-known technique that was briefly presented. Further, two TDD frame schemes was introduced to enable pilot skipping and CSI prediction. We show by simulation results the performance of the CSI Map on increasing the number of antennas at the BS. The results on sum-rate, spectral efficiency and energy efficiency outperform the conventional Massive MIMO system with a scale factor.
The introduced CSI Map can be further used to model the user mobility in an indoor scenario. CSI Map is a useful tool that can be used in many applications including query out critical what-if scenarios to take an optimal decision considering wireless resources management. We look forward to implementing CSI map in future researches on outdoor Massive MIMO.

10 References

[1] F. Rusek *et al.*, “Scaling up MIMO : Opportunities and challenges with very large arrays,” *IEEE Signal Process. Mag.*, vol. 30, no. 1, pp. 40–60, 2013.

[2] H. Q. Ngo, E. G. Larsson, and T. L. Marzetta, “Energy and spectral efficiency of very large multiuser MIMO systems,” *IEEE Trans. Commun.*, vol. 61, no. 4, pp. 1436–1449, 2013.

[3] J. Jose, A. Ashikhmin, T. L. Marzetta, and S. Vishwanath, “Pilot Contamination and Precoding in Multi-Cell TDD Systems,” pp. 1–23, 2009.
[4] T. L. Marzetta, “Noncooperative cellular wireless with unlimited numbers of base station antennas,” *IEEE Trans. Wirel. Commun.*, vol. 9, no. 11, pp. 3590–3600, 2010.
[5] H. Q. Ngo, T. L. Marzetta, and E. G. Larsson, “Analysis of the pilot contamination effect in very large multicell multiuser MIMO systems for physical channel models,” *ICASSP, IEEE Int. Conf. Acoust. Speech Signal Process. - Proc.*, vol. 2, no. 2, pp. 3464–3467, 2011.
[6] C. Song, Z. Qu, N. Blumm, and A.-L. Barabasi, “Limits of Predictability in Human Mobility,” *Sci. 327*, no. 5968, pp. 1018–1021, 2010.
[7] J. Kolodziej *et al.*, “An Application of Markov Jump Process Model for Activity-Based Indoor Mobility Prediction in Wireless Networks,” in *Frontiers of Information Technology (FIT)*, 2011, no. IEEE.
[8] A. K. Papazafeiropoulos, H. Q. Ngo, and T. Ratnarajah, “Uplink Performance of Conventional and Massive MIMO Cellular Systems with Delayed CSIT,” in *2014 IEEE 25th Annual International Symposium on Personal, Indoor, and Mobile Radio Communication (PIMRC)*, 2014.
[9] J. H. Sørensen and E. de Carvalho, “Pilot Decontamination Through Pilot Sequence Hopping in Massive MIMO Systems,” in *2014 IEEE Global Communications Conference*, 2014.
[10] A. Yang, Z. He, C. Xing, Z. Fei, and J. Kuang, “The Role of Large-Scale Fading in Uplink Massive MIMO Systems,” in *IEEE Transactions on Vehicular Technology 65.1 (2016)*, 2016.
[11] T. L. Marzetta, “How much training is required for multiuser MIMO?,” *Conf. Rec. - Asilomar Conf. Signals, Syst. Comput.*, pp. 359–363, 2006.
[12] K. Upadhya, S. A. Vorobyov, and S. Member, “Superimposed Pilots are Superior for Mitigating Pilot Contamination in Massive MIMO — Part II : Theory and Channel,” *Unpubl. -arXiv Prepr. arXiv1603.00648*, pp. 1–31.
[13] H. Yin, D. Gesbert, M. Filippou, and Y. Liu, “A coordinated approach to channel estimation in large-scale multiple-antenna systems,” *IEEE J. Sel. Areas Commun.*, vol. 31, no. 2, pp. 264–273, 2013.
[14] K. Li, X. Song, M. Omair Ahmad, and M. N. S. Swamy, “An improved multicell MMSE channel estimation in a massive MIMO system,” *Int. J. Antennas Propag.*, vol. 2014, 2014.

Chapter 6: Pilot Shifting with Coherence Interval Classification

Minor shift in the right direction will cause a major change ~AHB Kingman

This chapter considers the uplink pilot overhead in a time division duplexing (TDD) massive Multiple Input Multiple Output (MIMO) mobile systems. A common scenario of conventional massive MIMO systems is to serve all user terminals (UTs) in the cell with the same TDD frame format that used to fit within the coherence interval of the worst-case scenario of user mobility (e.g. a moving train with velocity 300 Km/h). Within the same cell, pedestrian and low mobility UTs (e.g. moving 1.38 m/s) share the same short TDD frame and thus are obliged to upload their pilots each time-slot. Also, the Base Station (BS) must estimate all the channels each time-slot for all users even for those with long coherence intervals. The channel coherence interval of the pedestrian UTs with a carrier frequency of 1.9 GHz can be as long as 60 times that of the train passenger users. In other words, conventional techniques waste 59-uploaded pilot sequences for channel estimation.
In this chapter, we are aware of the resources waste due to various coherence intervals among different user mobility. We classify users based on their coherence interval length, and then we propose to skip uploading pilots of UTs with large coherence intervals, then we shift frames with the same pilot reused sequence toward an empty pilot time-slot. Simulation results had proved that the proposed technique overcome the performance of conventional massive MIMO systems in both energy and spectral efficiency. It also shows an average pilot reuse factor of approximately 24 with 60 classes.

1 INTRODUCTION

Massive MIMO systems is a promising technology to serve as 5G wireless networks. Indeed such systems boost the spectral efficiency and the energy efficiency [1],[2]. In this regard, a large number of antennas M at the base station (BS) are utilized to communicate with a significantly smaller number of single-antenna user terminals (UTs) K over the same frequency and time domain [3]. However, several tasks challenging the optimal performance of massive MIMO persist even with a large number of antennas at the BS where uplink pilot contamination in Time Division Duplexing (TDD) is the most worthy [1]. During a limited coherence interval and under a TDD reciprocity scheme, UTs in each cell must upload a sequence of orthogonal pilot sequences to their BS for channel estimation lagged with the uplink data; then the BS will precede the downlink data based on the estimated channel matrix using uploaded pilots. This scenario limits the size of the orthogonal uplink pilot sequences that can be generated, which will lead to pilot reuse in adjacent cells and inter-cell interference [4]. In view of this, many research efforts had been made to mitigate uplink pilot contamination in massive MIMO systems [5], [6]. Most efforts in this field can be categorized into two groups, pilot-based estimation approach and subspace-based estimation approach [7]. Selective uplink training based on channel temporal correlation had been recently proposed by [8] to reduce training overhead; the authors exploits the

temporal correlation of UT channels to classify them into two groups. In each channel block, the BS select part of the UTs for training, while prediction determines the other UT CSIs. This approach adds channel prediction complexity to the training channel block, where our technique makes use of pilot sparsity to shift frames into empty pilot spectral space.

1.1 State of Art

This chapter proposes to use heterogeneous TDD frame structure by skipping pilots upload in some frames to reduce pilot contamination and increase energy efficiency on the uplink of massive MIMO systems. We introduce a sparse pilot model with time-shifted TDD frames to increase system spectral efficiency and make reuse of the same pilot sequence while preserving pilot orthogonality. We classify users into different classes according to their coherence intervals and assign each class a pool of sparse shifted pilot sequences that best matches their coherence intervals length, taking into consideration optimizing the overall system performance. We then prove the effect of our proposed technique by simulation results.

1.2 Related Works

Our work is different from [6], [5], [8] in the sense that these works present time-shifted pilots in an inter-cell manner. In the mentioned works, each group of cells uses a time-shift frame, while in our work we group users according to their coherence interval length and we use time shift of unit length equal to an entire time-slot. Further, we skip pilot upload in some time-slots for classes that encountered longer coherence intervals. This skipping makes it possible to reuse the same pilot in the same cell several times without encountering pilot contamination. Till this end, we are not aware of any work that contributes UTs classification based on their coherence interval length coped with time-shifted TDD frame structure.

2 SYSTEM MODEL

To present this proposed technique, we consider the same system model used in Chapter 5. A hexagonal cellular system with L cells each served by one BS holding M-antennas and communicating with K single-antenna UTs that share the same bandwidth. We assume the use of Orthogonal Frequency Division Multiplexing (OFDM) flat fading channel for each subcarrier.
For the upload session, the $M \times 1$ received at the *l-th* BS can be represented by Equation (6.2.1)

$$\boldsymbol{y}_l = \sum_{j=1}^{L} \sum_{\boldsymbol{k=1}}^{\boldsymbol{K}} \sqrt{P_{jk}} \boldsymbol{h}_{ljk} s_{ljk} + \boldsymbol{w}_l \qquad (6.2.1)$$

We follow the system model represented in Chapter 5, and we denote by *K'* the number of UTs that uploads their pilots in the current time-slot and by *K"* the number of UTs that does not upload their pilots during the same current time-slot where *K= K' +K".* Considering the uplink pilot session of length $\tau_p \times 1$, then the received training signal at the *l*-th BS will be presented as follows:

$$\boldsymbol{Y}_{\boldsymbol{l}}^{\boldsymbol{p}} = \sum_{j=1}^{L} \boldsymbol{H}_{lj} \boldsymbol{P}_{\boldsymbol{j}}^{1/2} \boldsymbol{\phi}'^{H}_{j} + \boldsymbol{W}_{\boldsymbol{l}}^{\boldsymbol{p}} \quad (6.2.2)$$

Given that $\left[\boldsymbol{H}_{lj} \in \mathbb{C}^{M \times K}\right]_k = \boldsymbol{h}_{ljk}$ being the channel matrix, $[\boldsymbol{P}_j^{\frac{1}{2}}] \in \mathbb{C}^{K \times 1}]_k = \sqrt{P_{jk}}$ being the SNR, $\left[\boldsymbol{S}_j \in \mathbb{C}^{1 \times K}\right]_k = s_{ljk}$ being the symbol vector and $\boldsymbol{w}_l \in \mathbb{C}^{M \times 1}$ denote the AWGN noise with zero mean and unit variance.

with $\boldsymbol{\phi'}_j^{\boldsymbol{p}} = \left[\boldsymbol{\phi}_j^P \odot \boldsymbol{q}_j\right]$, where $\boldsymbol{q}_j$ is a $K \times 1$ binary matrix of the *j-th* cell with elements $q_k \in \{0,1\}$ as follows:

$$[\boldsymbol{q}]_k = \begin{cases} 1 & if\ the\ k^{th}\ user\ sends\ an\ initiative\ frame \\ 0 & if\ the\ k^{th}\ user\ sends\ a\ predictive\ frame \end{cases}$$

The ratio to encounter pilot upload in any cell will be $\alpha = \frac{K'}{OP}$ where OP denotes the number of orthogonal pilot sequences in the system of L cells. Following this assumption $\int_j \subset \{1, \dots, L\}$ is the set

of cell indices related to the same reused cell pilots as j, and $\int'_j \subset \int_j$ is the set of indices with cardinality $L' = r(L \times \alpha)$ and where $r(.)$ is a function that rounds to the nearest integer.
Since we assumed that every pilot sequence is used once per cell, L' represents the approximate number of contaminated cell. This means that $\frac{L'}{L} \propto \frac{K'}{K}$ by reducing the number of users transmits their pilot in each cell is proportional to reducing the number of interfered cells. Using this proportionality, we can represent $\mathbf{y}_l^{\boldsymbol{p}}$ statistically as:

$$\boldsymbol{y}_l^{\boldsymbol{p}} = \sum_{j=1}^{L} \sum_{\boldsymbol{k=1}}^{\boldsymbol{K'}} \sqrt{P_{jk'}} \boldsymbol{h}_{ljk'} \phi'_{ljk'} + \boldsymbol{w}_l \quad (6.2.3)$$

$$= \underbrace{\sqrt{P_{lk}} \boldsymbol{h}_{llk'} \phi'_{llk}}_{Desired\ Signal} + \underbrace{\sum_{i \in \int'_l \setminus \{l\}}^{L} \sum_{\boldsymbol{k=1}}^{\boldsymbol{K}} \sqrt{P_{ik}} \boldsymbol{h}_{lik'} \phi'_{lik}}_{reused\ pilots} + \underbrace{\sum_{i \notin \int'_l}^{L} \sum_{\boldsymbol{k=1}}^{\boldsymbol{K}} \sqrt{P_{ik'}} \boldsymbol{h}_{lik} \phi'_{lik}}_{Orthogonal\ pilots} + \underbrace{\boldsymbol{w}_l}_{noise}$$

This expression was calculated in the same way as in chapter 5 Equation (5.2.3).

The estimated channel at the BS by a linear MMSE estimator can be represented as,

$$\widehat{\boldsymbol{h}}_{\boldsymbol{ljk}} = \overline{\boldsymbol{h}}_{\boldsymbol{ljk}} + \frac{\sqrt{P_{jk}} \tau_p \beta_{ljk}}{\sum_{i \in \int'_j}^{L} P_{ik} \tau_p \beta_{lik} + \sigma_{UL}^2} \left(\boldsymbol{Y}_{\boldsymbol{l}}^{\boldsymbol{p}} \boldsymbol{\phi}_{\boldsymbol{jk}} - \sum_{i \in \int'_j}^{L} \sqrt{P_{ik}} \tau_p \overline{\boldsymbol{h}}_{\boldsymbol{lik}} \right) \quad (6.2.4)$$

assuming uncorrelated Rayleigh fading channel with a distribution $\boldsymbol{h}_{lik} \sim \mathcal{CN}(\boldsymbol{0}, \beta_{lik} \boldsymbol{I}_M)$,
the estimated vector can be represented as,

$$\widehat{\boldsymbol{h}}_{\boldsymbol{ljk}} = \frac{\sqrt{P_{jk}} \tau_p \beta_{ljk}}{\sum_{i \in \int'_j}^{L} P_{ik} \tau_p \beta_{lik} + \sigma_{UL}^2} \left(\boldsymbol{Y}_{\boldsymbol{l}}^{\boldsymbol{p}} \boldsymbol{\phi}_{\boldsymbol{jk}} \right) \quad (6.2.5)$$

With circularly-symmetric complex Gaussian distributed, $\widehat{\boldsymbol{h}}_{\boldsymbol{ljk}} \sim \mathcal{CN}\left(\boldsymbol{0}, \left(\beta_{lik} - MSE_{ljk}\right) \boldsymbol{I}_M\right)$.

The uncorrelated error is expressed as $\boldsymbol{e}_{\boldsymbol{ljk}} = \widehat{\boldsymbol{h}}_{\boldsymbol{ljk}} - \overline{\boldsymbol{h}}_{\boldsymbol{ljk}}$, with zero mean and variance

$$\mathrm{MSE}_{ljk} = \beta_{ljk} \left(1 - \frac{P_{lk} \tau_p \beta_{ljk}}{\sum_{i \in \int'_j}^{L} P_{ik} \tau_p \beta_{lik} + \sigma_{UL}^2} \right) \quad (6.2.6)$$

Recall that $\beta_{jlk} = \mathbb{V}\{h_{ljkm}\}$ denotes the variance of h_{ljkm}.
The proof can be found in Appendix A, *Lemma 3.7.1.*

Following equation (3.7.5), the BS in the *l*-th cell separate the signal of the *k*-th UT by multiplying the received signal with a linear detector $\boldsymbol{v}_{\boldsymbol{lk}} \in \mathbb{C}^M$ as follows,

$$\boldsymbol{v}_{\boldsymbol{lk}}^H \boldsymbol{y}_{\boldsymbol{l}} = \sum_{i=1}^{L} \sum_{\boldsymbol{t=1}}^{\boldsymbol{K}} \sqrt{P_{it}} \boldsymbol{v}_{\boldsymbol{lk}}^H \boldsymbol{h}_{\boldsymbol{lit}} s_{it} + \boldsymbol{v}_{\boldsymbol{lk}}^H \boldsymbol{w}_l \quad (6.2.7)$$

$$= \underbrace{\sqrt{P_{lk}} \boldsymbol{v}_{\boldsymbol{ik}}^H \boldsymbol{h}_{\boldsymbol{jjk}} s_{jk}}_{preferred\ signal} + \underbrace{\sum_{\boldsymbol{t \neq k}}^{\boldsymbol{K}} \sqrt{P_{lt}} \boldsymbol{v}_{\boldsymbol{lk}}^H \boldsymbol{h}_{\boldsymbol{llt}} s_{it}}_{intra-cell\ interference} + \underbrace{\sum_{\boldsymbol{l \neq i}}^{\boldsymbol{L'}} \sum_{\boldsymbol{t \neq k}}^{\boldsymbol{K}} \sqrt{P_{lt}} \boldsymbol{v}_{\boldsymbol{ik}}^H \boldsymbol{h}_{\boldsymbol{ilt}} s_{lt}}_{inter-cell\ interference} + \underbrace{\boldsymbol{v}_{\boldsymbol{lk}}^H \boldsymbol{w}_l}_{AWGN\ noise} \quad (6.2.7)$$

With $\boldsymbol{v}_{\boldsymbol{jk}} = [\boldsymbol{V}_{\boldsymbol{j}}]_{\boldsymbol{k}}$, is the *k-th* vector of the $V \in \mathbb{C}^{M \times K}$ Matrix.

$$\boldsymbol{V_j} = \begin{cases} \widehat{\boldsymbol{H}}_{\boldsymbol{jj}} & for\ MRC \\ \widehat{\boldsymbol{H}}_{\boldsymbol{jj}} \left(\left(\widehat{\boldsymbol{H}}_{\boldsymbol{jj}}{}^{H} \right) \widehat{\boldsymbol{H}}_{\boldsymbol{jj}} \right)^{-1} & for\ ZF \\ \widehat{\boldsymbol{H}}_{\boldsymbol{jj}} \left(\widehat{\boldsymbol{H}}_{\boldsymbol{jj}}{}^{\boldsymbol{H}} \widehat{\boldsymbol{H}}_{\boldsymbol{jj}} + \frac{1}{P_{lk}} \boldsymbol{I}_K \right)^{-1} & for\ MMSE \end{cases} \quad (6.2.8)$$

Considering an uncorrelated Rayleigh fading channel between the *l-th* base station and the *k-th* user in the *i-th* cell, a lower bound on the ergodic uplink channel Spectral Efficiency can be written as,

$$SE_{lk}^{UL} = \gamma^{UL} \left(1 - \frac{\tau_p}{\tau_c}\right) \log_2(1 + SINR_{lk}^{UL}) \quad (6.2.9)$$

where,

$$SINR_{lk}^{UL} = \frac{G p_{lk} \beta_{llk} \frac{p_{lk} \tau_p \beta_{llk}}{\sum_{i\prime \in \int_{\prime l}} p_{i\prime k} \tau_p \beta_{li\prime k} + \sigma_{UL}^2}}{G \sum_{i \in \int_{\prime l} \setminus \{l\}} p_{lk} \beta_{lik} \frac{p_{lk} \tau_p \beta_{llk}}{\sum_{i\prime \in \int_{\prime l}} p_{i\prime k} \tau_p \beta_{li\prime k} + \sigma_{UL}^2} + \sum_{i=1}^{L\prime} \sum_{t=1}^{K} p_{it} U_{lit} + \sigma_{UL}^2} \quad (6.2.10)$$

The factor $\left(1 - \frac{\tau_p}{\tau_c}\right)$ characterize the payload data, where $\frac{\tau_p}{\tau_c}$ is the pilot sequence symbol length over the total frame length, and γ^{UL} is the fraction of the uplink data.

Considering MRC detection scheme, $G = M$ *and* $U_{lit} = \beta_{lit}$, while considering ZF detection scheme, $G = M - K$ and

$$U_{lit} = \begin{cases} MSE_{lit}, & for\ i \in \int_{\prime l} \\ \beta_{lit}, & otherwise \end{cases}$$

The proof can be found by *Theorem 4.4.1* and *Corollary 4.4.1* in Appendix A.
Energy Efficiency EE_n for Class n is expressed as:

$$EE_n = \frac{\gamma^{UL}}{P_{lk}} \left(\frac{n(T - \tau_p)}{nT - (n-1)\tau_p} \right) K_n log_2\left(1 + SINR_{lk}^{UL}\right)$$

where K_n is the number of users of Class n.

3 TIME-SHIFTED PILOTS

The diversity among UT coherence intervals depends on the propagation environment, user mobility, and the carrier frequency [3]. Since not all UTs encounter the same mobility within the cell, we can classify them according to their coherence interval length. Therefore, users belonging to Class 1 encounter the shortest coherence interval of length T, which is also considered as the TDD frame size. Indeed, users of Class 1 should upload their pilots each TDD frame. Furthermore, users of Class n with a coherence interval of length T'> nT should upload their pilots once each n TDD frames. Within one channel estimation during the coherence interval, BS can be precode all downlink data belong to this coherence interval based on the last estimated CSI. In Figure 6.3.1, we introduce an example of a sequence of TDD frames related to 3 UTs belonging to Class 3 using the same pilot sequence (represented by P). The 3 UTs exchange different data streams with the BS (represented by D). By shifting the frame toward a pilot free time-slot, users of Class n can reuse the same pilot n times subjected to T (n-1) ≤ Q. We denote by Q the maximum acceptable coherence interval which can be assigned by the network designers according to performance demands.

By following the definition of the sample duration of the slots, expressed in [9] as the number

of OFDM symbols times, the tone length of the Nyquist sampling interval $T = \frac{T_{slot}\, T_u}{T_s\, T_g}$. For typical OFDM parameters, symbol interval is $T_s = 1/14\, ms$, usable interval is $T_u = 1/15$ ms, guard interval is $T_g = 1/220\, ms$. Assuming delay-spread equals T_g, Nyquist interval is equivalent to $\frac{T_u}{T_g} = 14$ tones.

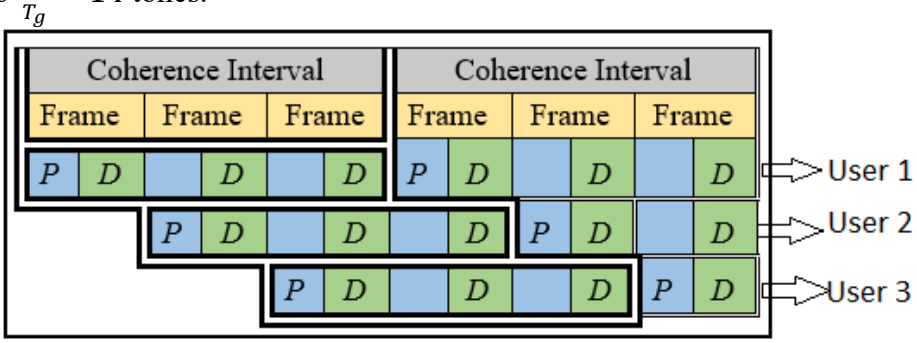

Figure 6.3.1: Time-Shifted frames of Class 3 UTs

Consider Class 1 corresponding to UTs moving in a train of speed 300 Km/h. Thus it took 473.7μs to pass ¼ wavelength at frequency 1.9 GHz which has an equivalent sample duration of T=92. If a pedestrian uses moves with an average speed of 1.38 m/s, their sample duration will be Tp= 400 which will lead to n=60 and hence, UTs related to this class can reuse the same pilot 60 times (ignoring the maximum shift delay limit).

4 User Terminals Classification

In this section, we propose a UTs classification algorithm that will allow us to take benefit from the proposed pilot shifting technique. One way to classify UTs is to monitor their consecutive CSI covariance matrices and classify them according to their speed of change among several time-slots. Indeed, UTs with high mobility profiles will be assigned to lower classes and low mobility UTs will be allocated to higher classes. Assume that the BS had a prior assigned Class C(k) corresponding to the coherence interval T of UT k. The BS can run the following algorithm (Figure 6.4.1) periodically or on SNR failure, to update the assigned class C(k) of the *k-th* UT.

1- i=1, C(k)=c
2- while (i ≤ C(k)+1)
3- if ($\frac{|\hat{h}_{lk}(t)(\hat{h}_{lk}(t-i))^H|}{\|\hat{h}_{lk}(t)\|} \geq (1 - |\varepsilon|)$
4- if(i > C(k) & C(k) < C(Q))
5- C(k)++
6- i++ , GoTo 2
7- else
8- C(k)= i – 1
9- end if
10- end while

Figure 6.4.1 User classification algorithm

Following the algorithm, depicted in Figure 6.4.1, the BS checks the covariance of the current channel vector $\hat{\boldsymbol{h}}_{\boldsymbol{lk}}(\boldsymbol{t})$ with the previous C(k) channel vectors. In the case that the channel persists with an acceptable error of $|\boldsymbol{\varepsilon}|$ for C(k)+1 consecutive time-slots and still below the limit Class C(Q), the Class C(k) of the k-th UT C(k) is promoted. Otherwise, if the channel

failed to persist for C(k) consecutive time-slots, the class assigned to the *k-th* UT will be degraded. After the *k-th* UT has been classified to Class C(k), he should upload his pilots once every C(k) consecutive time-slots, which will lead not only to the decrease of the uplink pilot contamination, but also to the reduction in the transmitted power at the UT and the increase of the density of UTs/cell.

Recent advances in massive MIMO systems recommend coordinating the pilot allocation between interfering cells by ensuring no pilot reuse between adjacent cells to avoid pilot contamination from the first tier of interfering cells. These techniques solve the pilot contamination problem radically for rational numbers of antennas. However, the number of UTs per cell decreases drastically since only a fraction of the pilot sequences are used in each cell. Interestingly, the proposed sparse pilot assignment allows pilot reuse within the same interference domain by shifting pilots toward a pilot free time-slot, which increases the UTs density per cell while mitigating inter and intra cell interference.

5 PILOT ALLOCATION

This section proposes a pilot allocation scheme that distributes pilot among UTs in the multi-cell scenario. The task must be handled by the Mobile Switching Center (MSC) or any central switch between BSs.

The following equation presented the number of possible shifts between two classes (e.g. m, n),

$$NS(m,n) = (GCD(m,n) - 1)\frac{\min(m,,n)}{GCD(m,n)}, \qquad (6.5.1)$$

with $GCD(m,n)$, stands for Greatest Common Divisor between the two natural numbers m, *n.*

A Greedy Pilot Allocation Algorithm is presented in Figure 6.5.1. This algorithm runs over the MSC

1. Create list of possible class pairs and with the corresponding number of shifts

CP (Class1, Class2, $NS(Class1, Class2)$*).*

2. Sort the list in descending order.
3. Do while there are unallocated pilots and there exist a UT without pilot
4. Pick a pilot *P* from an orthogonal array of pilots of length *OP*.
5. Pick a class pair from the head of *CP*
6. Search for maximum existing group of UTs with classes *m, n* that can fit *CP (m, n,* $NS(m,n)$*).*
7. Allocate the picked pilot *P* to the UTs found by step 6.
8. End do while

Figure 6.5.1 Greedy Pilot Allocation Algorithm

and is capable of allocating UTs in an efficient way such that each orthogonal pilot sequence is assigned to the maximum possible group of UTs from related to the same class or different class pair. Since the list of the possible class pair is sorted in descending order, MSC will start allocating orthogonal pilot sequences from the largest possible number of shifts to the least number. This will increase the reuse factor of pilot allocation which can be represented by, $Allocfact = \frac{Allocated\ UTs}{OP}$. The reuse factor of pilot allocation is also affected by the distribution of UTs among the Classes. In other words, the mobility of user terminals within the interference region will have a major impact on the pilot allocation reuse

factor. It is clear that, the higher the number of users in high classes, the higher the allocation reuse factor.

6 NUMERICAL RESULTS

In this section, we illustrate the performances of the proposed technique through Matlab simulations. We simulate a scenario with $L=7$ hexagonal cells. We assume pilot reuse once at the same time-slot in each cell, and that each cell owns τ=30 pilot sequences and $K=30$. The system uses a carrier frequency of 1.9 GHz, and we consider UTs with several channel coherence profiles. We also assume that the transmit power P_{lk} is upper bounded by 0.1 dB. We consider Class 1 time-slot of sample duration T=92 OFDM symbols and C(Q)=30.

In the first scenario, we simulate a conventional massive MIMO system (with only Class 1 users, i.e. all UTs send pilot every time slot) and a system with Class 3 users (every UTs uploads pilot once every 3-time slots). We recall that the time slot corresponds to the smaller coherence interval of all the UTs. Figures 6.6.1 and 6.6.2 illustrate the energy efficiency and the spectral efficiency of Class 1 and Class 3 UTs respectively. We can observe that Class 3 overcome the classical massive MIMO in both SE and EE, and the gap between Class 1 and 3 still increase with the number of antennas. Specifically, for 100 antennas, we can see that the EE of Class 3 UTs is almost 4 times better than conventional massive MIMO system. Note that, in conventional massive MIMO system, if there is only one UT having a coherence interval of Ts (Class 1) and all the other UTs have a coherence interval higher than 3*Ts (Class 3), all the UTs must upload pilot to the BS every Ts.

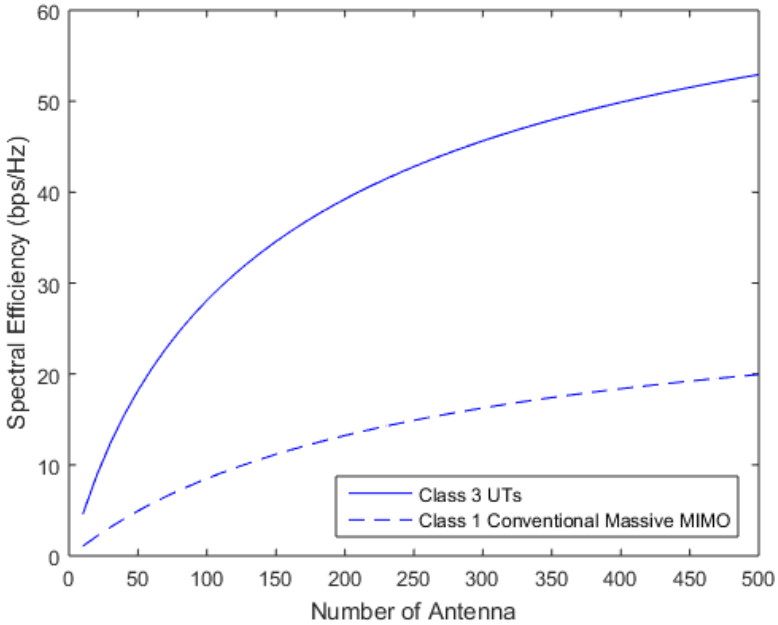

Figure 6.6.1 Spectral Efficiency Vs M

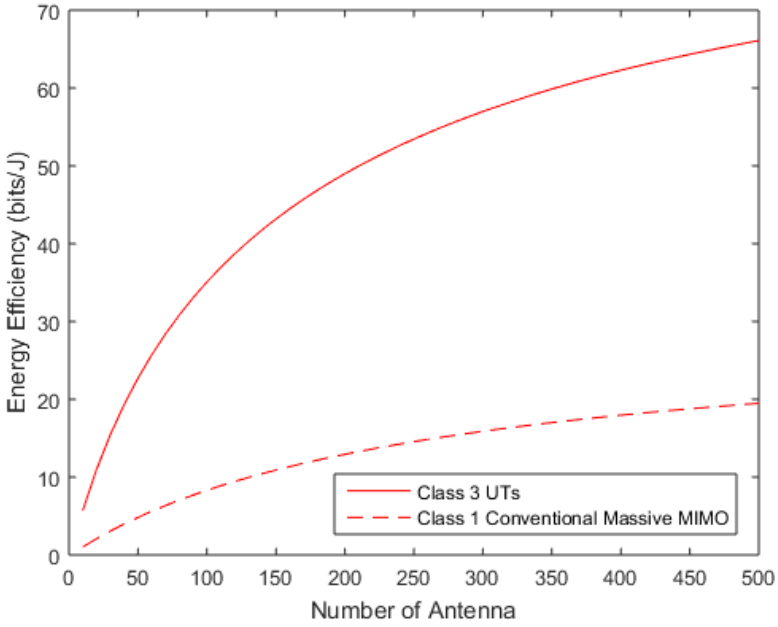

Figure 6.6.2 Energy Efficiency Vs M

To illustrate the performance of different classes of UTs, we further simulate the EE depending on the class index. In Figure 6.6.3, we consider *M=300* antennas and vary the class index from 1 to 30, wherein Figure 6.6.4 we vary M, and illustrate the EE of the set of classes from 1 to 30. Both figures demonstrate the significant advantage of using our proposed technique regarding both: energy efficiency and spectral efficiency. Indeed, there is a gap between the EE performance of the set of classes with indices greater than 1 and the EE performance of Class 1 (the curve at the bottom, Conventional massive MIMO). This result supports our claim about the utility of frame-shifting and sparse frame pilot for massive MIMO.

Note also that frame-shifting and sparse frame pilot reduce the computational estimation costs at the BS due to sparse received channel matrix. Moreover, by pilot skipping, pilot reuse will lead to the increase of the number of UTs/cell without any pilot contamination. Furthermore, the transmitted power of each UT can be reduced due to the reduction of inter and intra-cell interference.

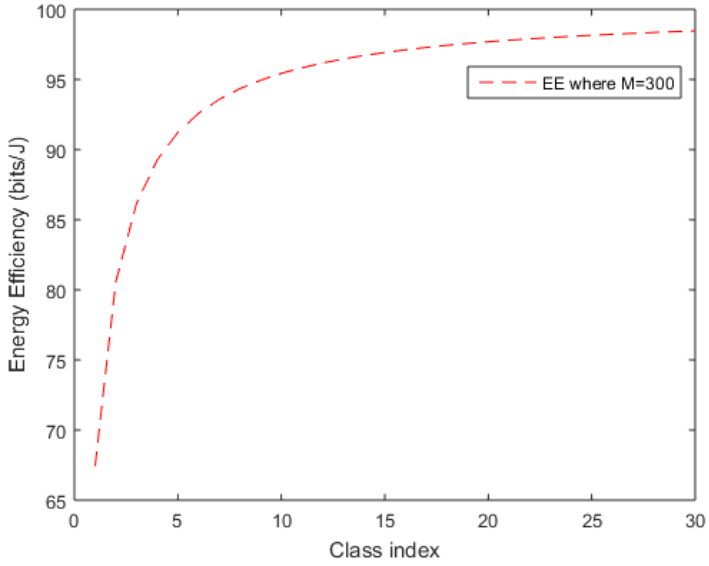

Figure 6.6.3 EE Vs Class index

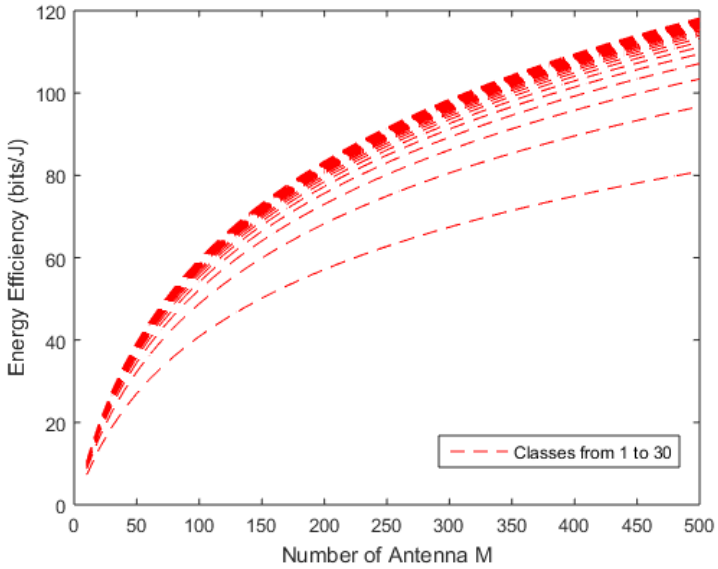

Figure 6.6.4 Classes indices from 1 to 30 Vs EE

To evaluate the reuse factor of the pilot allocation algorithm, we prepare a scenario of a 1000 UTs distributed over the same interference region and with a random normal distribution over the first 21 Classes with the mean class of 10 and a variance of 2.85, (see Figure 6.6.5).

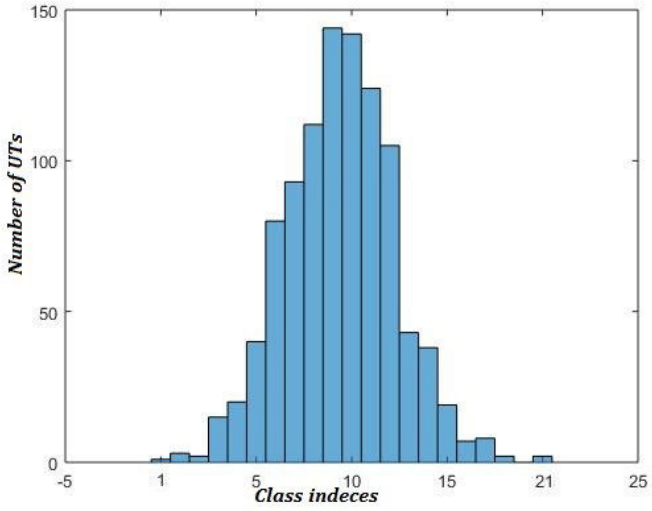

Figure 6.6.5 User Distribution among 21 Classes

OP=125 orthogonal pilot sequences are dedicated for pilot allocation; the obtained result is that 997 users of 1000 had been allocated to pilots and only three users still without pilots. By looking for the mobility of these users, one can find that those users are with the highest speed and they are related to class 1. The reuse factor of this allocation is $Allocfact = 7.976$. Another scenario where done with 3000 UTs distributed over 60 Classes using the same *OP=125,* we get an reuse factor of $Allocfact = 23.952$ with 2994 user allocated pilots (See figure 6.6.6).

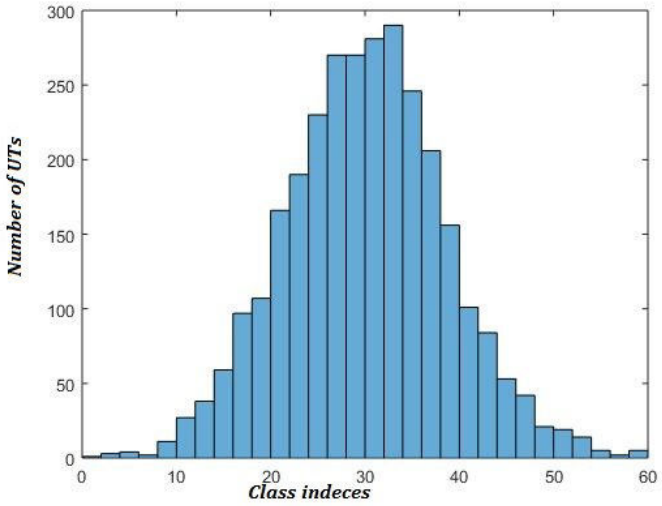

Figure 6.6.6 User Distribution among 60 Classes

7 CONCLUSION

In this chapter, we have introduced a novel technique to reduce the pilot overhead by classifying UTs based on their coherence interval. Then, we have shifted frames containing pilots to an empty time pilot space. Indeed, using sparse pilot and frame-shifting, a little number of orthogonal pilot sequences can serve a higher number of UTs and pilot reuse will be possible within the same cell without leading to pilot contamination. a user mobility classification algorithm was introduced to classify users based on their coherence interval length. The users were allocated to different classes that scales with the number of pilot skips. In other words, higher user classes correspond to more pilot skipping. Then frame shifting among users will take place to ensure orthogonality among pilots in the same time slot.

The proposed technique had proved its ability to mitigate pilot contamination, increase spectral and energy efficiency, increase UT/cell and reduces the computational estimation cost. Note that channel coherence based classification among UTs should be considered as a main issue in the future 5G mobile networks.

8 REFERENCES

[1] T. L. Marzetta, "Noncooperative cellular wireless with unlimited numbers of base station antennas," *IEEE Trans. Wirel. Commun.*, vol. 9, no. 11, pp. 3590–3600, 2010.

[2] H. Q. Ngo, E. G. Larsson, and T. L. Marzetta, "Energy and spectral efficiency of very large multiuser MIMO systems," *IEEE Trans. Commun.*, vol. 61, no. 4, pp. 1436–1449, 2013.

[3] E. Björnson, E. G. Larsson, and T. L. Marzetta, "Massive MIMO: Ten Myths and One Critical Question," pp. 1–10, 2015.

[4] J. Hoydis, S. ten Brink, and M. Debbah, "Massive MIMO: How many antennas do we need?," in *2011 49th Annual Allerton Conference on Communication, Control, and Computing (Allerton)*, 2011, pp. 545–550.

[5] K. Appaiah, A. Ashikhmin, and T. L. Marzetta, "Pilot contamination reduction in multi-user TDD systems," *IEEE Int. Conf. Commun.*, 2010.

[6] F. Fernandes, A. Ashikhmin, and T. L. Marzetta, "Inter-cell interference in noncooperative TDD large scale antenna systems," *IEEE J. Sel. Areas Commun.*, vol. 31, no. 2, pp. 192–201, 2013.

[7] O. Elijah, C. Y. Leow, A. R. Tharek, S. Nunoo, and S. Z. Iliya, "Mitigating pilot contamination in massive MIMO system - 5G: An overview," *2015 10th Asian Control Conf. Emerg. Control Tech. a Sustain. World, ASCC 2015*, no. c, 2015.

[8] C. Li, J. Zhang, S. Song, and K. B. Letaief, "Selective Uplink Training for Massive MIMO Systems," in *IEEE International Conference on Communications (ICC), Kuala Lumpur, Malaysia*, 2016.
[9] T. L. Marzetta, "Massive MIMO: An Introduction," *Bell Labs Tech. J.*, vol. 20, pp. 11–22, 2015.

Chapter 7: Conclusion and Future Work

A conclusion is the place where you get tired of thinking~ Arthur Bloch

This Chapter summarize the contributions of the thesis and suggests future research directions that from our point of view considered valuable. In general, this thesis presents in Chapter 1, an introductory overview of the 5G Mobile technology and its ongoing projects. Then in Chapter 2, a special focus on massive MIMO systems of the 5G was presented. Passing through benefits and challenges facing this technology. Chapter 3, introduce Downlink and uplink processing and focus on the TDD scheme. For instance, Linear and non-linear precoding techniques were briefly presented. Also, regarding the uplink processing techniques, brief linear detection techniques were introduced. Furthermore, linear and non-linear channel estimation had occupied a portion of the chapter. Regarding the challenges facing massive MIMO, that was introduced in Chapter 2; the interference problem was expanded in Chapter 4. This last presents the inter and intra-cell interference and some practical interference challenges in the 5G and massive MIMO for instance. Then a special focus on the uplink pilot contamination in massive MIMO system was expanded to cover contamination sources, the impact of pilot contamination on system performance and literary techniques to mitigate uplink pilot contamination. Chapter 5 and Chapter 6 introduce our contributions in this thesis. These contributions were directed toward mitigating uplink pilot contamination in massive MIMO mobile systems. For instance, Chapter 5 introduce a machine learning technique to predict channel state information rather than to estimate it. The prediction of the CSI is based on a map that stores a quantized version of the previous estimated CSI during the learning session. This technique considered a novel contribution to mitigating uplink pilot contamination. In Chapter 6, another novel technique to mitigate uplink pilot contamination and to increase the cell density was introduced. This was done by classifying users based on their mobility profile. Then exempting users with low mobility, (larger coherence interval) from uploading their pilots each TDD frame. At last, this ending chapter concludes the thesis contribution and summarize the results. Then suggests some future research directions extend this research.

1 Summary of Results

This section summarizes the results obtained by our contribution in this thesis. Hence, results of Chapter 5 and Chapter 6 were introduced.

1.1 CSI Map

The concept of mapping geographical locations within the cell into their corresponding CSI can be widely exploited to improve system performance. This is because the CSI is no more related to the user but to the position. On the dimension of system capacity and spectral efficiency, the ergodic capacity of the system was shown to overcome conventional techniques. Also, training overhead was significantly reduced, and just a limited number of UTs should upload their pilots.

On the dimension of energy efficiency, the reduced number of uploaded pilot had significantly reduced the power consumption on the UT side. Further, channel estimation process was compensated with low complexity search algorithm to predict the next possible CSI. Hence, a significant reduction of power consumption can be achieved.
On the dimension of network intelligence and user experience, the prediction of UT mobility can be exploited to improve resources management in the mobile network. For instance, cell density and roaming users can be easily predicted, and prior processing and resources allocation can be applied.

1.2 Pilot Shifting

By considering user mobility, a significant improves the overall system performance can take place. Chapter 6, presents an improve in spectral and energy efficiency over standard massive MIMO with a breaking bound on the number of users per cell.
Considering the spectral efficiency, the result shows a scale up with significant factor over the conventional massive MIMO systems. This is due to the increase in SINR and decrease of the uplink pilots. Hence, training overhead is also reduced allowing more users to be served within the same interference region.
Considering the energy efficiency, the skipped pilots reduce the transmission power and thus increase the energy efficiency of the system. Also, channel estimation process was mitigated, and less processing power should be used. As the SINR increases, the low transmission power is needed for symbol detection at the receiver.
The increase in the pilot reuse factor allows an enormous number of users to share the same pilot pool. For instance, 3000 UTs can use only 125 orthogonal pilot sequences.
Worth to mention that user mobility profile can be utilized as user experience information and exploited to manage system resources and to handle roaming and city traffic management.

2 FUTURE RESEARCH DIRECTIONS

As an extension of this research and to keep on improving the 5G Mobile Networks, several future types of research were suggested.

2.1 Outdoor CSI Map

Since the map size should increase with the geographical area it represents, it is not suitable for an outdoor scenario. Furthermore, the high mobility users in the outdoor scenario stand against implementing CSI map in outdoor.
We suggest an extension technique that adapts CSI map to the outdoor scenario and to still benefit from its significant performance improvements.

2.1.1 Shadowing Region Isolation

Massive MIMO proves its ability to mitigate the effect of fast fading noise by increasing the number of the antenna at the BS. Motivating by this fact, one can think of modeling the channel between the BS and the UT by the shadowing effect and the path loss effect (see Figure 7.2.1). Considering the last one, by having a knowledge of the position of the BS and the UT, it is easy to calculate the fading due to path loss. The only remaining factor to acquire the knowledge about the channel is the shadowing effect.

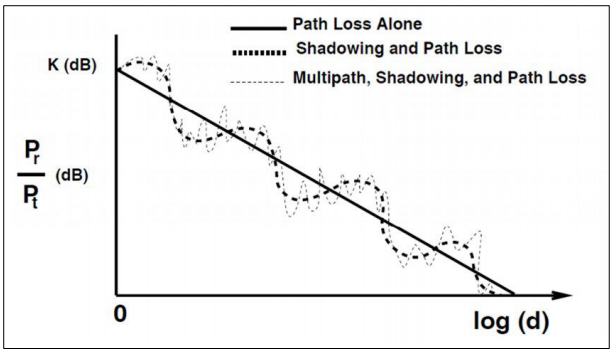

Figure 7.2.1 Fading effect

By learning several channels of known positions users, it is reasonable to construct a map of shadowing regions, where each region is subjected to the same shadowing effect (see Figure 7.2.2 and 7.2.3). If this region was learned, given any UT position, one can calculate the channel state information to this terminal. Hence, Outdoor CSI map can be easily applied, and channel prediction will take place instead of channel estimation.

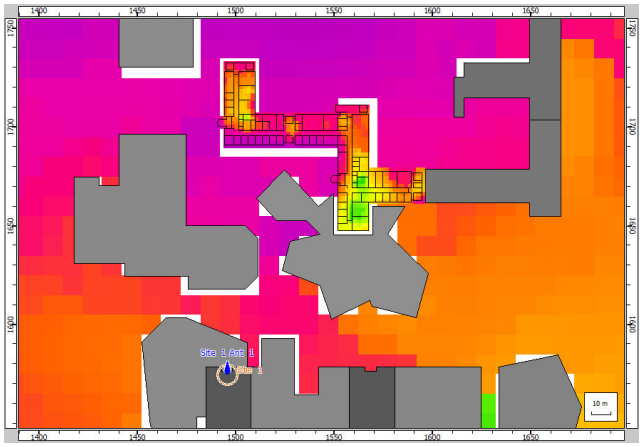

Figure 7.2.2 Shadowing regions indoor

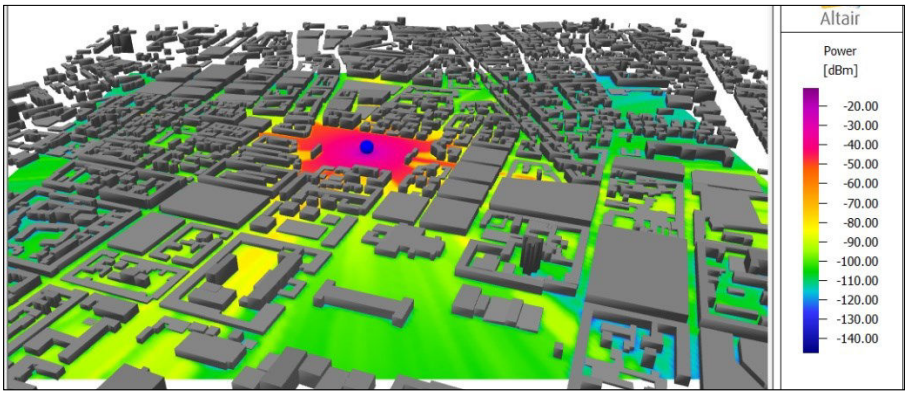

Figure 7.2.3 Shadowing region outdoor

2.1.2 Fast Mobility is region limited

Referring to the fact that fast mobility users must have a track e.g. (Railway, Roads), CSI map can be limited to the space occupied by the tracks in high mobility regions. Motivated by this fact, CSI map size can be reduced significantly and applying it to outdoor scenario will be no more a big challenge.

2.2 Cell-Free Mobile Network

The considerable number of antennas implemented at the BS, allow for a new physical dimension in multiplexing. This is referred to in the literature as "Spatial Multiplexing" and is defined by the ability of the base station to focus the signal to a specific space in the covered region. Hence, a substantial number of users can be served with the same frequency and time resources. This ability can be exploited to elevate from conventional predefined cells to a cell-free scenario.

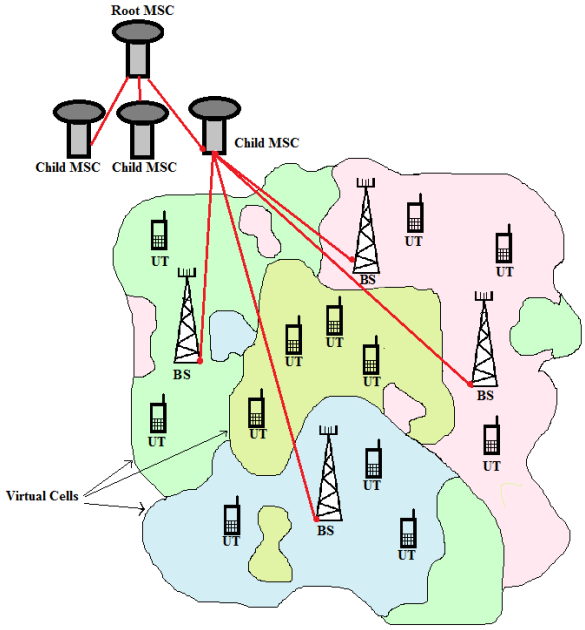

Figure 7.2.4 Cell Free Scenario

With cell-free, the user is no more dedicated to being served by a specific BS, but any BS in the interference region can serve it. This issue makes the network user-based and allows higher flexibility for user mobility and coverage (see figure 7.2.4). Hence, this flexibility is due to collaboration between BS's to serve a group of UTs in their coverage regions. Research in this direction can significantly improve system performance and apply CSI map.

2.3 Network Intelligence

Another direction for future research is the improvement in the network intelligence part of the Network. By network intelligence we mean the ability of the network to learn from system behavior, (including user mobility, and type of data), to take proper decisions. Those decisions can be among resources management or even infrastructure self-management.

Motivating by the flow toward Software Defined Networks (SDN) and Network Function Virtualization (NFV), that was considered a demand for 5G networks, network intelligence will improve the performance of the network to make it suitable to serve in future smart cities.

Worth to mention that the proposed CSI map can be part of this network intelligence.

Appendix A

Proof of Lemma 3.7.1.

The channel estimation of the k-th user in the l-th cell $\boldsymbol{h_{jlk}}$*, require the pilot sequence* $\boldsymbol{\phi_{lk}}$ *and can only appears as* $\boldsymbol{h_{jlk}\phi_{lk}^H}$ *where* $\boldsymbol{\phi_{lk}} \in \mathbb{C}^{\tau_p}$*. Estimating the channel by multiplying* $\boldsymbol{\phi_{lk}}$ *from the left side of the pilot signal in equation (3.7.2) gives,*

$$\boldsymbol{Y_j^p \phi_{lk}} = \sum_{l=1}^{L} \boldsymbol{H_{jl} P_l^{1/2} \phi_l^H \phi_{lk}} + \boldsymbol{W_j^p \phi_{lk}}$$
$$= \sum_{i \in \int_l}^{L} P_{ik} \tau_p \mathbf{h}_{ilk} + \boldsymbol{\widetilde{w}_{jlk}^p}$$

where $\boldsymbol{\widetilde{w}_{jlk}^p} = \boldsymbol{W_j^p \phi_{lk}} = [\widetilde{w}_{jlk1}^p, \dots, \widetilde{w}_{jlkM}^p]^T \sim \mathbb{CN}(\mathbf{0}, \tau_p \sigma_{UL}^2 \boldsymbol{I}_M)$*. This is true due to the pilot orthogonality assumption.*

We can further compute the linear MMSE of each element $y_{ilkm} \in \boldsymbol{Y_j^p \phi_{lk}}$ *(m-th row) as,*

$$\mathrm{y}_{ilkm} = \sum_{i \in \int_l}^{L} P_{ik} \tau_p \mathrm{h}_{ilkm} + \widetilde{w}_{jlkm}^p \qquad (A.1.1)$$

Linear MMSE estimation of the channel h_{ilkm} *is given in [11] by definition as*

$$\hat{h}_{ilkm} = \mathbb{E}\{h_{jlkm}\} + \frac{COV\{\mathrm{h}_{jlkm}, \mathrm{y}_{jlkm}\}}{\mathbb{V}\{y_{jlkm}\}} (\mathrm{y}_{ilkm} - \mathbb{E}\{y_{jlkm}\}) \quad (A.1.2)$$

We have

$$\bar{h}_{jlkm} = \mathbb{E}\{h_{jlkm}\}$$
$$\mathbb{E}\{y_{jlkm}\} = \sum_{i \in \int_l}^{L} P_{ik} \tau_p \bar{\mathrm{h}}_{ilkm}$$
$$\mathbb{V}\{y_{jlkm}\} = \sum_{i \in \int_l}^{L} P_{ik} {\tau_p}^2 \beta_{jik} + \tau_p \sigma_{UL}^2$$
$$COV\{\mathrm{h}_{jlkm}, \mathrm{y}_{jlkm}\} = \sqrt{P_{lk}} \tau_p \beta_{jlk}$$

Substituting this primary into the definition of $\hat{h}_{ilkm}$ *and write it in vector form, we will arrive on (2.7.3). The variance* $\mathbb{V}\{\hat{h}_{ilkm}\}$ *is expressed as follows,*

$$\mathbb{V}\{\hat{h}_{ilkm}\} = \frac{COV\{\mathrm{h}_{jlkm}, \mathrm{y}_{jlkm}\}^2}{\mathbb{V}\{y_{jlkm}\}} = \frac{P_{lk} \tau_p {\beta_{jlk}}^2}{\sum_{i \in \int_l}^{L} P_{ik} \tau_p \beta_{jik} + \sigma_{UL}^2} \qquad (A.1.3)$$

and the uncorrelated Estimation Error is expressed as,

$$MSE = \beta_{jlk} - \mathbb{V}\{\hat{h}_{ilkm}\}. \qquad (A.1.4)$$

Proof of Theorem 4.4.1

The ergodic capacity C_{lk}^{UL} is the supremum of the mutual information between the output $\boldsymbol{v_{jk}^H y_j}$ and the input s_{lk} represented in equation (3.7.5). Assume that the distribution of the input is $s_{lk} \sim \mathbb{CN}(0,1)$ and the supremum is taken over this distribution. Let $\widehat{\boldsymbol{H}}$ denoted the estimated channel at the receiver. Thus, we have

$$C_{lk}^{UL} \geq \gamma^{UL} \left(1 - \frac{\tau_p}{\tau_c}\right) I(s_{lk}; \boldsymbol{v_{lk}^H y_l}, \widehat{\boldsymbol{H}}) \qquad (A.2.1)$$

$$C_{lk}^{UL} = \gamma^{UL}\left(1-\frac{\tau_p}{\tau_c}\right)\left(h(s_{lk}) - h(s_{lk}|\boldsymbol{v}_{\boldsymbol{lk}}^H\boldsymbol{y}_{\boldsymbol{l}}, \widehat{\boldsymbol{H}})\right) \quad (A.2.2)$$

$$C_{lk}^{UL} = \gamma^{UL}\left(1-\frac{\tau_p}{\tau_c}\right)\left(\log_2(\pi e) - h(s_{lk}|\boldsymbol{v}_{\boldsymbol{lk}}^H\boldsymbol{y}_{\boldsymbol{l}}, \widehat{\boldsymbol{H}})\right) \quad (A.2.3)$$

Where we denote by $h()$, the differential entropy function and by $I(\,.\,;\,.\,)$, the mutual information under the assumed sub-optimal Gaussian distribution.
Equation (A.2.2) follows from the definition of mutual information while equation (A.2.3) follows from the entropy expression for the complex Gaussian random variables.
$\gamma^{UL}\left(1-\frac{\tau_p}{\tau_c}\right)$, represent the fraction of the uplink transmitted symbols over the coherence interval of length τ_c.
An upper bound of $h(s_{lk}|\boldsymbol{v}_{\boldsymbol{lk}}^H\boldsymbol{y}_{\boldsymbol{l}}, \widehat{\boldsymbol{H}})$ is characterized by,

$$h\left(s_{lk}\middle|\boldsymbol{v}_{\boldsymbol{lk}}^H\boldsymbol{y}_{\boldsymbol{l}}, \widehat{\boldsymbol{H}}\right) = h\left(s_{lk} - \alpha\,\boldsymbol{v}_{\boldsymbol{lk}}^H\boldsymbol{y}_{\boldsymbol{l}}\middle|\boldsymbol{v}_{\boldsymbol{lk}}^H\boldsymbol{y}_{\boldsymbol{l}}, \widehat{\boldsymbol{H}}\right) \quad (A.2.4)$$

$$h\left(s_{lk}\middle|\boldsymbol{v}_{\boldsymbol{lk}}^H\boldsymbol{y}_{\boldsymbol{l}}, \widehat{\boldsymbol{H}}\right) \le h\left(s_{lk} - \alpha\,\boldsymbol{v}_{\boldsymbol{lk}}^H\boldsymbol{y}_{\boldsymbol{l}}\right) \quad (A.2.5)$$

$$h\left(s_{lk}\middle|\boldsymbol{v}_{\boldsymbol{lk}}^H\boldsymbol{y}_{\boldsymbol{l}}, \widehat{\boldsymbol{H}}\right) \le \log_2\left(\pi e\,\mathbb{E}\left\{\left|s_{lk} - \alpha\,\boldsymbol{v}_{\boldsymbol{lk}}^H\boldsymbol{y}_{\boldsymbol{l}}\right|^2\right\}\right) \quad (A.2.6)$$

where (A.2.4) follows from the fact that subtracting a known variable $\alpha\,\boldsymbol{v}_{\boldsymbol{lk}}^H\boldsymbol{y}_{\boldsymbol{l}}$, does not change the entropy, given that α is some deterministic scalar. (A.2.5) can be explained by the fact that, dropping the knowledge of $\boldsymbol{v}_{\boldsymbol{lk}}^H\boldsymbol{y}_{\boldsymbol{l}}, \widehat{\boldsymbol{H}}$ will increase the entropy, while (A.2.6) is claimed based on the fact that the maximum entropy can be obtained when $s_{lk} - \alpha\,\boldsymbol{v}_{\boldsymbol{lk}}^H\boldsymbol{y}_{\boldsymbol{l}}$ is a zero mean complex Gaussian random variable and has a second order moment as the original variable.
Finally, to complete the proof, α should be selected in a way to obtain the nearest upper bound in (A.2.6), while this can be done by solving the minimization problem below.

$$\min_{\alpha} \mathbb{E}\left\{\left|s_{lk} - \alpha\,\boldsymbol{v}_{\boldsymbol{lk}}^H\boldsymbol{y}_{\boldsymbol{l}}\right|^2\right\} = \frac{1}{1+SINR_{lk}^{UL}} \quad (A.2.7)$$

The minimizing problem can be solved by computing the expectation problem over all the entries of *l,k* then finding the optimal *α*. From equation (A.2.6 and A.2.7) we can write,

$$C_{lk}^{UL} \ge \gamma^{UL}\left(1-\frac{\tau_p}{\tau_p}\right)\left(\log_2(\pi e) + \log_2\left(\pi e\,\frac{1}{1+SINR_{lk}^{UL}}\right)\right) \quad (A.2.8)$$

$$C_{lk}^{UL} = \gamma^{UL}\left(1-\frac{\tau_p}{\tau_p}\right)\log_2(1+SINR_{lk}^{UL})$$

which proof the theorem.

Proof of Corollary 4.4.1

Before we start, let's recall the following:

$$MSE_{lit} = \beta_{lit}\left(1 - \frac{P_{it}\tau_p\beta_{lit}}{\sum_{i\prime\in\S_l}^{L} P_{i\prime t}\tau_p\beta_{li\prime t} + \sigma_{UL}^2}\right) \quad (A.3.1)$$

$$\mathbb{V}\{h_{litm}\} = \beta_{lit} \quad (A.3.2)$$

$$\mathbb{V}\{\hat{h}_{litm}\} = \frac{P_{it}\tau_p(\beta_{lit})^2}{\sum_{i\prime\in\S_l}^{L} P_{i\prime t}\tau_p\beta_{li\prime t} + \sigma_{UL}^2} \quad (A.3.3)$$

for Rayleigh fading channels between the t-th user terminal in the i-th cell and the m-th antenna in the l-th BS assuming similar channel variance for all antennas.
In case of MR detection, then $\boldsymbol{v}_{lk} = \widehat{\boldsymbol{h}}_{llk}$ *which by substituting in Theorem 4.4.1 gives,*

$$SINR_{lk}^{MR,UL} = \frac{p_{lk}\left|\mathbb{E}\left\{\widehat{\boldsymbol{h}}_{llk}{}^{H}\boldsymbol{h}_{llk}\right\}\right|^2}{\sum_{i=1}^{L}\sum_{t=1}^{K} p_{it}\mathbb{E}\left\{\left|\widehat{\boldsymbol{h}}_{llk}{}^{H}\boldsymbol{h}_{lit}\right|^2\right\} - p_{lk}\left|\mathbb{E}\left\{\widehat{\boldsymbol{h}}_{llk}{}^{H}\boldsymbol{h}_{llk}\right\}\right|^2 + \sigma_{UL}^2\mathbb{E}\left\{\left\|\widehat{\boldsymbol{h}}_{llk}\right\|^2\right\}} \quad (A.3.4)$$

Computing the expectation values in $(A.3.4)$ *:*
From Lemma 3.7.1, $\boldsymbol{h}_{llk} = \widehat{\boldsymbol{h}}_{llk} + \boldsymbol{e_{llk}}$ *,thus the expectation in the numerator can be computed as*

$$p_{lk}\left|\mathbb{E}\left\{\widehat{\boldsymbol{h}}_{llk}{}^{H}\boldsymbol{h}_{llk}\right\}\right|^2 = M^2 p_{lk}(\mathbb{V}\{\hat{h}_{llkm}\})^2 \quad (A.3.5)$$

The first term of the denominator will be decomposed into three parts, where the first two parts group the cells reusing the same pilots as the l-th cell while the last part for the remaining cells.

$$\sum_{i=1}^{L}\sum_{t=1}^{K} p_{it}\mathbb{E}\left\{\left|\widehat{\boldsymbol{h}}_{llk}{}^{H}\boldsymbol{h}_{lit}\right|^2\right\} - p_{lk}\left|\mathbb{E}\left\{\widehat{\boldsymbol{h}}_{llk}{}^{H}\boldsymbol{h}_{llk}\right\}\right|^2 + \sigma_{UL}^2\mathbb{E}\left\{\left\|\widehat{\boldsymbol{h}}_{llk}\right\|^2\right\}$$

$$= \sum_{i\in\int_l} p_{ik}\mathbb{E}\left\{\left|\widehat{\boldsymbol{h}}_{llk}{}^{H}\boldsymbol{h}_{lik}\right|^2\right\} + \sum_{i\in\int_l}\sum_{t=1,t\neq k}^{K} p_{it}\mathbb{E}\left\{\left|\widehat{\boldsymbol{h}}_{llk}{}^{H}\boldsymbol{h}_{lit}\right|^2\right\}$$
$$+ \sum_{i\notin\int_l}\sum_{t=1}^{K} p_{it}\mathbb{E}\left\{\left|\widehat{\boldsymbol{h}}_{llk}{}^{H}\boldsymbol{h}_{lit}\right|^2\right\} - p_{lk}\left|\mathbb{E}\left\{\widehat{\boldsymbol{h}}_{llk}{}^{H}\boldsymbol{h}_{llk}\right\}\right|^2 + \sigma_{UL}^2\mathbb{E}\left\{\left\|\widehat{\boldsymbol{h}}_{llk}\right\|^2\right\}$$

$$= M^2\mathbb{V}\{\hat{h}_{llkm}\}\sum_{i\in\int_l\setminus\{l\}} p_{ik}\mathbb{V}\{\hat{h}_{likm}\} + M\mathbb{V}\{\hat{h}_{llkm}\}\sum_{i\in\int_l}\sum_{t=1}^{K} p_{it}\mathbb{V}\{\hat{h}_{litm}\}$$
$$+ M\mathbb{V}\{\hat{h}_{llkm}\}\sum_{i\notin\int_l}\sum_{t=1}^{K} p_{it}\mathbb{V}\{\hat{h}_{litm}\} + M\mathbb{V}\{\hat{h}_{llkm}\}\sigma_{UL}^2 \quad (A.3.6)$$

$\sum_{i\in\int_l} p_{ik}\mathbb{E}\left\{\left|\widehat{\boldsymbol{h}}_{llk}{}^{H}\boldsymbol{h}_{lik}\right|^2\right\}$ *in (A.3.6) is computed using (4.4.8) with the fact of independence between the MMSE estimate the estimation error, and it presents the effect of pilot contamination.*
$\sum_{i\in\int_l}\sum_{t=1,t\neq k}^{K} p_{it}\mathbb{E}\left\{\left|\widehat{\boldsymbol{h}}_{llk}{}^{H}\boldsymbol{h}_{lit}\right|^2\right\}$ *in (A.3.6) is computed based on the assumption that the remaining users in* $\int_l$ *uses orthogonal pilot sequences to that of the k-th user.*
$M\mathbb{V}\{\hat{h}_{llkm}\}\sum_{i\notin\int_l}\sum_{t=1}^{K} p_{it}\mathbb{V}\{\hat{h}_{litm}\}$ *in (A.3.6) is done based on the assumption that the channel estimates in the l-th cell are independent from the estimates that does not belong to* $\int_l$.
$M\mathbb{V}\{\hat{h}_{llkm}\}\sigma_{UL}^2$ *was the result of the* $\mathbb{E}\left\{\left\|\widehat{\boldsymbol{h}}_{llk}\right\|^2\right\} = M\mathbb{V}\{\hat{h}_{llkm}\}$.

Using equation (A.3.5) and (A.3.6), the SINR expression of equation (A.3.4) becomes,

$$SINR_{l,k}^{MR,UL} = \frac{Mp_{lk}\mathbb{V}\{\hat{h}_{llkm}\}}{\sum_{i\in\int_l\{l\}} p_{ik}\mathbb{V}\{\hat{h}_{likm}\} + \sum_{i\in\int_l}\sum_{t=1}^{K} p_{it}\mathbb{V}\{\hat{h}_{litm}\} + \sigma_{UL}^2} \quad (A.3.7)$$

After substituting equation (A.3.1) - (A.3.3) into (A.3.7) the expression in the corollary will be proved.

In the case of ZF detection, the following property will be valid due channel inversion structure.

$$\mathbb{E}\{\boldsymbol{v}_{lk}^{H}\boldsymbol{h}_{llk}\} = 1 \quad (A.3.8)$$

and the noise term can be solved by,

$$\sigma_{UL}^2\mathbb{E}\{\|\boldsymbol{v}_{lk}\|^2\} = \sigma_{UL}^2\mathbb{E}\left\{tr\left[\left(\left(\widehat{\boldsymbol{H}}_{ll}\right)^{H}\widehat{\boldsymbol{H}}_{ll}\right)^{-1}\right]_{k,k}\right\} = \frac{\sigma_{UL}^2}{(M-K)\mathbb{V}\{\hat{h}_{llkm}\}} \quad (A.3.9)$$

The SINR expression in (A.3.10), using ZF detection, can be done after substituting equation (A.3.8) and (A.3.9) into (4.4.4).

$$SINR_{l,k}^{ZF,UL} = \frac{p_{lk}}{\sum_{i=1}^{L}\sum_{t=1}^{K} p_{it}\mathbb{E}\{|\boldsymbol{v}_{lk}{}^{H}\boldsymbol{h}_{lit}|^2\} - p_{lk} + \frac{\sigma_{UL}^2}{(M-K)\mathbb{V}\{\hat{h}_{llkm}\}}} \quad (A.3.10)$$

The expectation term at the denominator of equation $(A.3.10)$ *can be computed as follows*

$$\sum_{i=1}^{L}\sum_{t=1}^{K} p_{it}\mathbb{E}\{|\boldsymbol{v}_{lk}{}^{H}\boldsymbol{h}_{lit}|^2\}$$

$$= \sum_{i\in\mathfrak{J}_l} p_{ik}\mathbb{E}\{|\boldsymbol{v}_{lk}{}^{H}\boldsymbol{h}_{lit}|^2\} + \sum_{i\in\mathfrak{J}_l}\sum_{t=1}^{K} p_{it}\mathbb{E}\{|\boldsymbol{v}_{lk}{}^{H}\boldsymbol{e}_{lit}|^2\} + \sum_{i\notin\mathfrak{J}_l}\sum_{t=1}^{K} p_{it}\mathbb{E}\{|\boldsymbol{v}_{lk}{}^{H}\boldsymbol{h}_{lit}|^2\}$$

$$= \sum_{i\in\mathfrak{J}_l} \frac{p_{ik}{}^2(\beta_{lik})^2}{p_{lk}(\beta_{llk})^2} + \sum_{i\in\mathfrak{J}_l}\sum_{t=1}^{K} \frac{p_{it}MSE_{lit}}{(M-K)\mathbb{V}\{\hat{h}_{llkm}\}} + \sum_{i\notin\mathfrak{J}_l}\sum_{t=1}^{K} \frac{p_{it}\mathbb{V}\{\hat{h}_{litm}\}}{(M-K)\mathbb{V}\{\hat{h}_{llkm}\}} \quad (A.3.11)$$

By substituting (A.3.11) into (A.3.10) and exploiting the equations (A.3.1) - (A.3.3), we will arrive in the SINR for ZF detection.

Proof of Theorem 4.4.2

The received signal at the k-th user in the l-th cell is

$$y_{lk} = \sum_{i=1}^{L}(\boldsymbol{h}_{ilk})^H \sum_{t=1}^{K}\sqrt{\rho_{it}}\,\boldsymbol{w}_{it}s_{it} + n_{lk} \quad (A.4.1)$$

$$= \underbrace{\sqrt{\rho_{lk}}(\boldsymbol{h}_{llk})^H\boldsymbol{w}_{lk}s_{lk}}_{Desired} + \underbrace{\sum_{t=1,t\neq l}^{K}\sqrt{\rho_{lk}}(\boldsymbol{h}_{llk})^H\boldsymbol{w}_{lk}s_{lk}}_{Intra-cell\ interfernce} + \underbrace{\sum_{i=1,i\neq l}^{L}\sum_{t=1}^{K}\sqrt{\rho_{it}}(\boldsymbol{h}_{ilk})^H\boldsymbol{w}_{it}s_{it}}_{Inter-cell\ interference} + \underbrace{n_{lk}}_{Noise}$$

This can be computed by substituting equation (3.10.1) into (3.10.2). By taking into consideration a suboptimal Gaussian signal distribution, $s_{lk}\sim\mathbb{CN}(0,1)$, a lower bound on the mutual information between $s_{lk}$and y_{lk} can be expressed as follows:

$$\boldsymbol{C}_{l,k}^{DL} \geq \gamma^{DL}(1-\frac{\tau_p}{\tau_c})I(s_{lk};y_{lk})$$

$$\geq \gamma^{DL}\left(1-\frac{\tau_p}{\tau_c}\right)\left(\log_2(\pi e) - h(s_{lk}|y_{lk})\right)$$

$$\geq \log_2\left(1+SINR_{l,k}^{DL}\right) \quad (A.4.2)$$

where the inequality is computed based on the procedure written in equation (A.2.4) -(A.2.8). However, the receiver does not know any information about the estimated CSI.

Proof of Corollary 4.4.2

This proof is similar to the proof of ***Corollary 4.4.1****, so we will use the same technique to solve the expectations.*
In case of MR precoding
First the expectations in equation (4.4.13).

$$\rho_{lk}\left|\mathbb{E}\{\boldsymbol{h}_{llk}{}^{H}\boldsymbol{w}_{lk}\}\right|^2 = \frac{\rho_{lk}}{M\mathbb{V}\{\hat{h}_{llkm}\}}\left|\mathbb{E}\left\{\|\widehat{\boldsymbol{h}}_{llk}\|^2\right\}\right|^2 = M\rho_{lk}\mathbb{V}\{\hat{h}_{llkm}\} \quad (A.5.1)$$

The denominator can be solved as follows,

$$\sum_{i=1}^{L}\sum_{t=1}^{K}\rho_{it}\mathbb{E}\left\{\left|\widehat{\boldsymbol{h}}_{ilk}{}^{H}\boldsymbol{w}_{it}\right|^2\right\}-\rho_{lk}\left|\mathbb{E}\left\{\widehat{\boldsymbol{h}}_{llk}{}^{H}\boldsymbol{w}_{llk}\right\}\right|^2+\sigma_{DL}^2$$

$$=\sum_{i\in\mathfrak{J}_l}\rho_{ik}\mathbb{E}\left\{\left|\widehat{\boldsymbol{h}}_{ilk}{}^{H}\boldsymbol{w}_{lik}\right|^2\right\}+\sum_{i\in\mathfrak{J}_l}\sum_{t=1,t\neq k}^{K}\rho_{it}\mathbb{E}\left\{\left|\widehat{\boldsymbol{h}}_{ilk}{}^{H}\boldsymbol{w}_{ilt}\right|^2\right\}$$
$$+\sum_{i\notin\mathfrak{J}_l}\sum_{t=1}^{K}\rho_{it}\mathbb{E}\left\{\left|\widehat{\boldsymbol{h}}_{ilk}{}^{H}\boldsymbol{w}_{ilt}\right|^2\right\}-\rho_{lk}\left|\mathbb{E}\left\{\widehat{\boldsymbol{h}}_{llk}{}^{H}\boldsymbol{w}_{llk}\right\}\right|^2+\sigma_{DL}^2$$

$$=M\sum_{i\in\mathfrak{J}_l\setminus\{l\}}\rho_{ik}\mathbb{V}\{\hat{h}_{iikm}\}+\sum_{i\in\mathfrak{J}_l}\sum_{t=1}^{K}\rho_{it}\mathbb{V}\{\hat{h}_{ilkm}\}+\sigma_{DL}^2\qquad(A.5.2)$$

After substituting (A.5.1) and (A.5.2) into equation (4.4.13), we will arrive in the expression stated in the corollary for MR precoding.

In the case of ZF precoding:

notice that,

$$\mathbb{E}\left\{\left\|\widehat{\boldsymbol{H}}_{ii}\boldsymbol{r}_{it}\right\|^2\right\}=\mathbb{E}\left\{\left[\left(\left(\widehat{\boldsymbol{H}}_{ii}\right)^{H}\widehat{\boldsymbol{H}}_{ii}\right)^{-\mathbf{1}}\right]_{\boldsymbol{t},\boldsymbol{t}}\right\}=\frac{1}{(M-K)\mathbb{V}\{\hat{h}_{iitm}\}}\qquad(A.5.3)$$

Exploiting the fact that $\left(\widehat{\boldsymbol{H}}_{ii}\right)^{H}\widehat{\boldsymbol{H}}_{ii}$ *is considered a central Wishart matrix and has M degree of freedom, the ZF precoding vector can be expressed as,*

$$\boldsymbol{w}_{it}=\sqrt{(M-K)\mathbb{V}\{\hat{h}_{iitm}\}}\widehat{\boldsymbol{H}}_{ii}\boldsymbol{r}_{it}\qquad(A.5.4)$$

Substituting $(A.5.4)$ *in equation (4.4.13), the numerator and the denominator can be solved as follows,*

$$\rho_{lk}\left|\mathbb{E}\{\boldsymbol{h}_{llk}{}^{H}\boldsymbol{w}_{lk}\}\right|^2=(M-K)\rho_{lk}\mathbb{V}\{\hat{h}_{llkm}\}\ ,\qquad(A.5.5)$$

$$\sum_{i=1}^{K}\sum_{t=1}^{K}\rho_{it}\mathbb{E}\left\{\left|\widehat{\boldsymbol{h}}_{ilk}{}^{H}\boldsymbol{w}_{it}\right|^2\right\}-\rho_{lk}\left|\mathbb{E}\left\{\widehat{\boldsymbol{h}}_{llk}{}^{H}\boldsymbol{w}_{lk}\right\}\right|^2+\sigma_{DL}^2$$
$$=(M-K)\sum_{i\in\mathfrak{J}_l\setminus\{l\}}\rho_{ik}\mathbb{V}\{\hat{h}_{ilkm}\}+\sum_{i\in\mathfrak{J}_l}\sum_{t=1}^{K}\rho_{it}MSE_{ilk}+\sum_{i\notin\mathfrak{J}_l}\sum_{t=1}^{K}\rho_{it}\mathbb{V}\{h_{itm}\}$$
$$+\sigma_{DL}^2\qquad(A.5.6)$$

The ZF precoding expression in the corollary can be found by substituting (A.5.5) and (A.5.6) into equation (4.4.13).